



QEX

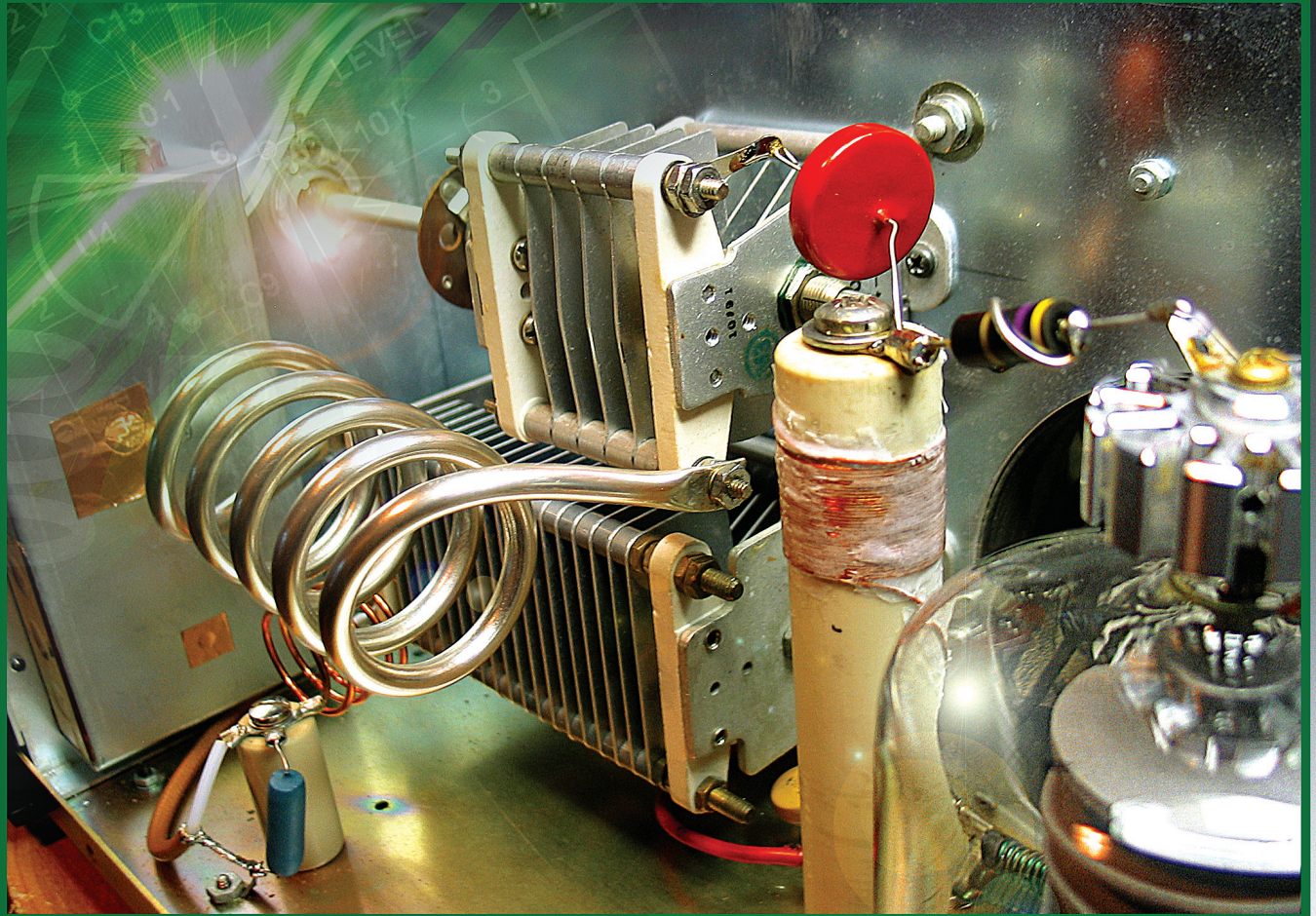
\$5

May/June 2016

www.arrl.org

A Forum for Communications Experimenters

Issue No. 296



WB3LHD converts a classic Heathkit HF linear amplifier and breathes new life into it for 6 meter band service.

EchoLink® Ready



TM-V71A

With the Kenwood TM-V71A you have a choice of where you want your speaker, on the top or on the bottom of the radio. Simply remove the faceplate and flip the main body, then reattach the face, it's that simple! Yet another Kenwood 1st, this dual band transceiver has ten dedicated EchoLink® memory channels as well as EchoLink sysop-mode operation. EchoLink connection to your PC via the optional PG-5H cable kit is easy with no expensive interface needed.

EchoLink® is a registered trademark of Synergenics, LLC. For more information please see: www.echolink.org.



Large dual color amber or green thirteen segment LCD.

KENWOOD

Customer Support: (310) 639-4200
Fax: (310) 537-8235



Scan with your phone to download TM-V71A Brochure.


www.kenwood.com/usa



ADS#09216

QEX (ISSN: 0886-8093) is published bimonthly in January, March, May, July, September, and November by the American Radio Relay League, 225 Main Street, Newington, CT 06111-1494. Periodicals postage paid at Hartford, CT and at additional mailing offices.

POSTMASTER: Send address changes to: QEX, 225 Main St, Newington, CT 06111-1494 Issue No 296

Kazimierz "Kai" Siwiak, KE4PT
Editor

Lori Weinberg, KB1EIB
Assistant Editor

Zack Lau, W1VT
Ray Mack, W5IFS
Contributing Editors

Production Department

Steve Ford, WB8IMY
Publications Manager

Michelle Bloom, WB1ENT
Production Supervisor

Sue Fagan, KB1OKW
Graphic Design Supervisor

David Pingree, N1NAS
Senior Technical Illustrator

Brian Washing
Technical Illustrator

Advertising Information Contact:

Janet L. Rocco, W1JLR
Business Services
860-594-0203 – Direct
800-243-7768 – ARRL
860-594-4285 – Fax

Circulation Department

Cathy Stepina, QEX Circulation

Offices

225 Main St, Newington, CT 06111-1494 USA
Telephone: 860-594-0200
Fax: 860-594-0259 (24 hour direct line)
e-mail: qex@arrl.org

Subscription rate for 6 issues:

In the US: ARRL Member \$24,
nonmember \$36;

US by First Class Mail:
ARRL member \$37, nonmember \$49;

International and Canada by Airmail: ARRL member
\$31, nonmember \$43;

Members are asked to include their membership
control number or a label from their QST when
applying.

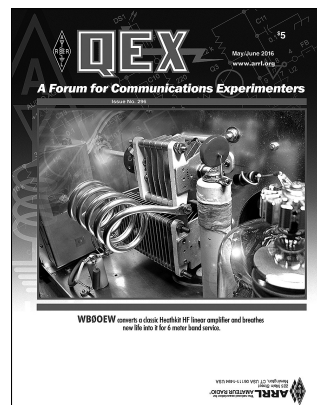
In order to ensure prompt delivery, we ask that you periodically check the address information on your mailing label. If you find any inaccuracies, please contact the Circulation Department immediately. Thank you for your assistance.



Copyright © 2016 by the American Radio Relay League Inc. For permission to quote or reprint material from QEX or any ARRL publication, send a written request including the issue date (or book title), article, page numbers and a description of where you intend to use the reprinted material. Send the request to the office of the Publications Manager (permission@arrl.org).

About the Cover

Ron Berry, WB3LHD, takes a classic Heathkit SB-1000 linear amplifier out of retirement from HF duty, then modifies and presses it into 6 meter monoband service. He gives step by step details of his modifications to the RF deck, input and output circuits, and component changes that result in 650 W RF output on the "magic band."



In This Issue

Features

2 Perspectives
Kazimierz "Kai" Siwiak, KE4PT

3 6 m Monoband Conversion for Heathkit SB-1000 Amplifier
Ron Berry, WB3LHD

8 Open Source Soft-Decision Decoder for the JT65 (63, 12) Reed-Solomon Code
Steven J. Franke, K9AN and Joseph H. Taylor, K1JT

18 Measuring Propagation Attenuation Using a Quadcopter
Glenn E. Elmore, N6GN

24 Using a Wide-Band Noise Generator with a Spectrum Analyzer
Dr. George R. Steber, WB9LVI

30 Geodetic and Maidenhead Locator System Conversion
Bill Echols, NI5F

36 SDR Simplified
Ray Mack, W5IFS

44 Upcoming Conferences

Index of Advertisers

ARRL Cover III
Down East Microwave Inc: 7
DX Engineering: 23
Kenwood Communications: Cover II
Nemal Electronics International, Inc: 17

Quicksilver Radio Products Cover IV
RF Parts: 41, 43
Roger Palmer, VE7AP 22
Tucson Amateur Packet Radio: 17

The American Radio Relay League



The American Radio Relay League, Inc. is a noncommercial association of radio amateurs, organized for the promotion of interest in Amateur Radio communication and experimentation, for the establishment of networks to provide communications in the event of disasters or other emergencies, for the advancement of the radio art and of the public welfare, for the representation of the radio amateur in legislative matters, and for the maintenance of fraternalism and a high standard of conduct.

ARRL is an incorporated association without capital stock chartered under the laws of the state of Connecticut, and is an exempt organization under Section 501(c)(3) of the Internal Revenue Code of 1986. Its affairs are governed by a Board of Directors, whose voting members are elected every three years by the general membership. The officers are elected or appointed by the Directors. The League is noncommercial, and no one who could gain financially from the shaping of its affairs is eligible for membership on its Board.

"Of, by, and for the radio amateur," ARRL numbers within its ranks the vast majority of active amateurs in the nation and has a proud history of achievement as the standard-bearer in amateur affairs.

A *bona fide* interest in Amateur Radio is the only essential qualification of membership; an Amateur Radio license is not a prerequisite, although full voting membership is granted only to licensed amateurs in the US.

Membership inquiries and general correspondence should be addressed to the administrative headquarters:

ARRL
225 Main Street
Newington, CT 06111 USA
Telephone: 860-594-0200
FAX: 860-594-0259 (24-hour direct line)

Officers

President: Rick Roderick, K5UR
PO Box 1463, Little Rock, AR 72203

Chief Executive Officer: DAVID SUMNER, K1ZZ

The purpose of QEX is to:

- 1) provide a medium for the exchange of ideas and information among Amateur Radio experimenters,
- 2) document advanced technical work in the Amateur Radio field, and
- 3) support efforts to advance the state of the Amateur Radio art.

All correspondence concerning *QEX* should be addressed to the American Radio Relay League, 225 Main Street, Newington, CT 06111 USA. Envelopes containing manuscripts and letters for publication in *QEX* should be marked Editor, *QEX*.

Both theoretical and practical technical articles are welcomed. Manuscripts should be submitted in word-processor format, if possible. We can redraw any figures as long as their content is clear. Photos should be glossy, color or black-and-white prints of at least the size they are to appear in *QEX* or high-resolution digital images (300 dots per inch or higher at the printed size). Further information for authors can be found on the Web at www.arrl.org/qex/ or by e-mail to qex@arrl.org.

Any opinions expressed in *QEX* are those of the authors, not necessarily those of the Editor or the League. While we strive to ensure all material is technically correct, authors are expected to defend their own assertions. Products mentioned are included for your information only; no endorsement is implied. Readers are cautioned to verify the availability of products before sending money to vendors.

Kazimierz "Kai" Siwiak, KE4PT

Perspectives

Constants and Standards

QEX is a forum for the free exchange of ideas among communications experimenters. We regularly delve into the physics, science and engineering of radio technologies, and we invariably use physical constants and units of measure in our calculations. Wherever possible, we should use standard symbols and exact quantities, especially in computer programs. For example, the speed of light c is *defined* as exactly 299,792,458 m/s. The magnetic constant μ_0 is *exactly* $4\pi \times 10^{-7}$ H/m. These are two defined fundamental constants of nature. It follows that the derived electric constant ϵ_0 is *exactly* $1/(\mu_0 c^2)$ F/m. Likewise, the derived intrinsic impedance of free space η_0 is *exactly* $(\mu_0 c)$ Ω . Why do so? Because it is correct. Who came first, the chicken or the egg? The exact defined constants come first, the derived constants come next. That said, there is nothing wrong with using approximations like 300,000,000 m/s for the speed of light or 377 Ω for the free space intrinsic impedance, or for that matter 3.14 for π as illustrative examples, but in calculations let's use the exact values. You can find the accepted values of physical constants at physics.nist.gov/cuu/Constants/archive2010.html.

The wonderful thing about standards is there are so many to choose from (oft quipped by pundits). What weighs more, an ounce of gold or an ounce of feathers? What weighs more, a pound of gold or a pound of feathers? The answers are "an ounce of gold weighs more than an ounce of feathers" and "a pound of feathers weighs more than a pound of gold!" Gold is "weighed" in Troy measure, one Troy ounce has a mass of about 31.1 grams, and there are 12 Troy ounces to the Troy pound (about 373.2 grams). Feathers are "weighed" in Avoirdupois measure, and one ounce Av equals about 28.4 grams. There are 16 Av ounces to the Av pound (about 453.6 grams). The answers are immediately obvious in the metric units!

Good standards deny us silly riddles, but they can also save us money. The cause of the NASA Mars Climate Orbiter crash into Mars was that one NASA team used English units (inches, feet and pounds) while another team used metric units for key spacecraft maneuvers required to place the spacecraft in the proper Mars orbit. The subsequent US \$357 M loss of the spacecraft was due to the failed translation of English units into metric units in a segment of ground-based, navigation-related mission software.

Final riddle. What do the United States, Liberia, and Myanmar have in common? They are the only three remaining non-metric countries in the world. That brings us to Amateur Radio standards. I make the plea to use metric units in *QEX* where ever possible, with the imperial (English) values in parentheses.

Remember that the content of *QEX* is driven by you, the reader and prospective author. If you don't write it, we can't publish it. So please, put your favorite topic or innovative measurement on paper, and share it on these pages. Just follow the details on the www.arrl.org/qex-author-guide web page, and contact us at qex@arrl.org. We value your feedback, comments and opinions about these pages.

In this issue, our *QEX* authors touch upon several aspects of Amateur Radio — decoding procedures for a powerful Reed-Solomon code, PLLs and PID loops, a linear amplifier conversion project, measuring circuits using a noise generator, and airborne propagation measurements. Steven J. Franke, K9AN, and Joe Taylor, K1JT, share an under-the-hood description of the JT65 decoding procedure, and include a wholly new algorithm for its powerful error-correcting code. Ron Berry, WB3LHD, converts the classic Heathkit SB 1000 HF amplifier into a 6 m band work horse. Bill Echols, N15F, extends the definition of Maidenhead grid locators from the currently defined 8 characters to 16 characters, which improves location precision to inches. Glenn Elmore, N6GN, uses a quadcopter to measure 10 m band propagation attenuation in a local environment. George Steber, WB9LVI, uses a wide-band noise generator as an alternative to a tracking generator to measure components and circuits with a spectrum analyzer, and compares the two methods showing several examples. Ray Mack, W5IFS, Demystifies proportional-integral-differential (PID) control loops and gives insights into how to build and tune one.

Please continue to support *QEX*, and help it remain a strong technical publication.

73,

Kazimierz "Kai" Siwiak, KE4PT

6 m Monoband Conversion for Heathkit SB-1000 Amplifier

Convert this classic HF amplifier into a 6-m band work horse.

After 38 years of chasing DX on the HF bands, I decided it was time to explore a new frontier and push the 50 MHz button on my transceiver. I eagerly erected a 6 m two element quad antenna and started working some Maidenhead grid squares.¹ I soon realized that a bigger antenna and more than 100 W of power would be most helpful. I could afford a bigger antenna, but purchasing a 6 meter amplifier would be difficult. This would be the perfect time to convert my old Heathkit SB-1000 amplifier to 6 meter operation. I had retired it 13 years ago from HF duty because of a twice-blown band switch. It has been sleeping in my closet ever since.

Since I was not an expert on the subject of amplifier conversions, and this was my first attempt, I felt it best to contact other hams who made the conversion successfully. I also consulted the *ARRL Handbook*, RF amplifier books, articles in *QST*, and searched the Internet for additional information.² Now confident, I began my HF to 6 meters amplifier conversion.

For convenience, I assigned the components with alpha-numeric designators directly from the original Heathkit SB-1000 amplifier schematic. You can download the complete manual from the Internet.³ Figure 1 shows the schematic diagram of my amplifier.

I needed to address the following details during my conversion: strip the RF deck, change the plate and loading capacitors, modify the π -input circuit and π -L output circuit, replace the parasitic choke, replace the blocking capacitor, and replace the RF plate choke. I also replaced the internal RF

output coax and safety choke.

First, I removed the amplifier cover, knobs, vernier pointers, and lowered the front panel. I saved all the hardware and parts in small plastic cups and labeled sandwich bags as I removed them. This saved me a lot of trouble later on. I didn't have to guess what screws or parts went where. Here are the details.

Stripping the RF Deck

With reference to the original schematic from the Heathkit SB-1000 manual, carefully remove V1, the 3-500Z tube, and set it aside. Remove the tank coils L7 and L8, inductor L9, plate RF choke RFC3, safety choke RFC1, door-knob capacitors C26, C28 and C29, plastic standoffs, the band switch SW2, and the switch enclosure. When you remove the band switch enclosure do not cut off the input matching section mini coax cables that pass through the grommet. Unsolder those cables to keep them as long as possible, they will be used again. Mark the cables as *input* and *output* so you don't get them reversed later. The input coax originates from pin 6 of relay K1, and the output coax connects to the 3-500Z cathode capacitors C18 and C19. Remove the band switch with all the capacitors, and the tunable slug inductors from the enclosure, except L6, the original 10 m inductor. L6 is the inductor with the least number of turns on it, and is located at the top next to the grommet hole. We will modify and reuse inductor L6 as described later in the " π input circuit" section.

Plate and Loading Capacitors

The plate and loading variable capacitors must be replaced but you can swap the upper plate capacitor for the bottom loading

capacitor. First remove the bottom loading capacitor C31 and set it aside for another project. Now remove the top plate capacitor C27 and mount it in the bottom loading capacitor position. When doing this you must reuse the original front mounting hole and drill a new rear mounting hole. Before you measure and drill the new rear hole, be sure the capacitor shaft is fully set into the vernier drive and is straight.

A new upper plate capacitor will require less capacitance than the original, and a higher voltage rating. I purchased a Cardwell #154-11-1 (9 – 38 pF) 4 kV air variable capacitor. There are several sources for these and they vary greatly in price. To mount it, you must reuse the rear mounting hole and drill a new front mounting hole. Be careful when drilling the hole, as the high voltage power supply is directly behind the panel. Again, make sure that you mount the capacitor straight. The newly mounted Cardwell capacitor has the same shaft height as the original capacitor, but the shaft will not reach the vernier drive. To fix that, I purchased a piece of 0.25 inch O.D. aluminum shaft. I cut off a piece approximately 2.5 inches long, and connected the two shafts together using a coupler that I had in my junk box. Before you cut the aluminum shaft, measure it carefully to be sure it's long enough to fit fully into the coupler and into the vernier drive.

The π Input Circuit

The original Heathkit input matching circuit is a π -type configuration that uses a variable inductor and two fixed capacitors. Some hams have opted to modify their 6 m conversions to a T-type network that has a variable capacitor and two fixed inductors. I wanted to retain the π circuit for its superior harmonic suppression and

¹Notes appear on page 7

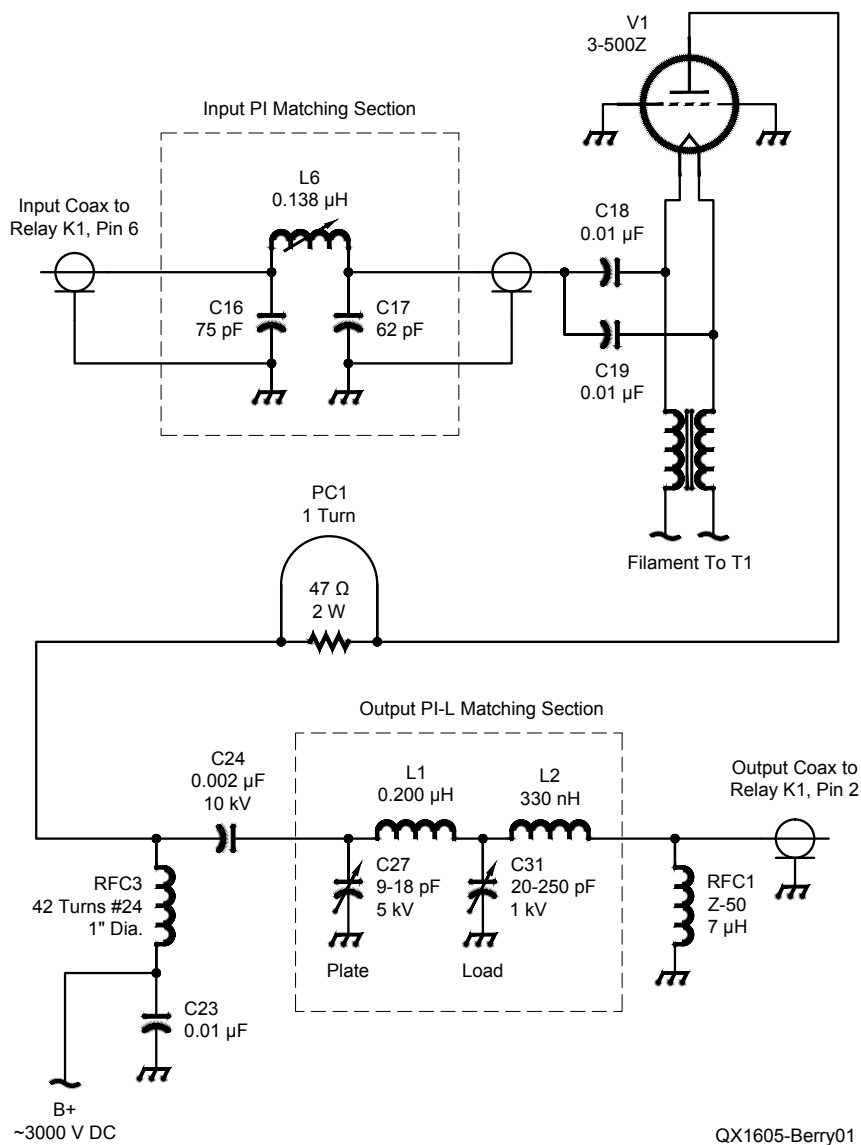


Figure 1 — Heathkit SB-1000 6 m band conversion schematic. See Table 1 for the project bill of materials.

Table 1.

Bill of Materials: Digi-Key, www.digikey.com; RF Parts, <https://www.rfparts.com/>; eBay, www.ebay.com; Amidon, www.amidoncorp.com/; Mouser, www.mouser.com.

Description	Part	Source	Part Number	Cost
C16	75 pF 500 V mica capacitor	Digi-Key	338-2835-ND	\$1.82
C17	62 pF 500 V mica capacitor	Digi-Key	338-2833-ND	\$1.82
C24	0.002 μF 10 kV capacitor	RF Parts	002-10KVHDA	\$2.95
C27	9-38 pF Capacitor	Cardwell	154-11-1	\$50.00
C401-408	Electrolytic Capacitors	RF Parts	CGS211T450R4	\$159.60
L1	0.25" OD Copper Tubing	eBay	N/A	\$10.00
RFC1	7.0 μH safety choke	Mouser	588-Z50E	\$5.61
RFC3	15' of #24 Thermozele wire	Amidon	AWG#24 HAPT	\$3.00
V1	Taylor 3-500ZG Tube	RF Parts	3-500ZG-TAY	\$169.95
Misc.	Q-Dope, GC Electronics	eBay	N/A	\$10.00
Misc.	0.25" OD Aluminum Shaft	ACE Hardware	N/A	\$5.00
Misc.	Hyper Plate Cap	73CNC	Cap for 3-500Z	\$39.99
Misc.	Silver Plating Solution	Amazon	Medallion Brand	\$16.99

My total cost \$476.73

improved efficiency. I also decided to make it broadband enough to cover the entire 6 m band. This way no adjustments would be necessary with changes in frequency, and I could keep the original enclosure without the band switch. I started by modeling the circuit using an online *Input Impedance Matching Designer*.⁴

In *Designer*, enter 50 Ω for *Source Resistance*, 110 Ω for *Load Resistance*, 52 MHz for *Frequency*, and *Desired Q* of 2. *Source Resistance* is the exciter output impedance, *Load Resistance* is the 3-500Z input impedance, and *Q* determines bandwidth of the circuit. After modeling the circuit, I built and tested it using a HP network analyzer. I added a 10 pF capacitor in parallel with the 110 Ω resistor at the output of the circuit to better simulate the 3-500Z input impedance. The final circuit has the following values: C16 is 75 pF, L6 is 0.138 μH, C17 is 62 pF. I measured less than 0.2 dB insertion loss, and return loss greater than 30 dB, which is equivalent to a VSWR of less than 1.1:1 across the entire 50 – 54 MHz span of the 6 m band.

Modify the 10 m band inductor L6 to the needed inductance as follows. Unsolder the top end of the coil from the lug, undo one turn, trim it to length, tin and re-solder it back on the lug. You should now have 2.75 turns (Figure 2). Apply some Q-Dope if necessary to hold the coil winding in place.

Solder capacitors C16 and C17, and the mini-coax cables between the L6 coil lugs and ground, see Figures 1 and 2. The input coax and the 75 pF capacitor C16 are on the left and below inductor L6. The output coax and the 62 pF capacitor C17 are on the right. I fastened the ground lug to one of the unused screw holes, and covered over the remaining holes with copper tape to help keep the enclosure RF tight. If you don't have copper tape, some aluminum duct tape will work as well. [Copper tape used for RF has copper filings embedded in the adhesive, so there is dc contact between the tape and its target. Aluminum duct tape does not make dc contact with its target through the adhesive — Ed.].

The π-L Output Circuit

The original Heathkit output tank circuit was a π configuration. I was concerned that the original π circuit would not have enough second harmonic suppression to meet the FCC Part 97 requirements of 60 dB suppression, so I decided to use a π-L configuration. A π-L network has a broader tuning range, higher Q, and greater harmonic suppression compared with the standard π network. I started by downloading the *PI-EL* output network designer.⁵

Make L2 from #12 AWG copper wire

stripped from a piece of 12-2 Romex®. Wind four turns, 0.75 inches long around a one inch O.D. form. The inductance of L2 should be about 330 nH. One end connects to the load capacitor and the other end to the RF output coax center lead and the safety choke. I had a ceramic standoff insulator in my junk box to secure and insulate these connections, see Figure 3.

I made L1 from 0.25 inch O.D. thin wall copper tubing. Thin wall tubing is much easier to form than solid conductor. Wind five turns, five inches long, around a 1.50 inch O.D. form, see Figure 4. A video I saw on YouTube suggested to fill the tubing with table salt and crimp the ends tightly. The salt will prevent the coil from flattening and kinking as you wind it. Be sure to knock the salt out when finished. I cut the ends to length and mashed them flat with a hammer. I then drilled holes in the flats and fastened the ends between the variable capacitors. The inductance of the finished coil will be around 0.20 μ H. I silver-plated the coil with silver plating solution.⁶ This not only looks nice, but will help make it as efficient as possible.

The Parasitic Choke

The original parasitic choke PC1 was 4.5 turns of wire wound around a 100 Ω 2 W resistor and was designed for an HF amplifier. I tried replacing it with four turns on a 47 Ω 2 W resistor. I measured a reactance of 16 Ω at 54 MHz. I felt the choke was far too aggressive so I wound a more 6 m friendly version. It has only one turn of #16 AWG buss wire wound around the 47 Ω 2 W resistor. This presented 1 Ω of reactance at 54 MHz but still has enough roll-off above the 6 m band to be an effective parasitic choke.

The Blocking Capacitor

I wanted a higher voltage rating on the blocking capacitor to provide a higher margin of safety, so I replaced the original two-parallel 0.001 μ F 6 kV blocking capacitors C24 and C25 with a single 0.002 μ F 10 kV, capacitor C24 (Figure 1).

RF Plate Choke

The original RF plate choke RFC3 measured 120 μ H inductance, which has good reactance for the HF bands, but way more than necessary for 6 m, and it might have a self-resonance somewhere within the 6 m band. I removed all the original coil wires but reused the original 1 inch diameter ceramic form. I close-wound 42 turns of #24 AWG heavy armored polythermaleze top-coated (HAPT) magnet wire about 0.25 inches down from the top, and secured the coil turns to the ceramic form with

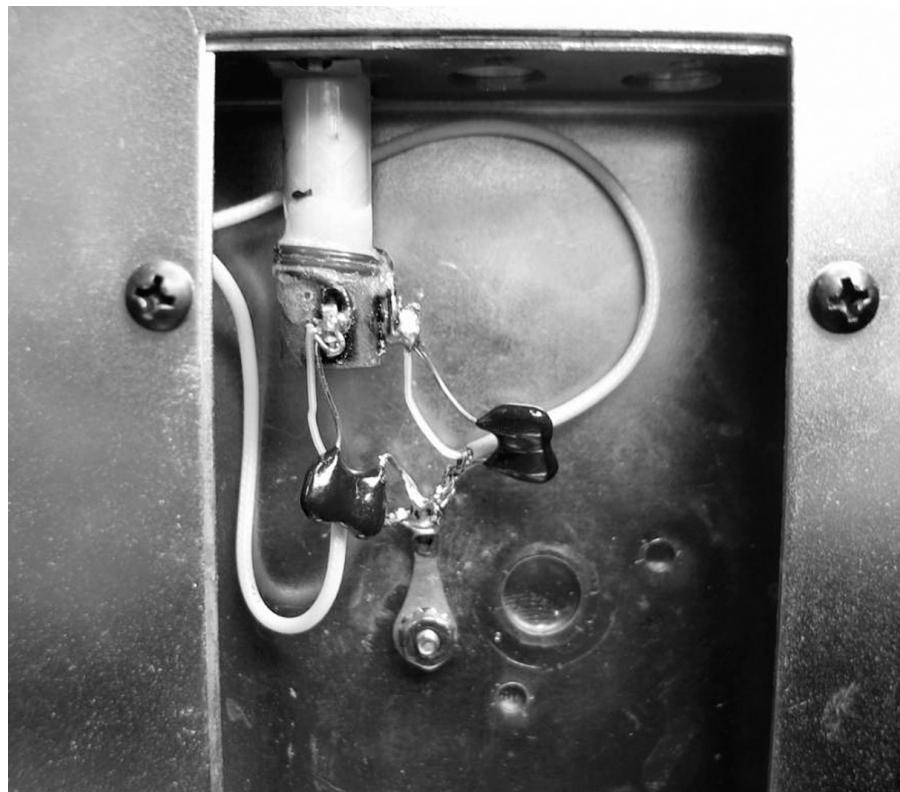


Figure 2 — Modified inductor L6 and routing of the input coax (left) and output coax (right). Capacitors C16 (left) and C17 are below L6.



Figure 3 — Inductor L2 mounts on a ceramic stand-off and connects to the RF output coax (below and left) and to choke RFC1. The other end of RFC1, and the coax shield connect to the ground lug at the bottom.

Q-Dope. The finished inductor measured around 30 μH . Fasten the choke back into position (Figure 4) with the bottom screw and re-solder the red high voltage lead, the 0.001 μF capacitor C23, and the bottom choke wire to the bottom lug. Screw the top solder lug in place and solder the new parasitic choke PC1, the new blocking capacitor, and the top choke wire.

The RF Output Coax

The original type RG-58 output coax is marginal at 50 MHz for more than 500 W, so I replaced it with a section of 50 Ω RG-142 Teflon™ dielectric coax. Teflon has a much higher breakdown voltage rating than polyethylene. A section of RG-213 or RG-8 coax would work as well but because of its larger diameter you may have difficulty

routing it around. The coax center lead attaches to the end of L2 where the safety choke attaches. The shield attaches to a solder lug on the chassis ground, (Figure 3).

The Safety Choke

I replaced the original safety choke RFC1 with an Ohmite Z50 7 μH choke. The safety choke is there in case the dc blocking capacitor C24 shorts. This would place thousands of plate volts to your antenna system, possibly causing damage and potentially killing someone. The safety choke has high reactance at RF but is a dc short to ground. In the event that the blocking capacitor shorts, the safety choke shorts the 3,000 V plate supply to ground, rather than to your antenna system. This will cause the amplifier fuse to blow, stopping the threat. The safety choke attaches between L2 where the RF output coax attaches, and chassis ground as seen in Figure 3.

Putting It Back Together

Follow the procedure in the Heathkit manual when setting the vernier drive pointer position in relation to the capacitor rotor shafts. Carefully look around to be sure you didn't leave any hardware or cut-off wires laying around the chassis. The amplifier conversion is finished and should look similar to the views in Figures 4 and 5.

Reinstall the front cover and install the plate and load capacitor knobs. I wanted to have a clean looking front panel, so I retained the original lettering and knob indication. I installed a hole plug into the hole of the missing band switch, and added a "SIX METER AMPLIFIER", and a "6 METER" label for the band switch on the front panel as seen in Figure 6. You can, of course, repaint or label your front panel as you wish.

Input Matching Alignment

Turn the amplifier on, and follow the Heathkit manual alignment procedure on pages 55 and 56 of the Heathkit SB-1000 manual. In my case, I set the PLATE capacitor to approximately the two o'clock position and the LOAD capacitor to approximately 7. I tuned my exciter to 52 MHz and adjusted the π input matching inductor L6 for minimum VSWR. I achieved a perfect 1:1 match. The design bandwidth Q of 2 is broad banded enough to cover the entire 50-54 MHz band without any farther adjustments. Just set it, and forget it!

Final Tune, Final Words

My amplifier tunes up nicely without any surprises and delivers 650 W with 50 to 60 W of drive across the 6 m band. On air reports

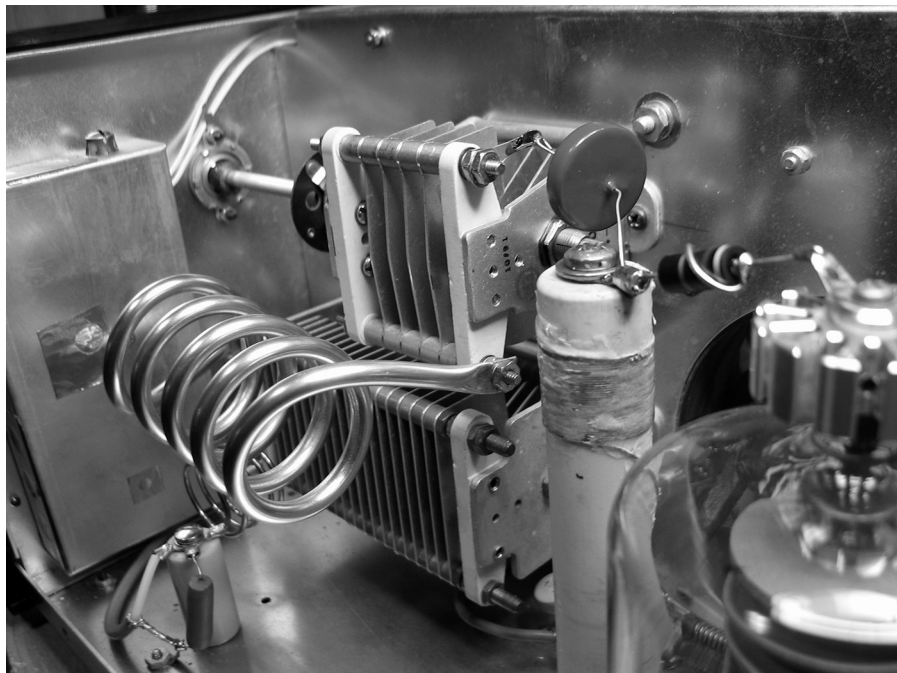


Figure 4 —Your finished modifications should resemble the parts placement seen in this view.

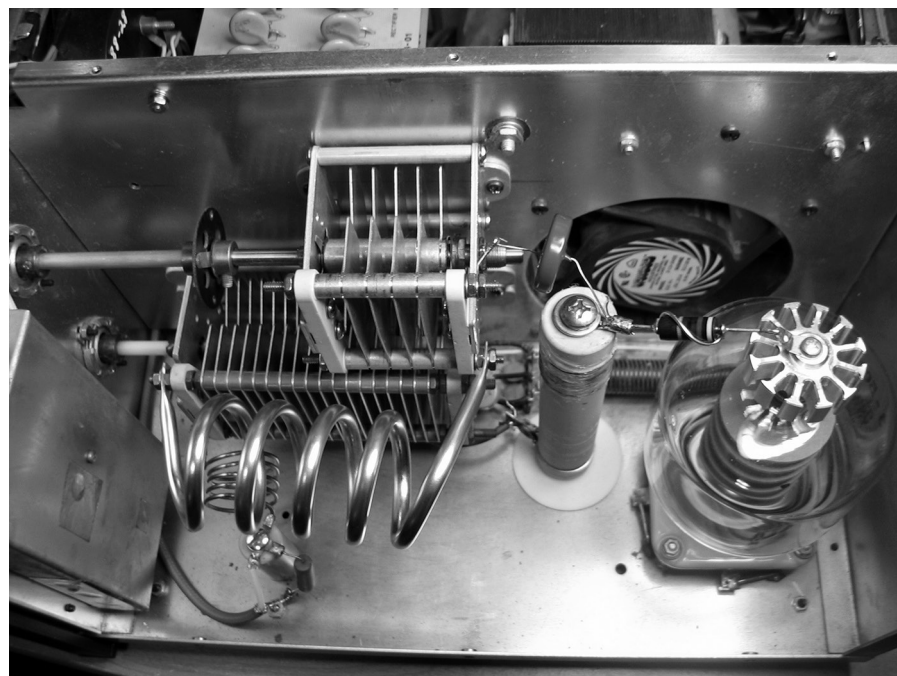


Figure 5 — Another internal view of the finished converted amplifier.

verified that it is clean and without distortion. I noted the following PLATE and LOAD front panel capacitor settings,

- 50 MHz: PLATE at the two o'clock position, LOAD at 7.0,
- 54 MHz: PLATE at the three o'clock position, LOAD at 8.0.

The original Eimac 3-500Z that came with my Heathkit was 27 years old and showed the dreaded gassy blue halo on first power up. I replaced it with a new 3-500ZG graphite tube. I also wanted the new tube to run as cool as possible, so I purchased a Hyper Plate Cap from 73CNC.⁷ As a precaution, I also replaced the eight 210 µF 450 V dc electrolytic capacitors, C401 – C408, on the high voltage power supply board. It was an expensive replacement but I felt it was good insurance considering the age of the original capacitors.

If you follow these instructions and layout exactly, you should not have any problems. The total cost for my conversion was about \$477, see the bill of materials in Table 1. You may not need to purchase everything I did, so you could conceivably do your conversion for a much lower cost.

Safety Note: please keep in mind that there is 3,000 V dc at the power supply and the tube plate circuit. *Contact could be lethal*, so please use caution, and NEVER turn on the amplifier with the cover completely off and with the ac interlock defeated.

Conclusion

This conversion took me many months and several iterations to complete successfully. The amplifier operates at a calculated efficiency of 45%. This was a low-cost and fun project for me, and I'm happy with the 650 W RF output. That's more than 8 dB advantage over my original 100 W.

If you have an old Heathkit SB-1000 sleeping in your closet, wake it up and give it new life! Good luck and I hope to work you on the Magic Band!

I extend my thanks to the hams whose great advice helped me with this project, and especially to Terry Osborn, K8SMC, Bob Unetich, K3NSC, Mike Penkas, WA8EBM, and John Nogan, AB5Q.

Ron Berry, WB3LHD, holds an Amateur Extra class license. He graduated from electronic school in 1969 with a degree in electronics technology. He has been an electronic technician for 47 years working in the TV broadcast industry for ITS Corporation, ADC Telecommunications and Axcera LLC, in Engineering and in the test department



Figure 6 — Front panel of the modified Heathkit amplifier.

performing transmitter final calibration. Ron is now semi-retired working at GigaHertz, LLC in the Engineering Department as an RF Engineering Technician. He is President of the GigaHertz Radio Club, K3ITS.

Ron's main interest is working DX using CW, SSB, RTTY, and other digital modes. He is on the DXCC Honor Roll and needs just 3 entities to achieve DXCC #1. Ron has been a ham and ARRL member for 38 years, and a member of INDEXA and SMIRK. Two of his most memorable events were visiting ARRL headquarters in 1994, and operating RTTY from his home station as W1AW/3 in the 2014 ARRL Centennial Celebration.

Notes

¹Maidenhead Locator System, see www.arrl.org/grid-squares.

²The ARRL Handbook, 2016 Edition, Available from your ARRL dealer or the ARRL bookstore, ARRL item number 0413 or 0420. Telephone 860-594-0355, or toll free in the US 888-277-5289; www.arll.org/shop; pubsales@arll.org.

³Heathkit SB-1000 manual and schematic, www.vintage-radio.info/heathkit.

⁴See home.sandiego.edu/~ekim/e194rfs01/jwmatcher/matcher2.html.

⁵PI-EL output matching designer www.tonnesoftware.com/piel.html.

⁶Silver plating solution from, www.medallioncare.com.

⁷73CNC, see www.73cnc.com/default.asp.

Down East Microwave Inc.

We are your #1 source for 50MHz to 10GHz components, kits and assemblies for all your amateur radio and Satellite projects.

Transverters & Down Converters, Linear power amplifiers, Low Noise preamps, coaxial components, hybrid power modules, relays, GaAsFET, PHEMT's, & FET's, MMIC's, mixers, chip components, and other hard to find items for small signal and low noise applications.

We can interface our transverters with most radios.

Please call, write or see our web site www.downeastmicrowave.com for our Catalog, detailed Product descriptions and interfacing details.

Down East Microwave Inc.
19519 78th Terrace
Live Oak, FL 32060 USA
Tel. (386) 364-5529

Open Source Soft-Decision Decoder for the JT65 (63,12) Reed-Solomon Code

Under-the-hood description of the JT65 decoding procedure, including a wholly new algorithm for its powerful error-correcting code.

1 — Background and Motivation

The JT65 protocol has revolutionized amateur-radio weak-signal communication by enabling operators with small or compromise antennas and relatively low-power transmitters to communicate over propagation paths not usable with traditional technologies. The protocol was developed in 2003 for Earth-Moon-Earth (EME, or “moonbounce”) communication, where the scattered return signals are always weak.¹ It was soon found that JT65 also enables worldwide communication on the HF bands with low power, modest antennas, and efficient spectral usage. Thousands of amateurs now use JT65 on a regular basis, making contacts on all bands from 160 meters through microwaves.

JT65 uses timed transmitting and receiving sequences one minute long. Messages are short and structured so as to streamline minimal exchanges between two amateur operators over potentially difficult radio paths. Most messages contain two callsigns and a grid locator, signal report, acknowledgment, or sign-off; one of the tokens CQ, QRZ, or DE may be substituted for the first callsign. Alternatively, a message may contain up to 13 characters of arbitrary text. All messages are efficiently compressed into exactly 72 bits of digital information. It should be obvious that the JT65 protocol is intended for the basic purpose of completing legitimate, documented two-way contacts,

but not for extended conversations. Full details of the message structure and encoding procedure were presented in an earlier publication.¹ For a concise description of the overall process of transmitting and receiving a JT65 message, see the accompanying sidebar *JT65 Message Processing*.

A major reason for the success and popularity of JT65 is its use of a strong error-correction code. Before transmission, each 72-bit message is divided into 12 six-bit *symbols* and augmented with 51 additional symbols of error-correcting information. These 51 *parity symbols* are computed according to information-theory rules that maximize the probability of correctly decoding the message, even if many symbols are received incorrectly. The JT65 code is properly described as a short block-length, low-rate Reed-Solomon code based on a 64-symbol *alphabet*. Characters in this alphabet are mapped onto 64 different frequencies for transmission.

Reed Solomon codes are widely used to ensure reliability in data transmission and storage. In hardware implementations, decoding is generally accomplished with a procedure such as the Berlekamp-Massey (BM) algorithm, based on *hard decisions* for each of the symbol values received. *Soft*

decisions are potentially more powerful, however. For each received JT65 symbol we can estimate not only the value most likely to be correct, but also the second, third, etc., most likely. Most importantly, we can also estimate the probability that each of those possible values is the correct one. Decoders that make use of such information are called *soft-decision decoders*.

Until now, nearly all programs implementing JT65 have used the patented Kötter-Vardy (KV) algebraic soft-decision decoder, licensed to and implemented by K1JT as a closed-source executable for use only in amateur radio applications.² Since 2001 the KV decoder has been considered the best known soft-decision decoder for Reed Solomon codes.

We describe here a new open-source alternative called the Franke-Taylor (FT, or K9AN-K1JT) soft-decision decoding algorithm. It is conceptually simple, built on top of the BM hard-decision decoder, and in this application it performs even better than the KV decoder. The FT algorithm is implemented in the popular programs *WSJT*, *MAP65*, and *WSJT-X*, widely used for amateur weak-signal communication using JT65 and other specialized digital protocols. These programs are open-source, freely available, and licensed under the GNU General Public License.³

The JT65 protocol specifies transmissions

¹Notes appear on page 17

that start one second into a UTC minute and last for 46.8 seconds. Receiving software therefore has more than ten seconds to decode a message before the start of the next minute, when the operator will send a reply. With today's personal computers, this relatively long time encourages experimentation with decoders of high computational complexity. With time to spare, the FT algorithm lowers the decoding threshold on a typical fading channel by many decibels over the hard-decision BM decoder, and by a meaningful amount over the KV decoder. In addition to its excellent performance, the new algorithm has other desirable properties, not least of which is its conceptual simplicity. Decoding performance and computational complexity scale in a convenient way, providing steadily increasing soft-decision decoding gain as a tunable parameter is increased over more than five orders of magnitude. Appreciable gain is available from our decoder even on very simple (and relatively slow) computers. On the other hand, because the algorithm benefits from a large number of independent decoding trials, further performance gains should be achievable through parallelization on high-performance computers.

The remainder of this paper is organized as follows. Section 2 presents a brief overview of the nature of Reed Solomon codes and their error-correcting capabilities. Section 3 provides statistical motivation for the FT algorithm, and Section 4 describes the algorithm in full detail. Material in these two sections is important because it documents our approach and underlines its fundamental technical contributions. These sections are heavier in formal mathematics than common in *QEX*; for this reason, some readers may choose to skip or skim them and proceed more quickly to the results. Most readers will benefit by reviewing the original paper on the JT65 protocol.¹ A procedure for *hinted decoding* — determining which one, if any, of a list of likely messages matches the one that was received — is outlined in Section 5. Finally, in Section 6 we present performance measurements of the FT and hinted decoding algorithms and make explicit comparisons to the BM and KV decoders familiar to users of older versions of *WSJT*, *MAP65* and *WSJT-X*. Section 7 summarizes some on-the-air experiences with the new decoder. Refer to the sidebar *Glossary of Specialized Terms* for brief definitions of some potentially unfamiliar language.

2 — JT65 Messages and Reed Solomon Codes

The JT65 message frame consists of a short, compressed 72-bit message encoded for transmission with a Reed-Solomon code. Reed-Solomon codes are *block*

codes characterized by n , the length of their *codewords*; k , the number of message symbols conveyed by the codeword; and the transmission alphabet, or number of possible values for each symbol in a codeword. The codeword length and the number of message symbols are specified with the notation (n, k) . JT65 uses a (63,12) Reed-Solomon code with an alphabet of 64 possible values for each symbol. Each of the 12 message symbols represents $\log_2 64 = 6$ message bits. The source-encoded message conveyed by a 63-symbol JT65 frame thus consists of 72 information bits. The JT65 code is *systematic*, which means that the 12 message symbols are embedded in the codeword without modification and another 51 parity symbols derived from the message symbols are added to form a codeword of 63 symbols.

In coding theory the concept of *Hamming distance* is used as a measure of disagreement between different codewords, or between a received word and a codeword. Hamming distance is the number of code symbols that differ in two words being compared. Reed-Solomon codes have guaranteed minimum Hamming distance d , where

$$d = n - k + 1. \quad (1)$$

With $n = 63$ and $k = 12$ the minimum Hamming distance of the JT65 code is $d = 52$. With 72 information bits in each message, JT65 can transmit any one of $2^{72} \approx 4.7 \times 10^{21}$ possible messages. The codeword for any message differs from every other codeword in at least 52 of the 63 symbol positions.

A received word containing some *errors* (incorrect symbols) can be decoded into the correct codeword using a deterministic, algebraic algorithm provided that no more than t symbols were received incorrectly, where

$$t = \left\lfloor \frac{n-k}{2} \right\rfloor. \quad (2)$$

For the JT65 code $t = 25$, so it is always possible to decode a received word having 25 or fewer symbol errors. Any one of several well-known algebraic algorithms, such as the BM algorithm, can carry out this hard-decision decoding. Two steps are necessarily involved in this process. We must (1) determine which symbols were received incorrectly, and (2) find the correct value of the incorrect symbols. If we somehow know that certain symbols are incorrect, that information can be used to reduce the work involved in step (1) and allow step (2) to correct more than t errors. In the unlikely event that the location of every error is known, and if no correct symbols are accidentally labeled as errors, the BM

algorithm can correct up to $d - 1 = n - k$ errors.

The FT algorithm creates lists of symbols suspected of being incorrect and sends them to the BM decoder. Symbols flagged in this way are called *erasures*. With perfect erasure information up to $n - k = 51$ incorrect symbols can be corrected for the JT65 code. Imperfect erasure information means that some erased symbols may be correct, and some other symbols in error. If s symbols are erased and the remaining $n - s$ symbols contain e errors, the BM algorithm can find the correct codeword as long as

$$s + 2e \leq d - 1. \quad (3)$$

If $s = 0$, the decoder is said to be an *errors-only* decoder. If $0 < s \leq d - 1$, the decoder is called an *errors-and-erasures* decoder. The possibility of doing errors-and-erasures decoding lies at the heart of the FT algorithm. On that foundation we have built a capability for using soft information on the reliability of individual symbol values, thereby producing a soft-decision decoder.

3 — Statistical Framework

The FT algorithm uses the estimated quality of received symbols to generate lists of symbols considered likely to be in error, thus enabling decoding of received words with more than 25 errors. Algorithms of this type are generally called *reliability-based* or *probabilistic* decoding methods.⁴ Such algorithms involve some amount of educated guessing about which received symbols are in error or, alternatively, about which received symbols are correct. The guesses are informed by quality metrics associated with the received symbols. To illustrate why it is absolutely essential to use such soft-symbol information in these algorithms it helps to consider what would happen if we tried to use completely random guesses, ignoring any available soft-symbol information.

As a specific example, consider a received JT65 word with 23 correct symbols and 40 errors. We do not know which symbols are in error. Suppose that the decoder randomly selects $s = 40$ symbols for erasure, leaving 23 unerased symbols. According to Eq. (3), the BM decoder can successfully decode this word as long as e , the number of errors present in the 23 unerased symbols, is 5 or less. The number of errors captured in the set of 40 erased symbols must therefore be at least 35.

The probability of selecting some particular number of incorrect symbols in a randomly selected subset of received symbols is governed by the hypergeometric probability distribution. Let us define N as the number of symbols from which erasures will be selected, X as the number of incorrect

symbols in the set of N symbols, and x as the number of errors in the symbols actually erased. In an ensemble of many received words X and x will be random variables, but for this example we will assume that X is known and that only x is random. The conditional probability mass function for x with stated values of N , X , and s may be written as

$$P(x = \varepsilon | N, X, s) = \frac{\binom{X}{\varepsilon} \binom{N-X}{s-\varepsilon}}{\binom{N}{s}} \quad (4)$$

where $\binom{n}{k} = \frac{n!}{k!(n-k)!}$ is the binomial coefficient. The binomial coefficient can be calculated using the function `nchoosek(n, k)` in the numerical computing language *GNU Octave*, or with one of many free online calculators. The hypergeometric probability mass function defined in Eq. (4) is available in *GNU Octave* as function `hygepdf(x, N, X, s)`. The cumulative probability that at least ε errors are captured in a subset of s erased symbols selected from a group of N symbols containing X errors is

$$P(x \geq \varepsilon | N, X, s) = \sum_{j=\varepsilon}^s P(x = j | N, X, s). \quad (5)$$

Example 1:

Suppose a received word contains $X = 40$ incorrect symbols. In an attempt to decode using an errors-and-erasures decoder, $s = 40$ symbols are randomly selected for erasure from the full set of $N = n = 63$ symbols. The probability that $x = 35$ of the erased symbols are actually incorrect is then

$$P(x = 35) = \frac{\binom{40}{35} \binom{63-40}{40-35}}{\binom{63}{40}} \approx 2.4 \times 10^{-7}$$

Similarly, the probability that $x = 36$ of the erased symbols are incorrect is $P(x = 36) \approx 8.6 \times 10^{-9}$. Since the probability of erasing 36 errors is so much smaller than that for erasing 35 errors, we may safely conclude that the probability of randomly choosing an erasure vector that can decode the received word is approximately $P(x = 35) \approx 2.4 \times 10^{-7}$. The odds of producing a valid codeword on the first try are very poor, about 1 in 4 million.

Example 2:

How might we best choose the number of symbols to erase, in order to maximize the probability of successful decoding? By

exhaustive search over all possible values up to $s = 51$, it turns out that for $X = 40$ the best strategy is to erase $s = 45$ symbols. According to Eq. (3), with $s = 45$ and $d = 52$ then e must be 3 or less. Decoding will be assured if the set of erased symbols contains at least $40 - 3 = 37$ errors. With $N = 63$, $X = 40$, and $s = 45$, the probability of successful decode in a single try is $P(x \geq 37) \approx 1.9 \times 10^{-6}$. This probability is about 8 times higher than the probability of success when only 40 symbols were erased. Nevertheless, the odds of successfully decoding on the first try are still only about 1 in 500,000.

Example 3:

Examples 1 and 2 show that a random strategy for selecting symbols to erase is unlikely to be successful unless we are prepared to wait a long time for an answer. So let's modify the strategy to tip the odds in our favor. Let the received word contain $X = 40$ incorrect symbols, as before, but suppose we know that 10 received symbols are significantly more reliable than the other 53. We might therefore protect the 10 most reliable symbols and select erasures from the smaller set of $N = 53$ less reliable ones. If $s = 45$ symbols are chosen randomly for erasure in this way, it is still necessary for the erased symbols to include at least 37 errors, as in Example 2. However, the probabilities are now much more favorable: with $N = 53$, $X = 40$, and $s = 45$, Eq. (5) yields $P(x \geq 37) \approx 0.016$. Even better odds are obtained by choosing $s = 47$, which requires $x \geq 38$. With $N = 53$, $X = 40$, and $s = 47$, $P(x \geq 38) \approx 0.027$. The odds for producing a codeword on the first try are now about 1 in 38. A few hundred independently randomized tries would be enough to all-but-guarantee production of a valid codeword by the BM decoder.

4 — The Franke-Taylor Decoding Algorithm

Example 3 shows how statistical information about symbol quality should make it possible to decode received frames having a large number of errors. In practice the number of errors in the received word is unknown, so our algorithm simply assigns a high erasure probability to low-quality symbols and relatively low probability to high-quality symbols. As illustrated by Example 3, a good choice of erasure probabilities can increase the chance of producing a codeword by many orders of magnitude. Once erasure probabilities have been assigned to each of the 63 received symbols, the FT algorithm uses a random number generator to decide whether or not to erase each symbol, according to its assigned erasure probability. The list of

erased symbols is then submitted to the BM decoder, which produces either a codeword or a flag indicating failure to decode.

The process of selecting the list of symbols to erase and calling the BM decoder comprises one cycle of the FT algorithm. The next cycle proceeds with a new selection of erased symbols. At this stage we must treat any codeword obtained by errors-and-erasures decoding as no more than a *candidate*. Our next task is to find a metric that can reliably select one of many proffered candidates as the codeword that was actually transmitted.

The FT algorithm uses quality indices made available by a noncoherent 64-FSK demodulator (see the sidebar *JT65 Message Processing*). The demodulator computes binned power spectra for each signaling interval; the result is a two-dimensional array $S(i, j)$, where the frequency index i assumes values 0 to 63 and the symbol index j has values 1 to 63. The most likely value for each symbol is taken as the frequency bin with largest signal-plus-noise power over all values of i . The fractions of total power in the two bins containing the largest and second-largest powers, denoted respectively by p_1 and p_2 , are computed for each symbol and passed from demodulator to decoder as soft-symbol information. The FT decoder derives two metrics from p_1 and p_2 , namely p_1 -rank (the rank $\{1, 2, \dots, 63\}$ of the symbol's fractional power $p_{1,j}$ in a sorted list of p_1 values) and the ratio p_2/p_1 . High ranking symbols have larger signal-to-noise ratio than those with lower rank. When p_2/p_1 is close to 1, the most likely symbol value is only slightly more reliable than the second most likely one.

We use 3-bit quantization of the metrics p_1 -rank and p_2/p_1 to index the entries in an 8×8 table of symbol error probabilities. The probabilities were derived empirically from a large data set of received words that were successfully decoded. The table provides an estimate of the *a priori* probability of symbol error based on the metrics p_1 -rank and p_2/p_1 . This table is a key element of the algorithm, as it determines which symbols are effectively protected from erasure. The *a priori* symbol error probabilities are close to 1 for low-quality symbols and close to 0 for high-quality symbols. Recall from Examples 2 and 3 that candidate codewords are produced with higher probability when the number of erased symbols is larger than the number of incorrect symbols. Correspondingly, the FT algorithm works best when the probability of erasing a symbol is somewhat larger than the probability that the symbol is incorrect. For the JT65 code we found empirically that good decoding performance is obtained when the symbol erasure probability is about 1.3 times the

symbol error probability.

The FT algorithm tries successively to decode the received word using independent educated guesses to select symbols for erasure. For each iteration a stochastic erasure vector is generated based on the symbol erasure probabilities. The erasure vector is sent to the BM decoder along with the full set of 63 hard-decision symbol values. When the BM decoder finds a candidate codeword it is assigned a quality metric d_s , the *soft distance* between the received word and the codeword:

$$d_s = \sum_{j=1}^n \alpha_j (1 + p_{1,j}). \quad (6)$$

Here $\alpha_j = 0$ if received symbol j is the same as the corresponding symbol in the codeword, $\alpha_j = 1$ if the received symbol and codeword symbol are different, and $p_{1,j}$ is the fractional power associated with received symbol j . Think of the soft distance as made up of two terms: the first is the Hamming distance between the received word and the codeword, and the second ensures that if two candidate codewords have the same Hamming distance from the received word, a smaller soft distance will be assigned to the one where differences occur in symbols of lower estimated reliability.

In practice we find that d_s can reliably identify the correct codeword if the signal-to-noise ratio for individual symbols is greater than about 4 in linear power units. We also find that significantly weaker signals can be decoded by using soft-symbol information beyond that contained in p_1 and p_2 . To this end we define an additional metric u , the average signal-plus-noise power in all received symbols according to a candidate codeword's symbol values:

$$u = \frac{1}{n} \sum_{j=1}^n S(c_j, j). \quad (7)$$

Here the c_j 's are the symbol values for the candidate codeword being tested.

The correct JT65 codeword produces a value for u equal to the average of $n = 63$ bins containing both signal and noise power. Incorrect codewords have at most $k - 1 = 11$ such bins and at least $n - k + 1 = 52$ bins containing noise only. Thus, if the spectral array $S(i, j)$ has been normalized so that the average value of the noise-only bins is unity, u for the correct codeword has expectation value (average over many random realizations) given by

$$\bar{u}_c = 1 + y, \quad (8)$$

where y is the signal-to-noise ratio in linear power units. If we assume Gaussian statistics

and a large number of trials, the standard deviation of measured values of u is

$$\sigma_c = \left(\frac{1 + 2y}{n} \right)^{1/2}. \quad (9)$$

In contrast, the expected value and standard deviation of the u -metric for an incorrect codeword (randomly selected from a population of all "worst case" codewords, *i.e.*, those with $k - 1$ symbols identical to corresponding ones in the correct word) are given by

$$\bar{u}_i = 1 + \left(\frac{k - 1}{n} \right) y, \quad (10)$$

$$\sigma_i = \frac{1}{n} [n + 2y(k - 1)]^{1/2}, \quad (11)$$

where the subscript i is an abbreviation for "incorrect".

If u is evaluated for a large number of distinct candidate codewords, one of which is correct, we should expect the largest value u_1 to be drawn from a population with statistics described by \bar{u}_c and σ_c . If no tested codeword is correct, u_1 is likely to come from the (\bar{u}_i, σ_i) population and to be several standard deviations above the mean. In either case the second-largest value, u_2 , will likely come from the (\bar{u}_i, σ_i) population, again several standard deviations above the mean. If the signal-to-noise ratio y is too small for decoding to be possible or the correct codeword is never presented as a candidate, the ratio $r = u_2/u_1$ will likely be close to 1. On the other hand, correctly identified codewords will produce u_1 significantly larger than u_2 and thus smaller values of r . We therefore apply a ratio threshold test, say $r < R_1$, to identify codewords with high probability of being correct. As described in Section 6, we use simulations to set an empirical acceptance threshold R_1 that maximizes the probability of correct decodes while ensuring a low rate of false positives.

As with all decoding algorithms that generate a list of possible codewords, a stopping criterion is necessary. FT accepts a codeword unconditionally if the Hamming distance X and soft distance d_s obey specified criteria $X < X_0$ and $d_s < D_0$. Secondary acceptance criteria $d_s < D_1$ and $r < R_1$ are used to validate additional codewords that fail the first test. A timeout is used to limit execution time if no acceptable codeword is found in a reasonable number of trials, T . Today's personal computers are fast enough that T can be set as large as 10^5 , or even higher. Pseudo-code for the FT algorithm is presented in an accompanying box, **Algorithm 1**.

Inspiration for the FT decoding algorithm came from a number of sources.^{4,5,6} After developing this algorithm, we became aware

that our approach is conceptually similar to a stochastic, erasures-only list decoding algorithm described in another reference.⁷ That algorithm is applied to higher-rate Reed-Solomon codes on a symmetric channel using binary phase-shift keying (BPSK). Our 64-ary input channel with 64-FSK modulation required us to develop unique methods for assigning erasure probabilities and for defining acceptance criteria to select the best codeword from the list of tested candidates.

5 — Hinted Decoding

The FT algorithm is completely general. With equal sensitivity it can recover any one of the $2^{72} \approx 4.7 \times 10^{21}$ different messages that can be transmitted with the JT65 protocol. In some circumstances it's easy to imagine a *much* smaller list of messages (say, a few thousand messages or less) that would be among the most likely ones to be received. One such favorable situation exists when making short Amateur Radio contacts that exchange minimal information including callsigns, signal reports, perhaps Maidenhead locators, and acknowledgments. On the EME path or a VHF or UHF band with limited geographical coverage, the most common received messages frequently originate from callsigns that have been decoded before. Saving a list of previously decoded callsigns and associated locators makes it easy to generate a list of hypothetical messages and their corresponding codewords at very little computational expense. The resulting candidate codewords can be tested in almost the same way as those generated by the probabilistic method described in Section 4. We call this approach "hinted decoding;" it is sometimes referred to as the *Deep Search* algorithm. In certain limited situations it can provide enhanced sensitivity for the principal task of any decoder, namely to determine precisely what message was sent.

For hinted decoding we again invoke a ratio threshold test, but in this case we use it to answer a more limited question. Over the full list of messages considered likely, we want to know whether a suitable metric can distinguish with confidence between the one correct codeword and all others in the generated list — or, alternatively, to determine that the correct codeword is *not* contained in the list. We again find that the most effective metric involves a comparison of u_1 and u_2 , the largest and second-largest values of total signal-plus-noise power among all the tested codewords. The criterion for comparison is chosen empirically to maximize the number of correct decodes while ensuring that false decodes are rare. Because tested candidate codewords are drawn from a list typically no longer than a few thousand entries, rather

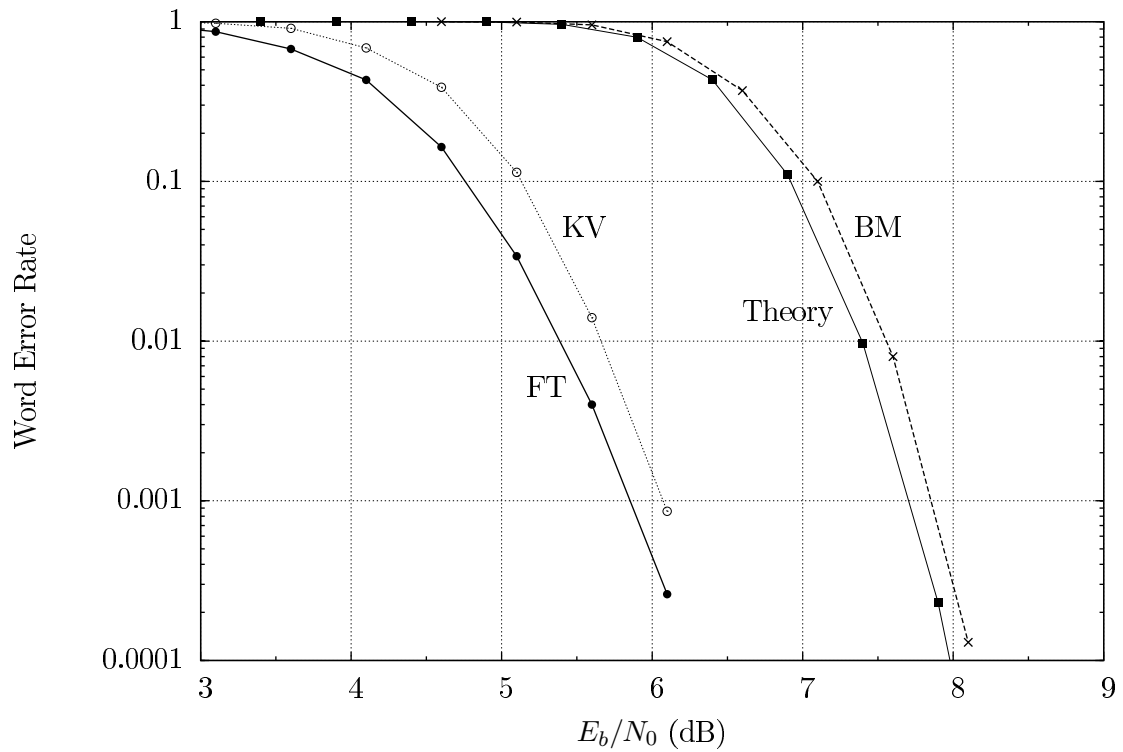


Figure 1 — Word error rates as a function of E_b/N_0 , the signal-to-noise ratio per information bit. The curve labeled 'Theory' shows a theoretical prediction for the hard-decision BM decoder. Remaining curves represent simulation results on an AWGN channel for the BM, KV, and FT decoders. The KV algorithm was executed with complexity coefficient $\lambda = 15$, the most aggressive setting historically used in the *WSJT* programs. The FT algorithm used timeout setting $T = 10^5$.

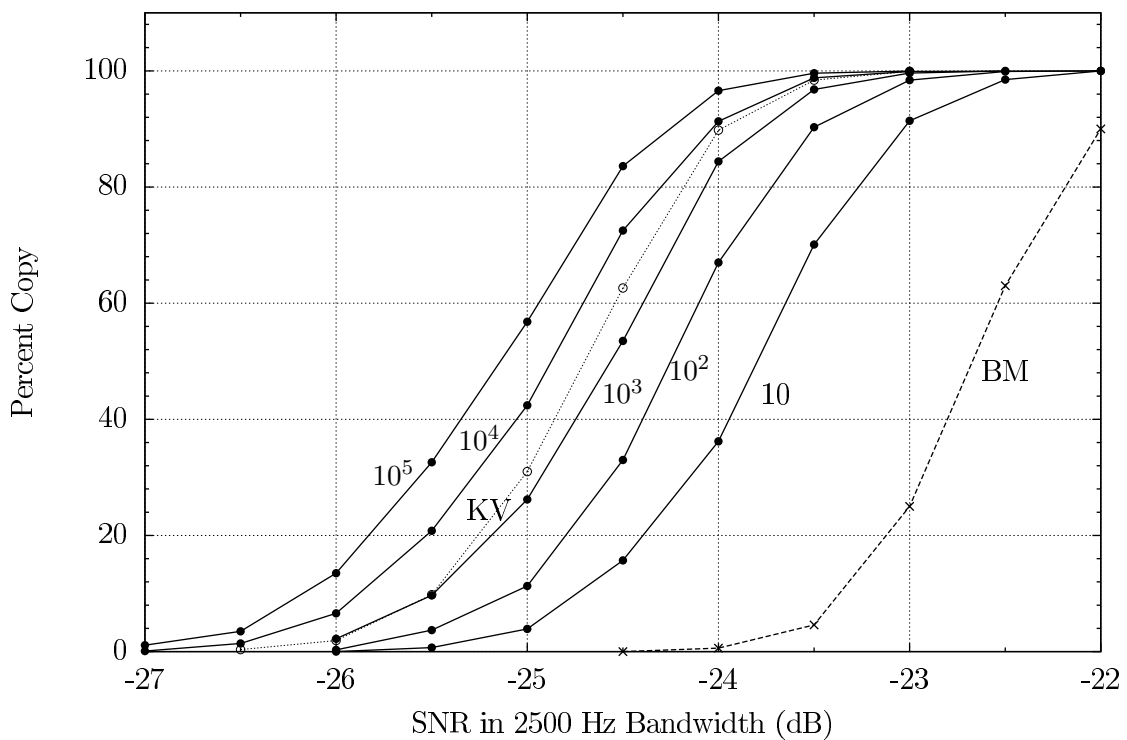


Figure 2 — Percent of JT65 messages copied as a function of SNR_{2500} , assuming additive white Gaussian noise and no fading. Numbers adjacent to curves specify values of timeout parameter for the FT decoder. Open circles and dotted line show results for the KV decoder with complexity coefficient $\lambda = 15$. Results for the BM algorithm are plotted with crosses and dashed line.

than 2^{72} , the limit can be more relaxed than that used in the FT algorithm. Thus, for the limited subset of messages suggested by previous experience to be likely, hinted decodes can be obtained at lower signal levels than required for the full universe of 2^{72} possible messages. Pseudo-code for the hinted-decoding algorithm is presented as **Algorithm 2**.

6 — Decoder Performance Evaluation

Comparisons of decoding performance are usually presented in the professional literature as plots of word error rate versus E_b / N_0 , the ratio of the energy collected per information bit to the one-sided noise power spectral density. For weak-signal Amateur Radio work, performance is more usefully presented as the probability of successfully decoding a received word plotted against SNR_{2500} , the signal-to-noise ratio in a 2500 Hz reference bandwidth. The relationship between E_b / N_0 and SNR_{2500} is described in Appendix A. Examples of both types of plot are included in the following discussion, where we describe simulations carried out to compare performance of the FT algorithm and hinted decoding with other algorithms and with theoretical expectations. We have also used simulations to establish suitable default values for the acceptance parameters X_0 , D_0 , D_1 , R_1 , and R_2 .

6.1 — Simulated results on the AWGN channel

Results of simulations using the BM, KV, and FT decoding algorithms on the JT65 code are presented in terms of word error rate versus E_b / N_0 in Figure 1. For these tests we generated at least 1000 signals at each signal-to-noise ratio, assuming the additive white Gaussian noise (AWGN) channel, and we processed the data using each algorithm. For word error rates less than 0.1 it was necessary to process 10,000 or even 100,000 simulated signals in order to capture enough errors to make the measurements statistically meaningful. As a test of the fidelity of our numerical simulations, Figure 1 also shows results calculated from theoretical probability distributions for comparison with the BM results. The simulated BM results agree with theory to within about 0.1 dB. The differences are caused by small errors in the estimates of time and frequency offset of the received signal in the simulated data. Such “sync losses” are not accounted for in the idealized theoretical results.

As expected, on the AWGN channel the soft-decision algorithms FT and KV are about 2 dB better than the hard-decision BM algorithm. In addition, FT has an edge over KV that increases from about 0.2 dB at

higher SNRs to nearly 0.5 dB at low SNR. With timeout parameter $T = 10^5$ execution time for FT is longer than that for the KV algorithm, but still small enough to be fully practical on today’s home computers.

Error-free transmission is important in commercial applications, so plots like Figure 1 are often extended downward to error rates of 10^{-6} or even less. The circumstances for minimal Amateur Radio contacts are very different, however. Decoding failure rates of order 0.1 or higher may be perfectly acceptable: they simply require repeat transmissions. In such circumstances the essential information is more usefully presented in a plot showing the percentage of transmissions copied correctly as a function of signal-to-noise ratio. Figure 2 shows the FT and KV results from Figure 1 in this format, along with additional FT results for $T = 10^4$, 10^3 , 10^2 and 10. It’s easy to see that the FT decoder produces more decodes than KV when T is greater than about 3000. As already noted in connection with Figure 1, FT with $T = 10^5$ has approximately 0.5 dB gain over KV at low SNR. It also provides very significant gains over the hard-decision BM decoder, even when limited to very small T .

Parameter T in the FT algorithm is the maximum number of symbol-erasure trials allowed for a particular attempt at decoding a received word. Most successful decodes take only a small fraction of the maximum allowed number of trials. Figure 3 shows the number of stochastic erasure trials required to find the correct codeword plotted as a function of X , the number of hard-decision errors in the received word. This test run used 1000 simulated transmissions at $SNR_{2500} = -24$ dB, just slightly above the decoding threshold, with timeout parameter $T = 10^5$. No points are shown for $X \leq 25$ because all such words are successfully decoded by a single run of the errors-only BM algorithm. Figure 3 shows that the FT algorithm decodes received words with as many as $X = 43$ symbol errors. It also shows that the average number of trials increases with the number of errors in the received word. The variability of decoding time also increases dramatically with the number of errors in the received word. These results provide insight into the mean and variance of execution time for the FT algorithm, since execution time is roughly proportional to the number of required erasure trials.

6.2 — Simulated results for Rayleigh fading and hinted decoding

Figure 4 presents the results of simulations for signal-to-noise ratios ranging from -18 to -30 dB, again using 1000 simulated signals for each plotted point. We include three curves for each decoding algorithm: one for the AWGN channel and no fading, and two

more for simulated Doppler spreads of 0.2 and 1.0 Hz. These simulated Doppler spreads are comparable to those encountered on HF ionospheric paths and also for EME at VHF and the lower UHF bands. For comparison we note that the JT65 symbol rate is about 2.7 Hz. It is interesting to note that while Rayleigh fading severely degrades the success rate of the BM decoder, the penalties are much smaller with both FT and Deep Search (DS) decoding. Simulated Doppler spreads of 0.2 Hz actually increased the FT decoding rate slightly at SNRs close to the decoding threshold, presumably because with the low-rate JT65 code, signal peaks provide the information needed for good copy.

7 — On-the-air Experience

The JT65 protocol has proven remarkably versatile. Today the mode is used by thousands of amateurs around the world, communicating over terrestrial paths on the MF and HF bands and over terrestrial as well as EME paths from 50 MHz through 10 GHz. Three *submodes* are in use, together accommodating a wide range of Doppler spreads and potential instrumental instabilities. All three submodes transmit the 63 data symbols interspersed with 63 synchronization symbols at keying rate $11025/4096 = 2.69$ baud. Submode JT65A uses tone spacing equal to the symbol rate; its total occupied bandwidth is $66 \times 2.69 = 177.6$ Hz. Submodes B and C have tone spacings and occupied bandwidths 2 and 4 times larger. In practice JT65A is generally used at 50 MHz and below, JT65B on 144 through 432 MHz, and JT65C at 1296 MHz and above.

Figure 5 shows portions of the main window and spectrogram displays from program *WSJT-X*, illustrating replies to a CQ from K1JT on 144.118 MHz using submode JT65B on the EME path. Speckled vertical lines on the waterfall at 1494 and 1515 Hz are the synchronizing tones of signals from DL7UAE and SP6GWB. Other visible speckles (barely above the noise) up to about 1870 Hz are some of the data tones from these two stations. Two lines of decoded text show that the estimated average signal strengths were $SNR_{2500} = -23$ and -24 dB, respectively, just one or two dB above decoding threshold for the FT decoder. Note that the two signals overlap throughout more than 90% of their occupied bandwidths, yet both are decoded cleanly and without errors. Such behavior is typical of the JT65 protocol.

As another example, Figure 6 shows activity in submode JT65A during a single minute on the 20 m amateur band. At this time the band was crowded with overlapping signals. With care you can count at least 19

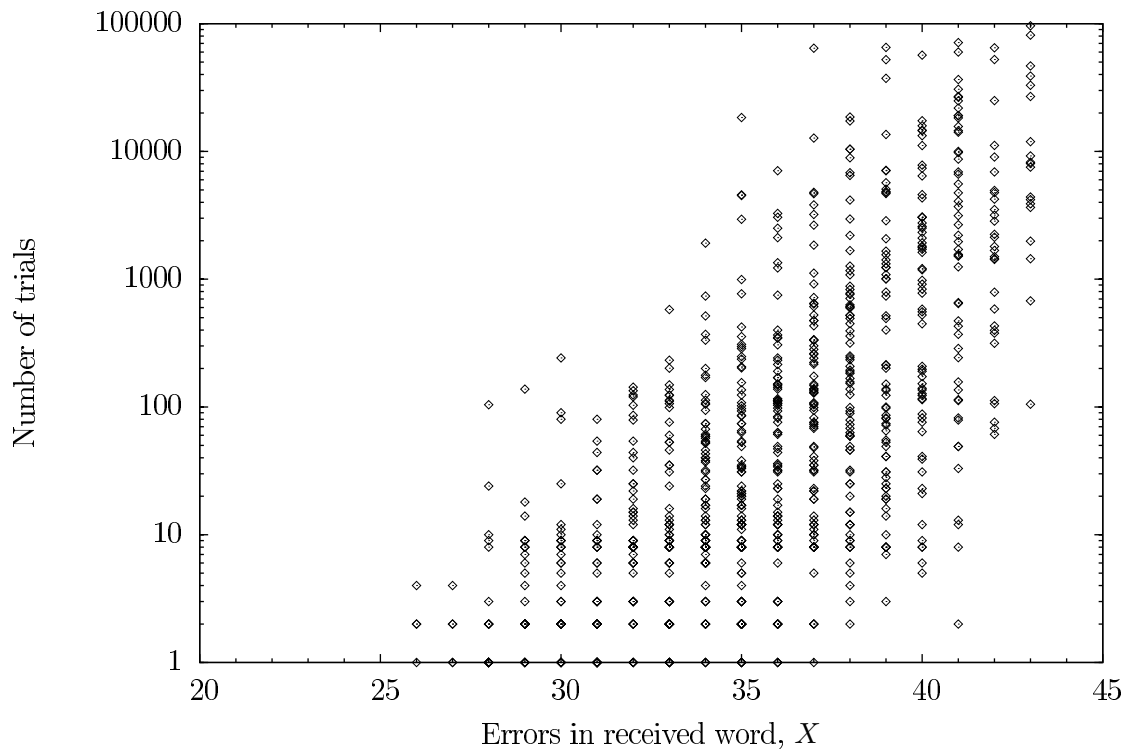


Figure 3 — Number of trials needed to decode a received word vs. Hamming distance X between received word and decoded codeword. We used 1000 simulated transmissions on an AWGN channel with no fading. The signal-to-noise ratio was $SNR_{2500} = -24$ dB, or $E_b/N_0 = 5.1$ dB.

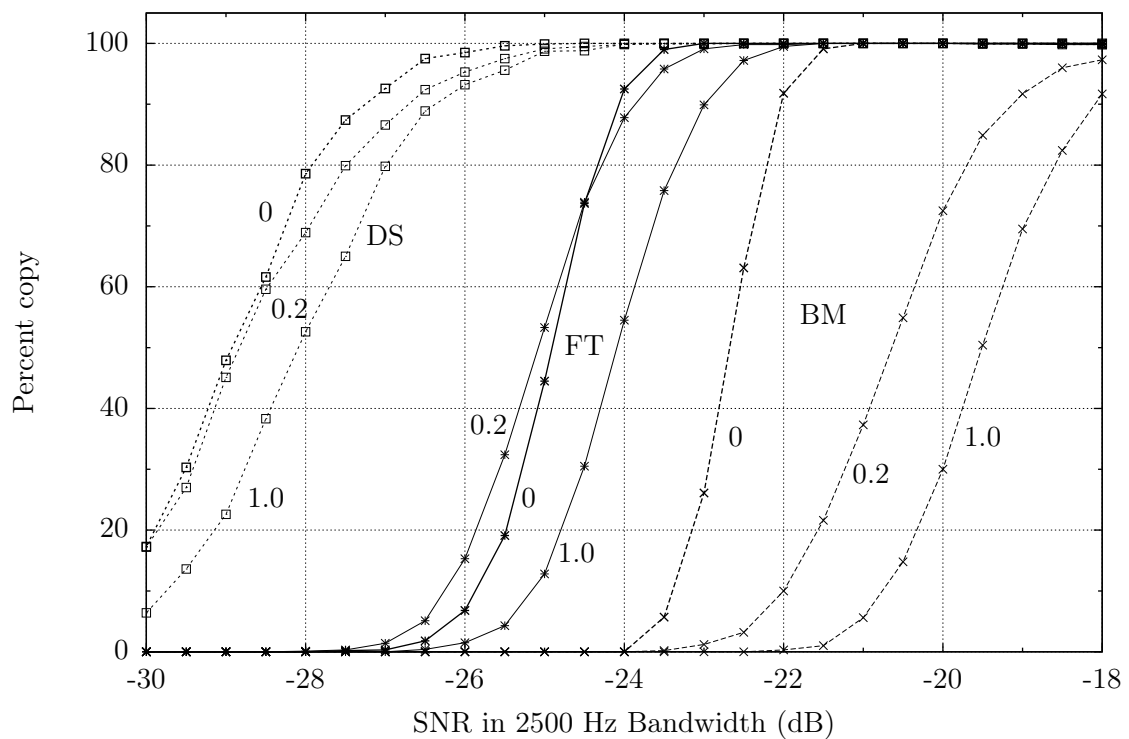


Figure 4 — Percentage of JT65 messages successfully decoded as a function of SNR_{2500} . Results are shown for the hard-decision Berlekamp-Massey (BM) and soft-decision Frank-Taylor (FT) decoding algorithms. Curves labeled 'DS' correspond to the hinted-decode (Deep Search) algorithm with a codeword list of length $L = 5850$. Numbers adjacent to the curves are simulated Doppler spreads in Hz. In the current version of *WSJT-X* the performance of the DS algorithm is limited by synchronization failures when SNR is less than about 28 dB.

distinct synchronizing tones (the speckled vertical lines in the Figure), and can see as many as four signals overlapping in some places. After signal processing to demodulate the signals and produce soft-symbol data for the FT decoder, program *WSJT-X* extracts and decodes 21 error-free messages from this recorded data segment. This result is achieved with a relatively small timeout parameter, $T = 1000$. For these results the decoder uses two successive sweeps over the spectrum. The strongest signals (12 in this example) are sequentially decoded and subtracted from the raw data after the first pass. Another 9 signals are decoded in the second pass. For comparison, the hard-decision BM decoder decodes only 12 messages from this recording (9 in the first pass and 3 more in a second).

Our implementation of the FT decoder, written in a combination of FORTRAN and C, is freely available as open-source code.⁸ For the Berlekamp-Massey part of the

algorithm we use routines written by Phil Karn, KA9Q, modified slightly so that the Reed-Solomon syndromes are computed only once in our most time-consuming loop (Steps 2 through 8, **Algorithm 1**).⁹ The FT algorithm has become an integral part of programs *WSJT*, *MAP65*, and *WSJT-X*. Improvement in sensitivity over the Kötter-Vardy decoder is small, only a few tenths of a dB, but especially on the EME path such small advantages are sometimes very important. Perhaps even more essential, programs in the *WSJT* family are now entirely open source. We no longer need to use the patented KV algorithm or the specially licensed executable program `kvasd [.exe]`.

8 — Acknowledgments

We thank Charlie Suckling, G3WDG; Bill Somerville, G4WJS; Casey Smith, KD9DSW; Edson Pereira, PY2SDR; Leif Asbrink, SM5BSZ; Rex Moncur,

VK7MO and Roger Rehr, W3SZ, for helpful comments on an earlier version of this paper.

A — Appendix: Signal to Noise Ratios

The signal to noise ratio in a bandwidth B , that is at least as large as the bandwidth occupied by the signal is:

$$SNR_B = \frac{P_s}{N_0 B} \quad (12)$$

where P_s is the average signal power (W), N_0 is one-sided noise power spectral density (W/Hz), and B is the bandwidth in Hz. In Amateur Radio applications, digital modes are often compared based on the SNR defined in a 2.5 kHz reference bandwidth, SNR_{2500} .

In the professional literature, decoder performance is characterized in terms of E_b / N_0 , the ratio of the energy collected per information bit, E_b , to the one-sided noise power spectral density, N_0 . Denote the duration of a channel symbol by τ_s (for JT65, $\tau_s = 0.3715$ s). JT65 signals have constant envelope, so the average signal power is related to the energy per symbol, E_s , by

$$P_s = E_s / \tau_s. \quad (13)$$

The total energy in a received JT65 message consisting of $n = 63$ channel symbols is $63E_s$. The energy collected for each of the 72 bits of information conveyed by the message is then

$$E_b = \frac{63E_s}{72} = 0.875E_s. \quad (14)$$

Using equations (12) – (14), SNR_{2500} can be written in terms of E_b / N_0 :

$$SNR_{2500} = 1.23 \times 10^{-3} \frac{E_b}{N_0} \quad (15)$$

If all quantities are expressed in dB, then:

$$\begin{aligned} SNR_{2500} &= (E_b / N_0)_{dB} - 29.1 \text{ dB} \\ &= (E_s / N_0)_{dB} - 29.7 \text{ dB} \end{aligned} \quad (16)$$

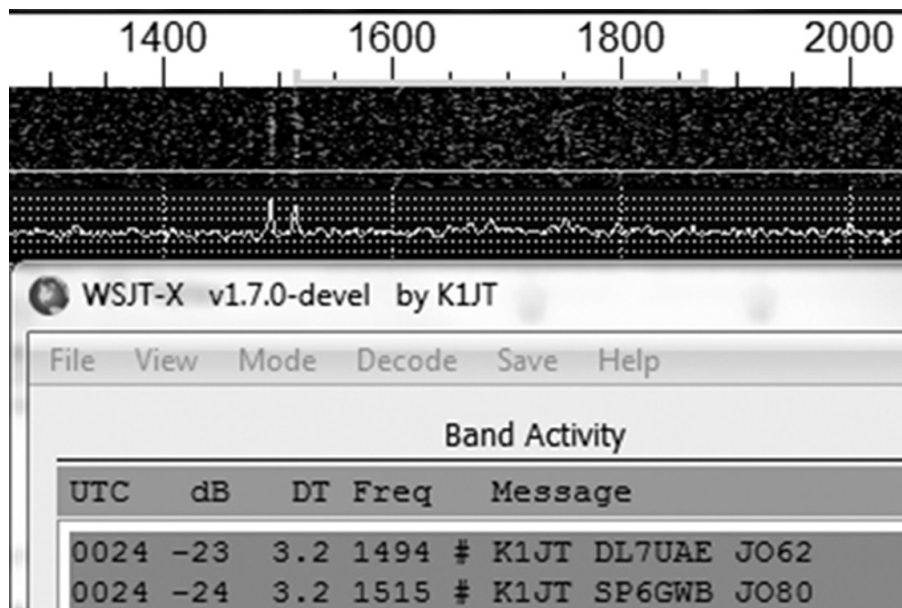


Figure 5 — Examples of JT65B EME signals recorded at K1JT. Numbers above the spectrogram are audio frequencies in Hz, and the spectrogram's vertical span is one minute of time. The horizontal green bar on the frequency axis indicates the bandwidth occupied by the second decoded signal, a reply from SP6GWB. See text for additional details.

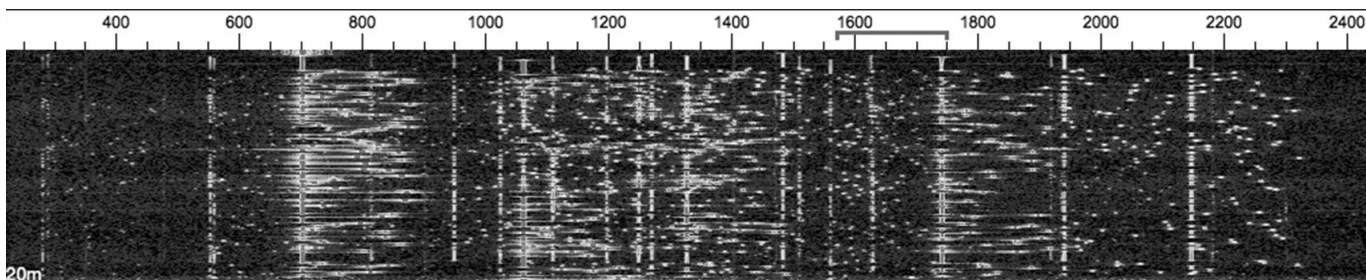


Figure 6 — Spectrogram from *WSJT-X* showing one minute of data collected under crowded band conditions on the 20 m band. Numbers on the scale are frequencies (in Hz) above 14.076 MHz.

JT65 Message Processing

1. User *A* enters or selects message consistent with formatting rules of JT65.
2. Transmitting software at *A*: compress message into 12 six-bit symbols, then add 51 six-bit parity symbols.
3. Intersperse 63 synchronizing symbols among the 63 information-carrying symbols.
4. Start transmission 1 s into a UTC minute. Transmit each symbol value at a distinct frequency.
5. Signal propagates from *A* to *B*, arriving much weaker and corrupted by noise, fading, and Doppler spread.
6. Receiving software at *B*: remove impulsive noise; detect synchronizing signal, measure its frequency and time offset.
7. Shift spectrum to put sync tone at zero frequency, correcting for any measured drift.
8. Compute binned power spectra $S(i, j)$ for all information symbols. (Index i runs over 64 possible symbol values, index j over 63 symbol numbers.)
9. Remove any possible spurs (signal appearing at same i for all j).
10. Apply **Algorithm 1**, the FT algorithm.
11. Optional: if FT decoding was unsuccessful apply **Algorithm 2**, hinted decoding.
12. Display decoded message for User *B*.

Algorithm 1

Pseudo-code for the FT algorithm.

1. For each received symbol, define the erasure probability as 1.3 times the *a priori* symbol-error probability determined from soft-symbol information $\{p_1 - \text{rank}, p_2/p_1\}$.
2. Make independent stochastic decisions about whether to erase each symbol by using the symbol's erasure probability, allowing a maximum of 51 erasures.
3. Attempt errors-and-erasures decoding using the BM algorithm and the set of erasures determined in step 2. If the BM decoder produces a candidate codeword, go to step 5.
4. If BM decoding was not successful, go to step 2.
5. Calculate the hard-decision Hamming distance X between the candidate codeword and the received symbols, along with the corresponding soft distance d_s and the quality metric u .
6. If u is the largest one encountered so far, preserve any previous value of u_1 by setting $u_2 = u_1$. Then set $u_1 = u$, $d_1 = d_s$, $X_1 = X$, and save the codeword.
7. If $X_1 < X_0$ and $d_1 < D_0$, go to step 11.
8. If the number of trials is less than the timeout limit T , go to step 2.
9. If $d_1 < D_1$ and $r = u_2/u_1 < R_1$, go to step 11.
10. Otherwise, declare decoding failure and exit.
11. An acceptable codeword has been found. Declare a successful decode and return the saved codeword.

Algorithm 2

Pseudo-code for hinted decoding

1. Generate a list of L codewords considered likely to be received. Set a pointer to the start of this list.
2. Fetch the next candidate codeword and calculate its metric u .
3. If u is the largest metric encountered so far, preserve any previous value of u_1 by setting $u_2 = u_1$. Then set $u_1 = u$ and save the codeword.
4. If the number of tested codewords is less than L , go to step 2.
5. If $r = u_2/u_1 < R_2$, go to step 7.
6. Otherwise, declare decoding failure and exit.
7. An acceptable codeword has been found. Declare a successful result and return the codeword and the value $q = 100(u_1 - bu_2)$ as a confidence indicator. (By default we use the value $b = 1.12$ for submode JT65A.)

Glossary of Specialized Terms

Alphabet	A sequence of possible symbol values used for signaling. JT65 uses a 64-character alphabet, values in the range 0 to 63.
Block code	An error-correcting code that treats data in blocks of fixed size.
Codeword	For the JT65 code, a vector of 63 symbol values each in the range 0 to 63.
Deterministic algorithm	A series of computational steps that for the same input always produces the same output.
Erasures	A received symbol may be "erased" when confidence in its value is so low that it is unlikely to provide useful information.
Hamming distance	The Hamming distance between two codewords, or between a received word and a codeword, is equal to the number of symbol positions in which they differ.
Hard decision	Received symbols are assigned definite values by the demodulator.
Received word	A vector of symbol values, possibly accompanied by soft information on individual reliabilities.
Soft decision	Received symbols are assigned tentative values (most probable, second most probable, etc.) and quality indicators.
Soft distance	The soft distance between a received word and a codeword is a measure of how greatly they differ, taking into account available soft information on symbol values.
Source encoding	Compression of a message to use a minimum number of bits. JT65 source-encodes all messages to 72 bits.
Stochastic algorithm	An algorithm involving chance or probability in determining the series of computational steps to be taken.
Symbol	The information carried in one signaling interval, usually an integral number of bits. JT65 uses 6-bit symbols.

Steve Franke, K9AN, holds an Amateur Extra class license. He was first licensed in 1971 and has previously held call signs WN9IIQ and WB9IIQ. An early and abiding fascination with radio science led to his current position as Professor of Electrical and Computer Engineering at the University of Illinois in Urbana-Champaign. Steve is a member of ARRL and a Fellow of the IEEE.

Joe Taylor was first licensed as KN2ITP in 1954, and has since held call signs K2ITP, WAILXQ, WIHFV, VK2BJX and K1JT. He was Professor of Astronomy at the University of Massachusetts from 1969 to 1981 and since then Professor of Physics at Princeton University, serving there also as Dean of the Faculty for six years. He was awarded the Nobel Prize in Physics in 1993 for discovery of the first orbiting pulsar, leading to observations that established the existence of gravitational waves. After retirement he has been busy developing and enhancing digital protocols for weak-signal communication by Amateur Radio, including JT65 and WSPR. He chases DX from 160 meters through the microwave bands.

References

- ¹J. Taylor, K1JT, "The JT65 Communications Protocol", *QEX*, Sep-Oct 2005, pp 3-12. Available also available at physics.princeton.edu/pulsar/K1JT/JT65.pdf.
- ²R. Kötter and A. Vardy, "Algebraic soft-decision decoding of Reed-Solomon codes", *IEEE Transactions on Information Theory*, Vol. 49, pp 2809-2825, 2003.
- ³WSJT Home Page: www.physics.princeton.edu/pulsar/K1JT/.
- ⁴Shu Lin and Daniel J. Costello, **Error Control Coding, 2nd Edition**, Pearson-Prentice Hall, 2004.
- ⁵Camille Leroux, Saïed Hemati, Shie Mannor, Warren J. Gross, "Stochastic Chase Decoding of Reed-Solomon Codes," *IEEE Communications Letters*, Vol. 14, No. 9, pp. 863-865, 2010.
- ⁶Soo-Woong Lee and B. V. K. Vijaya Kumar, "Soft-Decision Decoding of Reed-Solomon Codes Using Successive Error-and-Erasure Decoding," *IEEE "GLOBECOM" Proceedings*, 2008.
- ⁷Chang-Ming Lee and Yu T. Su, "Stochastic Erasure-Only List Decoding Algorithms for Reed-Solomon Codes," *IEEE Signal Processing Letters*, Vol. 16, pp 691-694, 2009.
- ⁸Source code for all programs in the WSJT project is stored in a Subversion repository at Sourceforge: <https://sourceforge.net/projects/wsjt/>.
- ⁹Errors-and erasures decoder for the Berlekamp-Massey algorithm written by Phil Karn, KA9Q, www.ka9q.net/code/fec/.

We Design And Manufacture To Meet Your Requirements

*Prototype or Production Quantities

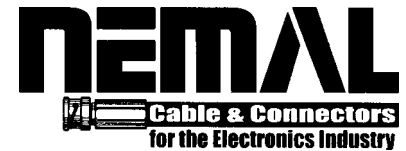
800-522-2253

This Number May Not Save Your Life...

But it could make it a lot easier! Especially when it comes to ordering non-standard connectors.

RF/MICROWAVE CONNECTORS, CABLES AND ASSEMBLIES

- Specials our specialty. Virtually any SMA, N, TNC, HN, LC, RP, BNC, SMB, or SMC delivered in 2-4 weeks.
- Cross reference library to all major manufacturers.
- Experts in supplying "hard to get" RF connectors.
- Our adapters can satisfy virtually any combination of requirements between series.
- Extensive inventory of passive RF/Microwave components including attenuators, terminations and dividers.
- No minimum order.



NEMAL ELECTRONICS INTERNATIONAL, INC.

12240 N.E. 14TH AVENUE

NORTH MIAMI, FL 33161

TEL: 305-899-0900 • FAX: 305-895-8178

E-MAIL: INFO@NEMAL.COM

BRASIL: (011) 5535-2368

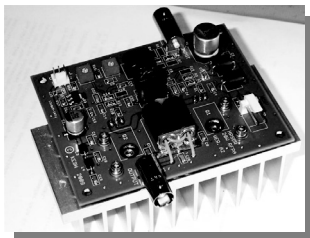
URL: WWW.NEMAL.COM



HPSDR is an open source hardware and software project intended to be a "next generation" Software Defined Radio (SDR). It is being designed and developed by a group of enthusiasts with representation from interested experimenters worldwide. The group hosts a web page, e-mail reflector, and a comprehensive Wiki. Visit www.openhpsdr.org for more information.

TAPR is a non-profit amateur radio organization that develops new communications technology, provides useful/affordable hardware, and promotes the advancement of the amateur art through publications, meetings, and standards. Membership includes an e-subscription to the *TAPR Packet Status Register* quarterly newsletter, which provides up-to-date news and user/technical information. Annual membership costs \$25 worldwide. Visit www.tapr.org for more information.

NEW!

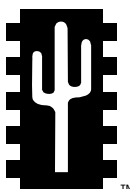


PENNYWHISTLE
20W HF/6M POWER AMPLIFIER KIT

TAPR is proud to support the HPSDR project. TAPR offers five HPSDR kits and three fully assembled HPSDR boards. The assembled boards use SMT and are manufactured in quantity by machine. They are individually tested by TAPR volunteers to keep costs as low as possible. A completely assembled and tested board from TAPR costs about the same as what a kit of parts and a bare board would cost in single unit quantities.

- **ATLAS** Backplane kit
- **LPU** Power supply kit
- **MAGISTER** USB 2.0 interface
- **JANUS** A/D - D/A converter
- **MERCURY** Direct sampling receiver
- **PENNYWHISTLE** 20W HF/6M PA kit
- **EXCALIBUR** Frequency reference kit
- **PANDORA** HPSDR enclosure

HPSDR Kits and Boards



TAPR

PO BOX 852754 • Richardson, Texas • 75085-2754

Office: (972) 671-8277 • e-mail: taproffice@tapr.org

Internet: www.tapr.org • Non-Profit Research and Development Corporation

Measuring Propagation Attenuation Using a Quadcopter

These tests show that the signal strength of a local station can be many tens of decibels weaker than from a DX station.

For the last several years I have been operating *WSPR* from N6GN on the 600 m through 70 cm Amateur Radio bands. I've found the large number of geographically spaced participants combined with the round-the-clock worldwide reporting make the WSPRnet.org web page and database an excellent tool for investigating propagation, and also for measuring and analyzing Amateur Radio station performance.

Among several local *WSPR* stations we noticed database entries that showed stations 1,000 to 2,000 miles away spotting our transmissions with significantly larger signal to noise ratio (SNR) than did local stations as close as four miles away. Assuming that the HF ionospheric propagation path follows an inverse-square law, one where the wave front expands spherically, it would seem at first glance that there should be a greater penalty for the greater distances. Distant signals (DX) should be much *weaker* than local signals.

From previous propagation experiments at UHF I knew that foliage and slight terrain variations in the propagation path could be responsible for extremely large attenuation at shorter wavelengths. It's also clear that HF antennas are usually closer to the ground, in terms of wavelength, than they are at UHF. Perhaps the peak of the main lobe of our HF antenna patterns getting pushed well above the horizon. This increases the signal incident on the ionosphere at the expense of signal levels measured at the local horizon. The question became, "How much of this greatly increased attenuation of

the local signal revealed by *WSPR* was due to foliage attenuation and how much was due to the HF antenna elevation pattern?" Our measurements using a quadcopter, see Figure 1, were designed to help answer that question.

Why is a Local Station Weaker than DX?

At my station, N6GN, I initially operated using an HF transceiver, then later with one of the Ultimate2 QRSS (U2) lower power beacon transmitters from QRP Labs.¹ On 10 m the U2 beacon delivers just 180 mW compared to the 5 W of my station HF transceiver. Even with just the lower power beacon, and a simple vertical antenna, it was very interesting to see where and when the signal can be spotted. Over several months of low power operation, I received spots from many US states and quite a few other countries.

It has been interesting to watch the reported SNRs to get an idea of propagation, and to compare them among other local stations at various distances, including several stations just 3 to 15 miles from my station. During the *WSPR* spotting activity, local stations often either could not hear my N6GN beacon at all, or reported 10 to 15 dB lower signal strength than stations 1000 to 2000 miles away. Upon discussing this over coffee with a few other local *WSPR* users one morning, we decided to see if we could determine the reasons for this.

What was limiting our signal?

From previous measurements at UHF I knew that local signals were often attenuated

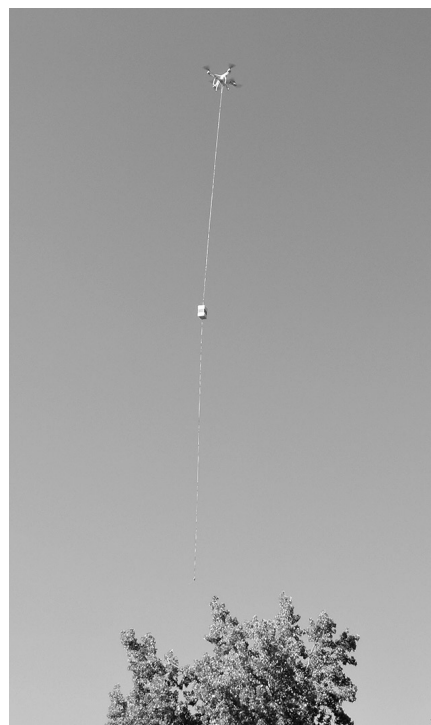


Figure 1 — Quadcopter shown towing a half-wave 10 m band vertical dipole with battery and beacon transmitter. [Photo courtesy of Glenn Elmore, N6GN].

a great deal more than if paths to the stations were truly in a free space and line-of-sight (LOS). RF path loss models indicated that many 10s of dB of additional attenuation could be expected for a 70 cm signal between typical amateur installations in a suburban environment. This is the same type of

¹Notes appear on page 22

environment our 10 m WSPR signals were encountering. We had previously measured a 70 cm path using a helium balloon supporting an elevated antenna fed with a surface wave transmission line to explore the “height gain” phenomenon.

Cross-polarization loss and pointing error

It was obvious that some of the local stations providing the WSPR spots were

cross-polarized, and encountered beam pointing errors, which attenuated their signals. Linear polarization refracted from the ionosphere results in both right and left hand circular polarized signals, so distant stations might not experience these polarization alignment issues. However, some of the locals were using vertical antennas, as I was at N6GN, so this didn’t explain all of the weak WSPR signal reports.

Antenna elevation pattern over Earth ground

We also know that the peak of the 10 meter signal is not directed at the horizon as it would be if we in free space. [There is always a ground reflection contribution for antennas elevated above Earth ground. — Ed.]. NEC based electromagnetic solvers (4nec2, EZNEC and other similar programs) predict a very considerable up-tilt in the peak of the antenna pattern due to the presence of real ground. We didn’t know precisely what our ground was like and what the ground reflections were doing to our antenna patterns. [NEC based electromagnetic solvers assume a perfectly flat and perfectly smooth ground. — Ed.].

Noise

Since the WSPR software and spotting network reports SNR referenced to an SSB bandwidth. It was possible that some of the reported differences were due to excess noise at the receiving station. We examined this possibility and found it is not always the case. Although local noise has become an increasingly serious problem everywhere, on 10 meters at least a few Amateur Radio stations can still boast about a fairly low noise floor. DX stations also often must fight local noise pollution, just as we do locally.

Excess absorptive attenuation

Referring to Figures 2, 3, and 4, one culprit for this “lost” signal was absorption by the environment. Several of the local hams were essentially at the same height above ground. They weren’t behind mountains or hills so we couldn’t blame obstruction losses from hills or mountains. We had a flat Earth between us. However, all of the local signals passed through trees and foliage in the propagation path to the N6GN antenna. We all live in suburban/rural areas, and there are lots of trees, with some that are well over 100 feet tall. I knew from previous measurements, as well as academic papers, that in UHF and microwave regions absorptive loss could be extremely high, with hardwood trees cited as producing excess attenuation of 0.25 dB per foot at 2.4 GHz. I had no data on what to expect from suburban California foliage at HF. Also, the wavelength in question was on the order of the height of many of the intervening trees.

When You Don’t Know, Measure!

We decided to make measurements to help separate some of the potential causes of signal loss. If we had a well characterized 10 m signal and antenna, and a station with an accurately known effective radiated power (ERP), we might raise and lower the radiating antenna over a wide range of

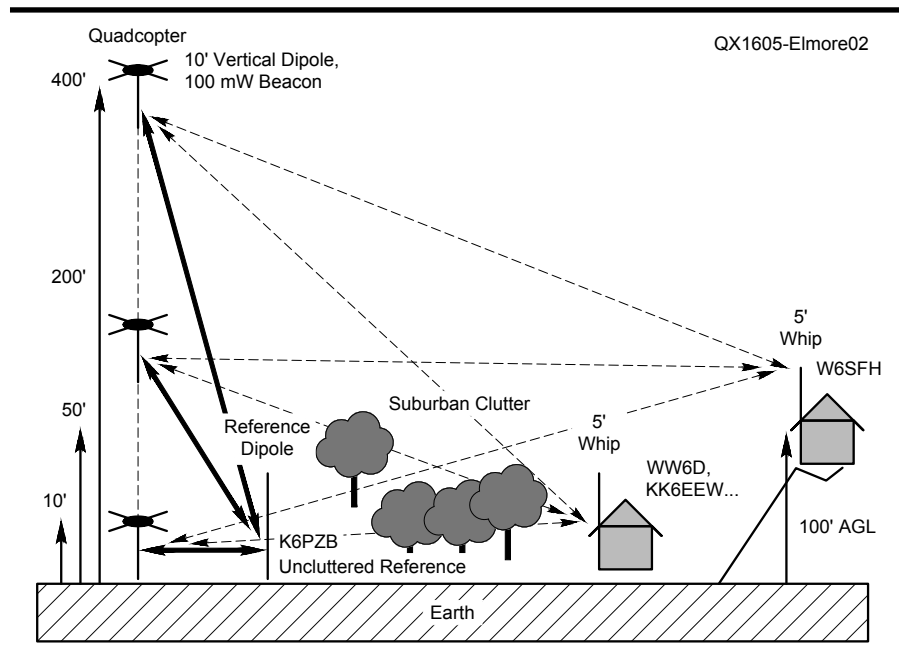


Figure 2 — Paths from various heights to a near-by station. The vertical scale is exaggerated.

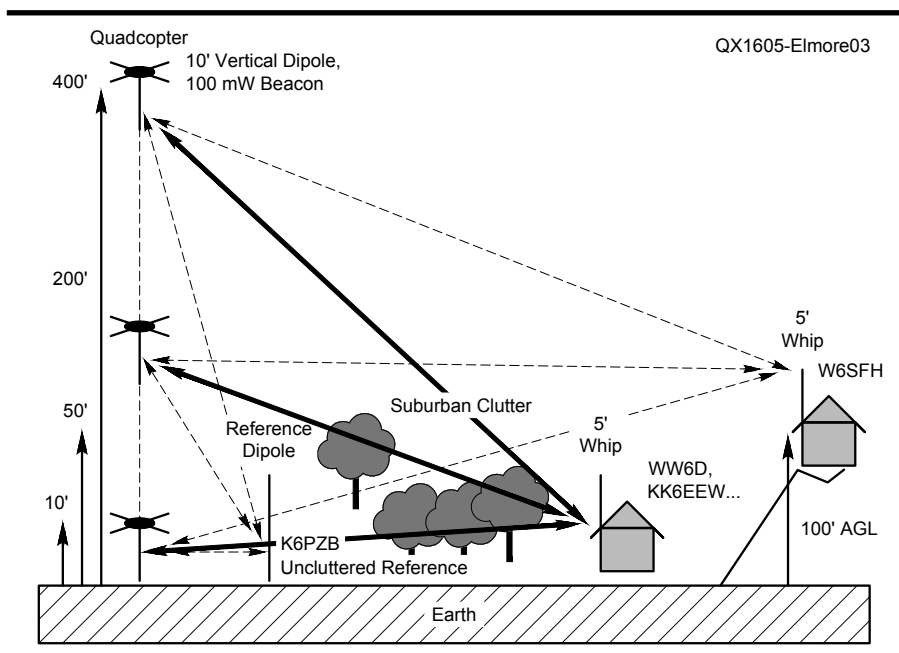


Figure 3 — Paths from various heights to mid-range stations. The vertical scale is exaggerated.

heights while measuring the field strength. This left the problem of placing the test transmitter and antenna at various heights in order to measure signal strength as a function of height.

I don't have a 400 foot variable height tower at my disposal. Furthermore, the weight of a 10 m dipole, transmitter and battery would be too much to lift with a small balloon. I then thought of the using an electric helicopter, a quadcopter that could easily lift several ounces of payload many hundreds of feet into the air. I have a DJI Phantom small quadcopter that has been modified to provide both GPS and barometric altitude telemetry data to the ground. This would allow gathering data as a function of antenna height and hopefully would help separate the potential contributors of attenuation to the signal.

Figure 2 shows the paths from various heights to a near-by station. Figure 3 shows the paths to mid-range stations. Figure 4 shows the paths to a more distant local station. The vertical dimension in the Figures is exaggerated, but you can see that at low test antenna heights, several potential contributors to attenuation were possible. The antenna lobe might be attenuated by reflections from the ground. Absorptive losses due to trees and other suburban clutter could also be involved. But as the transmitter and antenna height is increased, we thought that the effects from ground should vanish because for some stations the antennas would experience a LOS path. The path between the transmitter and receiving antenna, however, would still suffer the effects of a ground reflection.

The Tests

For the tests I chose a local park with about 1000 feet of flat ground — a completely clear sod playing field. A quadcopter lifted the payload (180 mW U2 beacon, lithium-polymer battery and a vertical dipole antenna) at one end of the park. We set the U2 to transmit a 100 Hz shift FSK-CW identifier and grid square on 28.1262 MHz.

This provided us with an accurate amplitude, and an almost constant frequency carrier for measurement by the several other stations. During the tests we used UHF FM radios to coordinate and report progress, and to report the test antenna height so all receiving stations could measure and record signal strength at the various known transmitting heights. We measured signals using either calibrated test spectrum analyzers or receivers that had previously been calibrated, so we knew the absolute signal level accurately.

We ran tests on two different occasions with two receive stations common to both sets of tests. Table 1 shows the stations participating in the tests along with some details.

Test 1

For the first test, we included a reference receive measurement quite close to the transmitter and with no clutter in between.

The reference station was K6PZB, located about 1000 feet away on the other side of the park. We set up a 10 m vertical dipole connected to a calibrated spectrum analyzer. The antenna was mounted on an insulating stand with the lower tip of the dipole a few feet above the ground. While the path would suffer the effects of the ground reflections, there was no other intervening clutter. Because this measurement path was so close, the effects of the two antennas beamwidths needed to be included in the calculated path loss. That is, as the test antenna was raised by the quadcopter, the broadside directions of the two antenna dipole patterns were no longer aligned. We used the known pattern of a dipole to correct for this in the final data. For more distant stations this effect was small, and we ignored it.

Two additional stations, WW6D and W6SFH, also listened and measured signals

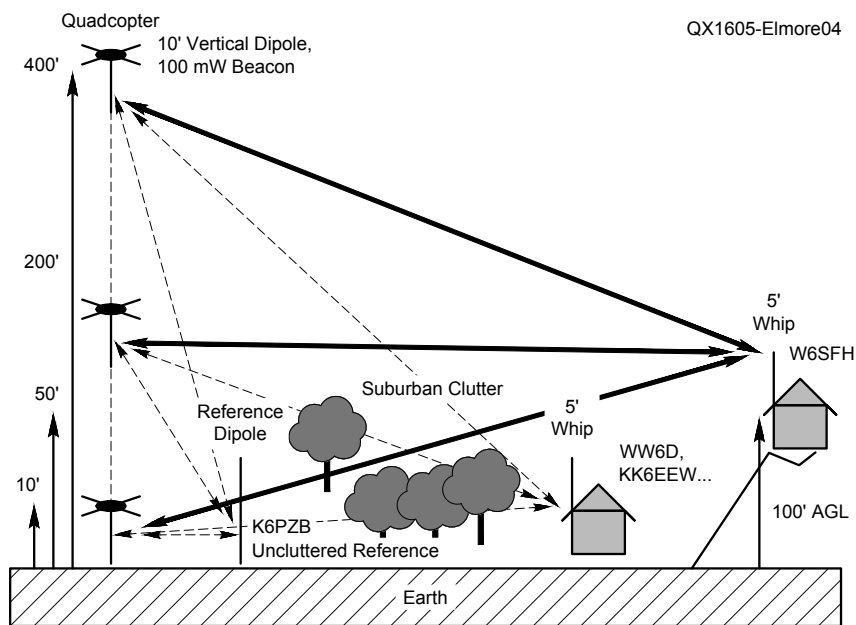


Figure 4 — Paths from various heights to a distant local station. The vertical scale is exaggerated.

Table 1.

First Test

Station	Details
K6PZB	Reference station, ground mounted half-wave vertical dipole, 1000 foot distant, LOS path in the same park as the transmitter.
W6SFH	About 3 miles NE, situated on a ~100 foot hill above most clutter, tri-band beam 40 feet above ground.
WW6D	About 2 miles N at same ground level height as test transmitter, tri-band beam at 40 feet above ground.

Second Test

Station	Details
KK6EEW	About 10 miles distant, vertical antenna and spectrum analyzer receiver, short whip with High-Z preamp.
K6PZB#2	Ground located half-wave vertical dipole about 3 miles NE, situated on a ~100 foot hill above most clutter, LOS to park.
W6SFH#2	About 3 miles NE and situated on a ~100 hill above most clutter, tri-band beam 40 feet above ground.

with either a spectrum analyzer or a calibrated SDR receiver. Both of these stations used relatively low horizontally polarized tri-band beams pointed toward the transmitting site. W6SFH was located on a ~100 foot hill above most of the intervening clutter. By the time the transmitter reached 100 to 150 foot elevation we expected to be in visual LOS of his beam. WW6D was located at the same ground level as the transmitter. This meant that there was a maximum of intervening clutter between his antenna and the test antenna at its lowest height. With the test antenna 400 feet (122 m) high, the path was still not LOS, but total clutter was reduced because only the clutter near WW6D was in the path between the transmitting and receiving antennas.

Test 2

For the second test the K6PZB reference antenna (K6PZB#2) was located at the 100 foot hill, about 1000 feet from receiving station W6SFH. Both of these stations used the same antennas and measuring systems as in the first test. K6PZB selected a location that would be LOS to the test transmitter once the test antenna was above approximately

100 feet. KK6EEW was the most distant of the reporting receiving stations. At 10 miles distance, there were very low rolling hills and very significant foliage in the path for all beacon elevations. Although still a local station, KK6EEW definitely did not have a LOS path.

Test Results

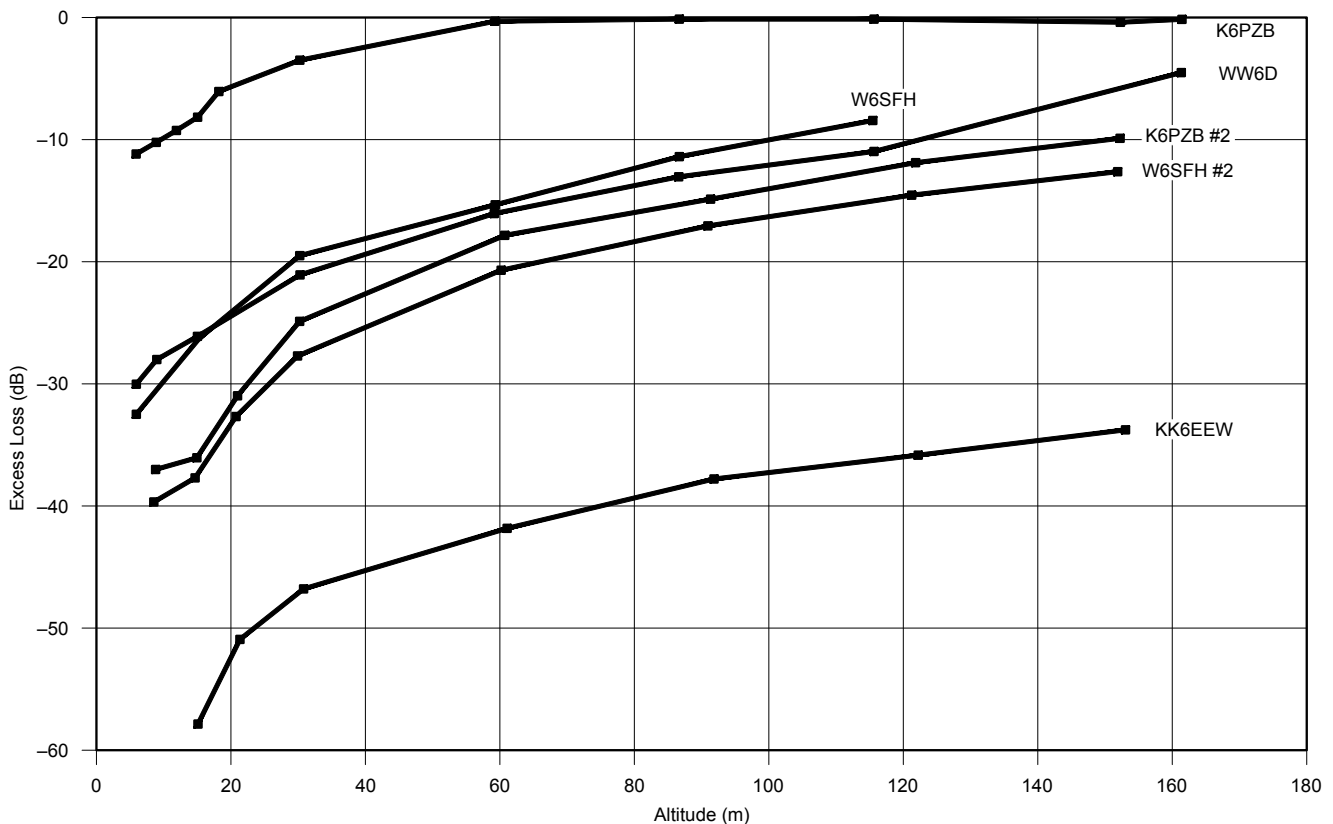
Figure 5 presents the measured results from the two tests. The vertical axis is the path loss in excess of free-space loss for the distance to each of the receive sites. The horizontal axis is the altitude of the beacon transmitter. The levels for each of these curves are different because they were referenced to the calculated free space loss for the particular distance.

The data of Figure 5 shows that the reference measurement matches calculated free space values and showed no excess attenuation once the test antenna exceeds a height of 60 meters — about six wavelengths at the test frequency. Each of the more distant sites showed additional attenuation, particularly at low test antenna altitudes. At the most distant receiving site, the

improvement created by altitude was most dramatic. Signals that had been lost in the noise from the test antenna when it was near ground level became quite strong by the time the test antenna reached a few wavelengths of altitude. One other monitoring station, about 8 miles distant (not included in the data), reported that although no signal was heard when the test antenna was at ground level it “...got very strong for only 200 mW” once the dipole and transmitter exceeded a 100 feet in altitude. The improvement from increasing antenna height was in excess of 50 dB. At maximum height the beacon generally became the strongest signal on the band for all receiving stations.

An Interpretation

Data from the K6PZB reference antenna seems to confirm that the ground affects the main dipole lobe and pushes the angle of peak radiation upward. This effect, 10 to 12 dB, was common to all stations and reveals a strong height dependency. There remains an additional 10 to 15 dB factor for the closer stations and at least 25 dB for the more distant receivers. This might make



QX1605-Elmore05

Figure 5 — Measurements of signals as a function of height using a quadcopter to support a “flying” 10 m transmitter and dipole.

intuitive sense. For closer stations, see Figure 2, the angle of the antenna increases more than for distant stations, Figures 3 and 4, and the proportional amount of intervening absorbers from trees, terrain and buildings decreases. The amount of intervening absorbers, however, decreases the most for elevation angles appropriate to DX station paths.

In a recent 432 MHz measurement, each doubling of height produced about 7 dB of improvement of SNR in a suburban/urban environment. Although that RF path attenuation model was not intended for HF, our data also follows this trend in the 10 meter band.

Conclusion

Our tests were not definitive. They could be improved, and they leave open questions. We investigated a single locale with one type of ground and generally similar foliage and terrain. Some of the data involved cross-polarized antennas. We did not investigate any “Brewster angle absorption” effects. Even so, all receiving sites reported a generally similar experience. Our data provided evidence that long distance contacts on 10 m by way of the ionosphere along paths involving elevation angles above 10 to 15 degrees can have considerably lower attenuation than some local contacts. We speculate that one reason is that when station antennas lower than a few wavelengths are used, there is on the order of 10 dB penalty due to the effect of ground reflection pushing the peak of the antenna

lobes upward, and putting the local station at a disadvantage. A second reason is that there is greater attenuation due to absorption by the local environment just as there is at VHF and above. The combination of these two effects can easily exceed 40 dB and serves to explain the differences we see in reported SNRs on WSPR.

These results add emphasis to the value of antenna height when working stations at or very near the local horizon, rather than via higher angle ionospheric propagation paths. As an HF band is just opening or closing, when the angle of the ionospheric path is extremely low, and the skip distance is long, the improvements possible from increasing antenna height may dominate other improvements that you can make to an Amateur Radio station. Height may have even more effect than antenna size — height gain may exceed the gains possible for practical HF antennas. Investments in tower height probably provides much greater return than investment in antenna size or number, since an antenna with a gain in excess of about 30 dB is not generally feasible below the microwave bands. The benefits of antenna height are perhaps most dramatic on VHF and higher frequencies as demonstrated in online videos.²

Next Steps

Our local 10 m band data seems to agree with the findings of previous 70 cm tests. Following our 10 m test, we have performed 2 m band test with WSPR on 2 m.

We used a balloon rather than a quadcopter. We would like to make similar height gain measurements out to several hundred miles using WSPR. We plan to report our progress on QEX.

Glenn Elmore, N6GN, has been a licensed Amateur Radio operator for 50 years. He's held the call signs WV6STS, WA6STS, and now N6GN. He holds the Amateur Extra class license since 1972. Glenn was an electrical engineer involved with the design of RF and microwave test and measurement equipment, notably scalar, vector network and spectrum analyzers. His Amateur Radio interests include weak signal VHF-microwave operation, meteor scatter, EME, terrestrial DX as well as higher speed amateur TCP/IP radios and networks. Glenn has been using WSPR for more than five years to examine VHF/UHF propagation. He operates a largely homebrew station using OpenHPSDR SDR hardware and software.

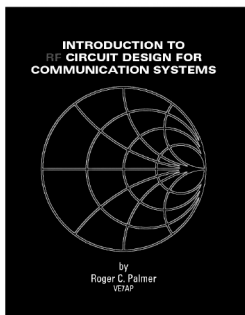
Over the years Glenn has authored professional papers and articles, Amateur Radio microwave hardware projects and more recently, several papers and articles on surface wave transmission line theory and applications, including a three-part series in QEX in 2012. Glenn is semi-retired and able to devote more time to applications and theory of SWTL and integrating these with an understanding of theoretical physics.

Notes

¹QRP Labs, www.qrp-labs.com.

²See the several videos at <https://youtu.be/-VWBUDJv2n0>.

³<https://www.dropbox.com/s/jkpyxkpci50hb4q/HaloTest.pdf?dl=0>



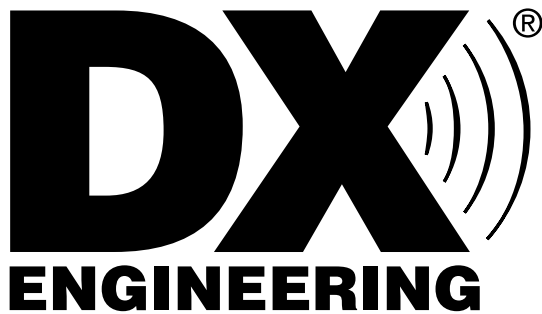
INTRODUCTION TO RF CIRCUIT DESIGN FOR COMMUNICATION SYSTEMS

New, practical, easy-to-read text book written for technicians and amateurs who want to learn more about RF Circuit Design techniques.

By Roger C. Palmer, VE7AP

www.paltec.ca

Now available from Amazon.com 208 pages, \$29



8:30 am to midnight ET, Monday-Friday
1230 to 0400 UTC March-October

8:30 am to 5 pm ET, Weekends
1230 to 2100 UTC March-October

International/Tech: 330-572-3200
8:30 am to 7 pm ET, Monday-Friday
9:00 am to 2 pm ET, Saturday
Country Code: +1 Sale Code: 1606QEX

**ORDER BY 10 PM
SAME-DAY
SHIPPING**
Mon-Fri, 10 pm ET
In-Stock Items

800-777-0703 | DXEngineering.com

See You at Hamvention®, Booths 0-7 Main Arena!



DX ENGINEERING®

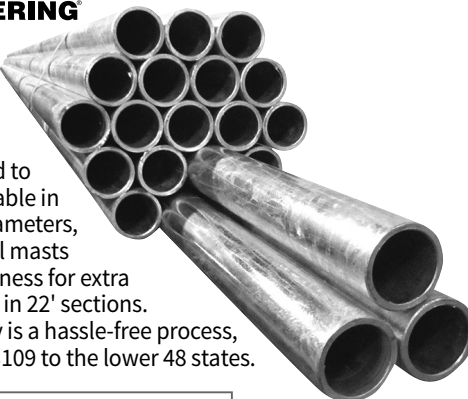
Coaxial Cable Tool Kits

Carry everything you need to prep and install solder connectors on your coaxial cable. The Basic Kit is tailored for RG-213 and RG-8 cable with PL-259 connectors. Upgrading to the Complete Kit gives you additional tools to work with RG-8/X size cable and Type N connectors.

DX ENGINEERING®

Heavy-Duty 4130 Chromoly Steel Masts

DX Engineering offers masts perfectly suited to Amateur Radio. Available in 2 or 3 inch outside diameters, these galvanized steel masts have a 1/4" wall thickness for extra rigidity. They are sold in 22' sections. Ordering and delivery is a hassle-free process, and shipping is only \$109 to the lower 48 states.



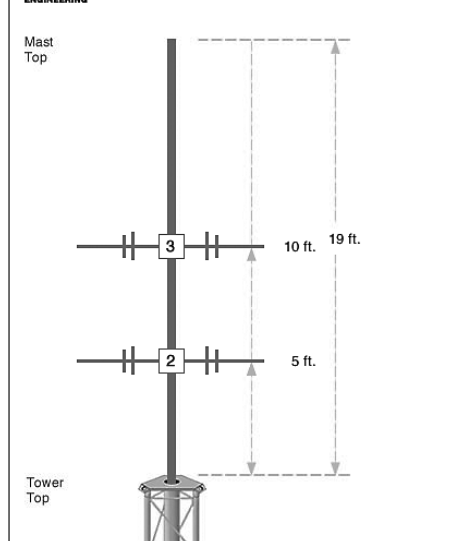
DX ENGINEERING®

Receive Four Square Packages

These receive antenna systems provide a better low band weak signal reception than is possible with a typical transmit antenna. They use time-delay phasing to deliver improved directivity, a better signal-to-noise ratio, and enhanced reliability—all in less space than a Beverage antenna. These phased arrays are directivity-optimized to produce wider and deeper nulls, along with a narrower main lobe, which results in fantastic front-to-rear response. Directivity is switchable in four 90 degree spaced directions. Several packages are available, find the right one for your station at DXEngineering.com.



DX ENGINEERING® MAST LOAD ESTIMATOR



Use the free Mast Load Estimator at DXEngineering.com to determine the right mast for your application.

DX ENGINEERING®

PRO-STACK Broadband Antenna Phasing Systems

DX Engineering's PRO-STACK phasing systems allow you to combine multiple Yagi, log periodic beam or quarter-wave verticals for enhanced performance. The PRO-STACK allows multiple selections of any or all antennas including in and out of phase combinations. There are 2- and 3-antenna systems, available with SO-239, Type N or 7-16 DIN connectors.



DX ENGINEERING®

Are you ready for Field Day? DX Engineering is your go to source for all of your Field Day needs!

DX Engineering supports the BS7 Scarborough Reef DXpedition.
www.DXEngineering.com/TechArticles/News/DXGeneralNews

Email Support 24/7/365 at DXEngineering@DXEngineering.com

Stay connected:

Using a Wide-Band Noise Generator with a Spectrum Analyzer

Low cost noise sources are being marketed today as an alternative to a tracking generator, so how does a broadband noise generator compare to a tracking generator in such applications? In this study these two very different methods are compared and several examples presented.

Noise in radio communication system is a most unwelcome. We constantly strive for the highest signal and the lowest noise. But in several measurement applications there are tasks where the controlled generation of noise is very useful. Examples include noise figure measurement, EMI testing, spectrum analyzer calibration and gain-bandwidth measurements.

A spectrum analyzer with a tracking generator can be useful for measuring the frequency response of components, coaxial networks, filters and more. In this paper we will take a look at using a wide-band noise generator — instead of a tracking generator — for frequency response measurements with a spectrum analyzer. There are many spectrum analyzers without tracking generators that perhaps could benefit from this addition. To examine this possibility, the responses obtained with a tracking generator are compared to those obtained with a noise generator. Several examples of measuring coaxial cables and filters using these two approaches will be presented. A low cost noise generator, commonly available on the Internet, is used for the study. To get started, let's take a closer look at noise.

Noise Characteristics

To be useful for frequency response measurements, the noise generator must have a flat power spectral density (PSD) function.

¹Notes appear on page 29

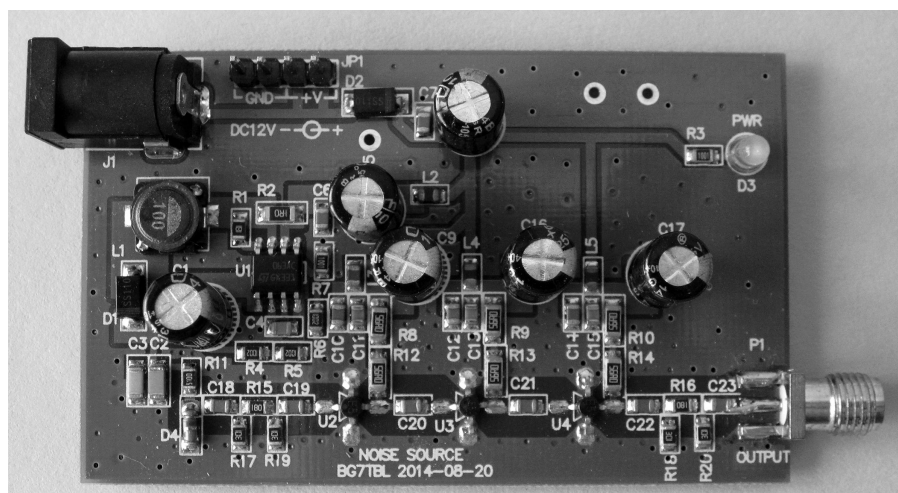


Figure 1 — The low-cost BG7TBL noise source used in this study.

A PSD function shows how much power is contained in each spectral component or unit of frequency. It is usually normalized to 1 Hz and written as dBm/Hz.

Noise with a constant PSD is defined as white noise. Because white noise has the same power density at all frequencies, the power passed by the device under test (DUT) is proportional to its bandwidth.

White noise bandwidth, while theoretically infinite, is limited in practice by the means of noise generation and by the finite capabilities of devices. Thus, a random signal is considered white noise if it is observed to have a flat spectrum over the

range of frequencies that is relevant to the task at hand.

Being random or uncorrelated in time does not restrict the values a noise signal can take on. Any distribution of values is possible, even binary values. However, the most common form of noise is additive white Gaussian noise (AWGN). This noise occurs as a result of the random motion of electrons. If the number of electrons involved is large, their motions are largely independent. Therefore the voltage amplitude distribution of noise sources, derived from a component such as a resistor or diode, follows a Gaussian probability density function (PDF). This



Figure 2 — Spectrum analyzer, oscilloscope and noise source used in this study.

distribution is conveniently characterized by its mean, standard deviation and bell-shaped curve. For Gaussian noise, the standard deviation of the noise voltage is the rms value of the voltage. Furthermore, if the Gaussian noise is band-limited, its Gaussian characteristics are not changed substantially.

Components generate AWGN in accordance with the temperature of the surrounding material, usually assumed to be 290K (17°C). The thermal noise density generated at this temperature equals -174 dBm/Hz, which in a 1 Hz bandwidth is in the attowatt range, and is of interest to astronomers. Much higher noise levels are needed for circuit measurements. Reverse biased Zener diodes can provide more than 25 dB above the -174 dBm/Hz thermal noise floor. Modern spectrum analyzers can measure these low-level noise signals and they are useful for noise figure measurements. For gain-bandwidth measurements, considerably more noise is required and the power must be increased by an additional 50 dB or more.

Excess noise ratio (ENR) — defined as $10 \log[(Th - 290)/290]$ — is a normalized

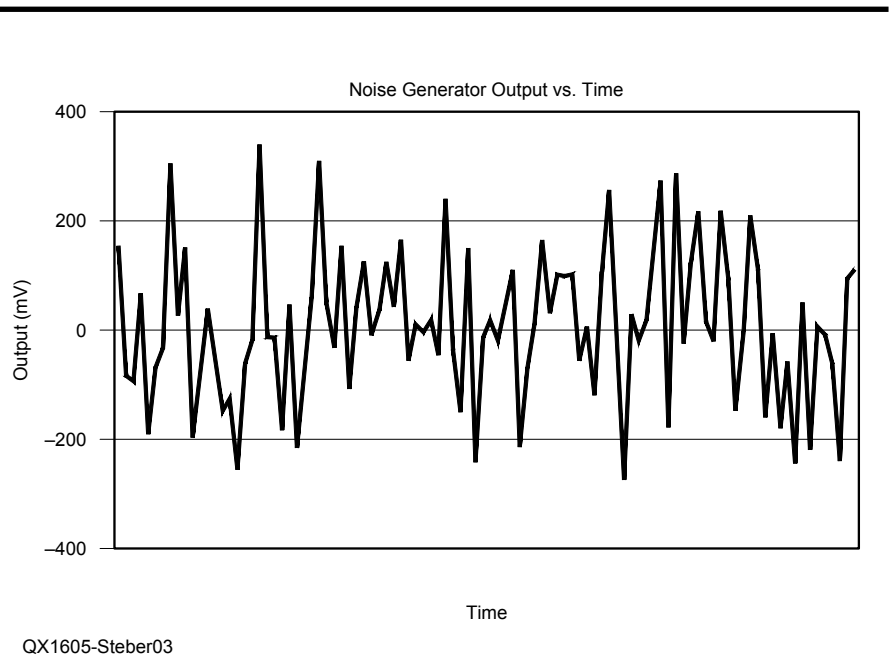


Figure 3 — Waveform of noise source captured with Owon oscilloscope.

measure expressed in dB of how much the noise source temperature (T_h) is above 290K. For ENR greater than 15 dB the power density can be approximated by adding ENR to -174 dBm/Hz. For example, given an ENR of 44 dB the power density is -130 dBm/Hz.

Commercially available white noise generators are usually very expensive. However a low cost, wide band noise source, shown in Figure 1, was recently for sale on eBay (www.ebay.com) that claimed a high excess noise ratio (ENR) and a large frequency range. Even more interesting, it was claimed that the unit, a model BG7TBL, could be used in place of a tracking generator for a spectrum analyzer. This unit is small in size (2.75 by 1.625 inches), but is well constructed from SMD parts. It operates from 12 V dc, and has an SMA connector for output. Since the cost was low, \$18.50 including shipping, I decided to send for one and see how well it works.

As noted above, a big reason that such a noise generator may prove useful is that many spectrum analyzers in the field do not have tracking generators. Hence, the usefulness of these instruments may be enhanced by enabling frequency response testing of components, filters and the like. In this study the BG7TBL noise source was evaluated for this application using a 2.6 GHz Advantest R3361C spectrum analyzer equipped with tracking generator, and a 200 MHz Owon SDS8202 digital oscilloscope.

Characteristics of the Noise Source and Test Equipment

The Advantest spectrum analyzer, Owon oscilloscope and BG7TBL noise generator used in this project are shown in Figure 2. The noise source is situated on a piece of protective cardboard on top of the spectrum analyzer and is also connected to the scope. Typically the scope is not needed or used when doing frequency response measurements. Also shown on top of the spectrum analyzer is a GPIB controller that is used to control the analyzer via a PC.

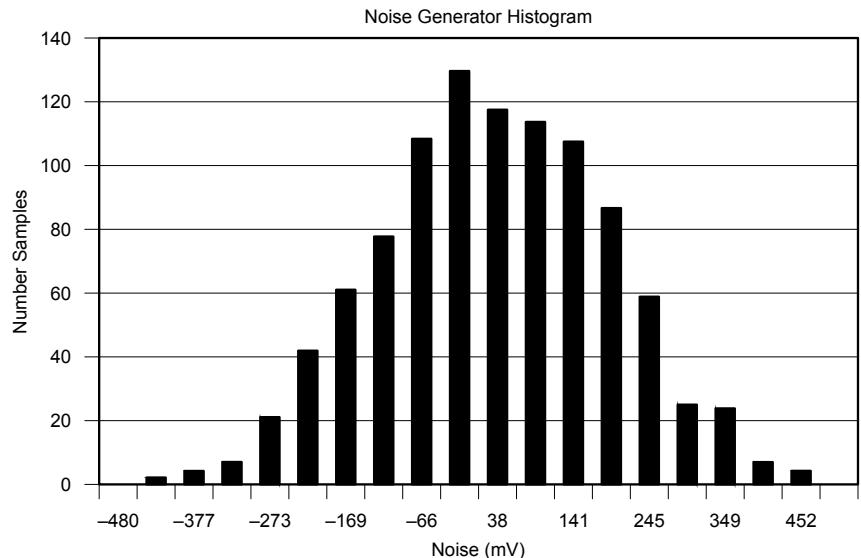
A circuit diagram was not provided with the noise generator but I believe it to be similar to one found in the Maxim application note AN3469.¹ The Maxim design uses a reverse biased Zener diode as the noise source followed by two MAX2650 amplifiers to increase the level. The Maxim circuit produces white noise up to several hundred MHz. On the other hand, the BG7TBL version used here appears to have three amplifiers and claims operation up to 2.5 GHz. It operates on 12 V dc, but there are versions, found on the web, that operate on 24 V dc. However, those versions reportedly suffer from overheating. Table 1 shows the claimed ENR for various frequency bands.

These values are not truly ENR, as they

Table 1.

Frequency range and claimed ENR of BG7TBL noise generator.

Frequency	0.1 GHz	0.5 GHz	1.0 GHz	1.5 GHz	2.0 GHz	2.5 GHz
ENR	60 dB	55 dB	52 dB	48 dB	38 dB	30 dB



QX1605-Steber04

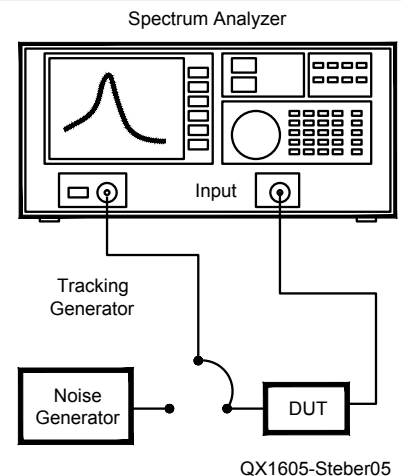
Figure 4 — Histogram of noise source obtained using Excel spreadsheet.

are be too low to provide useful results. My presumption is that they are estimates of the amount of noise that can be achieved above the noise floor of the spectrum analyzer. In that case they are useful and provide an indication of the dynamic range to be expected. These values are still well below the typical 80 dB or more dynamic range achievable with a tracking generator.

One of my first checks was to capture a noise waveform and observe the amplitude distribution. The signal was band limited to 20 MHz and the Owon scope captured 1000 data points of the noise signal. A typical noise waveform is shown in Figure 3. This data was then loaded into an Excel® spreadsheet to analyze and plot a histogram of the data. An example is shown in Figure 4. As you can see, the histogram appears to be Gaussian. I made no statistical tests to verify that the noise was Gaussian.

Frequency response tests were performed using the R3361C with its internal tracking generator and compared to the external wide-band noise source. The setup is illustrated in Figure 5. All connections are made with short coaxial cables. Note that the R3361C is a swept-spectrum analyzer as opposed to an FFT type. More information about FFT analyzers and RF samplers can be found in the Notes.^{2,3}

If you intend to repeat the following measurements, be sure to refresh your knowledge of your spectrum analyzer's operation. In particular review the function of the resolution bandwidth (RBW) setting, video bandwidth filter (VBW), reference level, detector options, attenuator settings, averaging settings, and the spectrum normalization procedure.



QX1605-Steber05

Figure 5 — Test setup for measuring components and cables.

Caution When Measuring Noise

An Agilent application note cautions about measuring noise or noise-like signals with a spectrum analyzer that can overdrive the input mixer.⁴ While displaying a signal in the normal display range, a very high noise signal can overdrive the front end of the spectrum analyzer. This can occur when the noise bandwidth (NB) of the noise signal is much wider than the RBW. For this situation

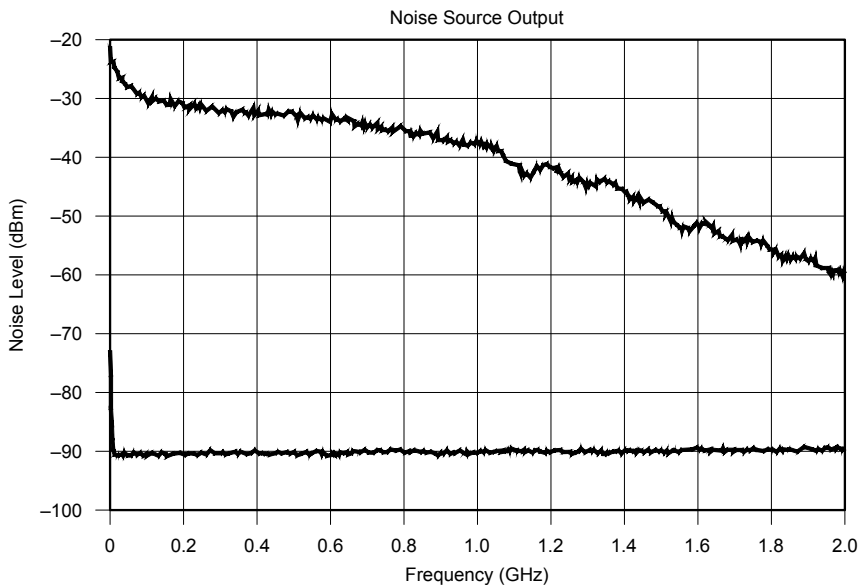
the power in the RBW will be lower than the total input power by about $10 \log(NB/RBW)$.

For example, a noise power with a 1 GHz bandwidth is 60 dB larger than the power in a RBW of 1 kHz. If the indicated power is -50 dBm with the 1 kHz RBW filter, then the mixer is seeing about +10 dBm. Many spectrum analyzers are specified for -10 dBm single tone (CW) signals at the input mixer. For CW signals, mixer compression is often

specified to be less than 1 dB with inputs of less than -5 dBm. However, good practice usually indicates keeping the total input power to the mixer below -10 dBm.

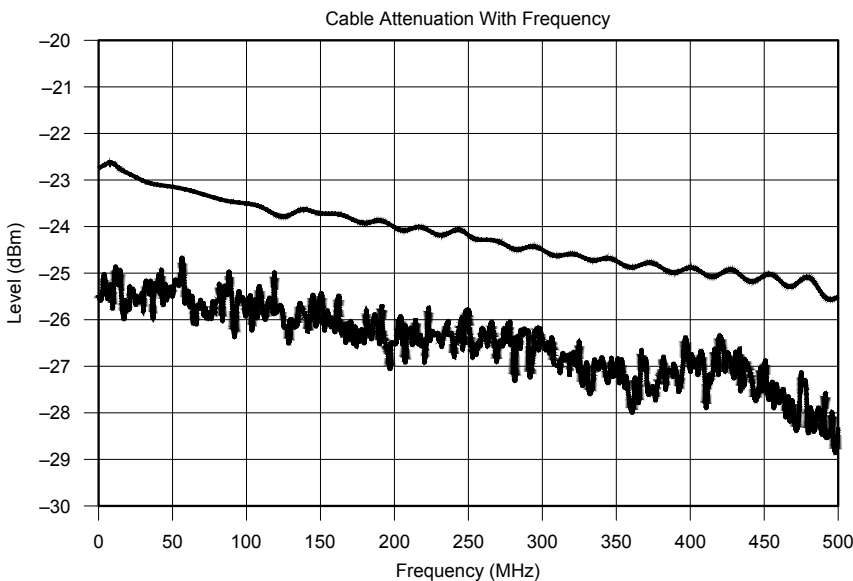
Unfortunately, the mixer behavior with Gaussian noise is not specified or guaranteed, especially because its peak-to-average ratio is much higher than that of CW signals. In any case we can take steps to keep the mixer input power low. This includes using sufficient RF attenuation at the input, increasing the RBW, and low-pass or bass-pass filtering the noise.

In general, to avoid damaging the mixer, it is a good idea to start the spectrum analyzer measurement with a high value of input attenuation. Then gradually reduce the attenuation until the indicated power is in a good range. I found that when using this noise source, 10 to 20 dB of input attenuation is sufficient when testing passive devices.



QX1605-Steber06

Figure 6 — Noise source output scan from 4 MHz to 2 GHz. Top trace is noise source. Bottom trace is spectrum analyzer noise floor.



QX1605-Steber07

Figure 7 — Attenuation of coaxial cable with frequency. Top trace is the tracking generator and bottom trace is noise source. The traces are intentionally off set from each other.

Determining the Noise Source Range

To look at the dynamic range of the noise source, the setup in Figure 5 is used with the input of the DUT connected to the noise source. A short-circuit replaces the DUT, essentially connecting the noise source to the spectrum analyzer 50 Ω input.

With noise source power OFF, and the spectrum analyzer settings as follows: RBW = 100 kHz, VBW = 1 kHz, input attenuator 10 dB; make a scan from 4 MHz to 2 GHz. This measures the noise floor of the spectrum analyzer as seen in the lower trace in Figure 6. Next, with noise source power ON and the other settings unchanged, the noise power level can be seen as the top trace in Figure 6.

We can see that, with these settings, the noise floor remains relatively flat at about -90 dBm. The noise source power at 100 MHz is about 60 dB above the floor. The response drops down to 30 dB above the noise floor at 2 GHz. This corresponds roughly to the values in Table 1. Because the noise level decreases with frequency it should be normalized over the range of interest before making measurements involving comparisons.

Measuring Cable Attenuation

To measure the transmission line (TL) loss in a coaxial cable, use the setup in Figure 5. The cable tested becomes the DUT. When testing the frequency response of cables and components it is customary to first plot the response of the fixture with a short in place of the DUT. This response can then be normalized, which removes the effects of the fixture and source variations, and provides a convenient reference plot for comparisons.

Figure 7 shows the results of testing a

short length (15 inches) of RG-58A/U cable over a 500 MHz span. Note that the vertical scale is expanded to 1 dB per division. This accentuates noise and ripples. The top trace is the output using the tracking generator. It is purposely offset from the lower trace using the noise source by about 2 dB to separate the curves. Averaging of the noise source, not done here, would make the noise curve much smoother. The response of the cable to the noise source compares well with the tracking generator. While the curve is somewhat bumpy, it can be smoothed out with averaging.

Measuring Filters

I had several types of RF filters on hand for testing. I used the same normalization procedure described above to remove the effects of the connecting cables, fixture and source variations.

Figure 8 shows an example of a 20 m band-pass filter response. The two curves, corresponding to the noise source and tracking generator, virtually overlap. I applied a RBW of 10 kHz, with no averaging for this measurement.

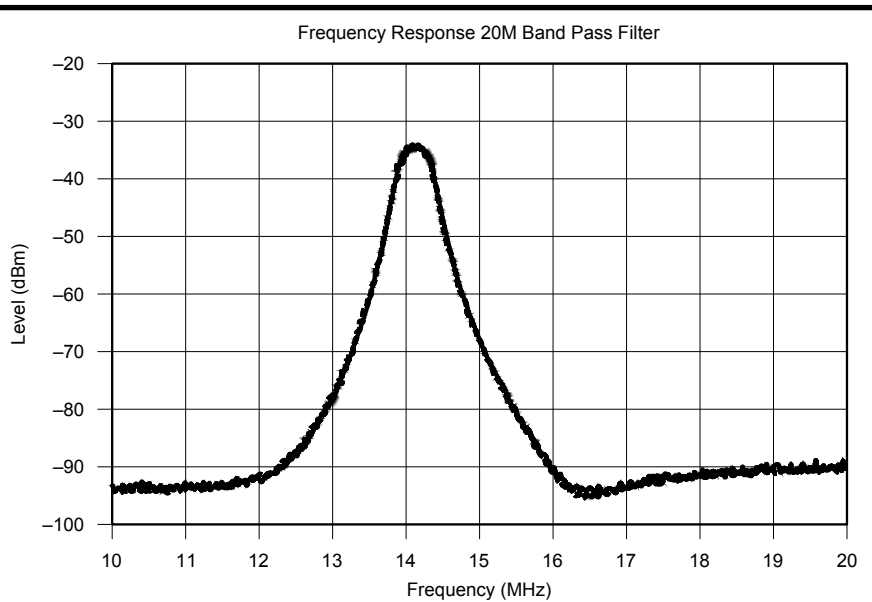
Figure 9 shows an example of a low pass filter. Again, the two curves are very close together with the slightly lower curve representing the tracking generator. I applied a RBW of 10 kHz, with no averaging for this measurement.

Finally, I measured a 14 MHz crystal. The measured response shown in Figure 10 was a great surprise for me. It shows what can be done with trace averaging. I used an average of ten times. Note the greatly expanded frequency scale (100 kHz span), and the 1 kHz RBW used for the measurement. The lower trace is from the tracking generator and does show more fine detail.

Measuring a Quarter Wavelength Stub

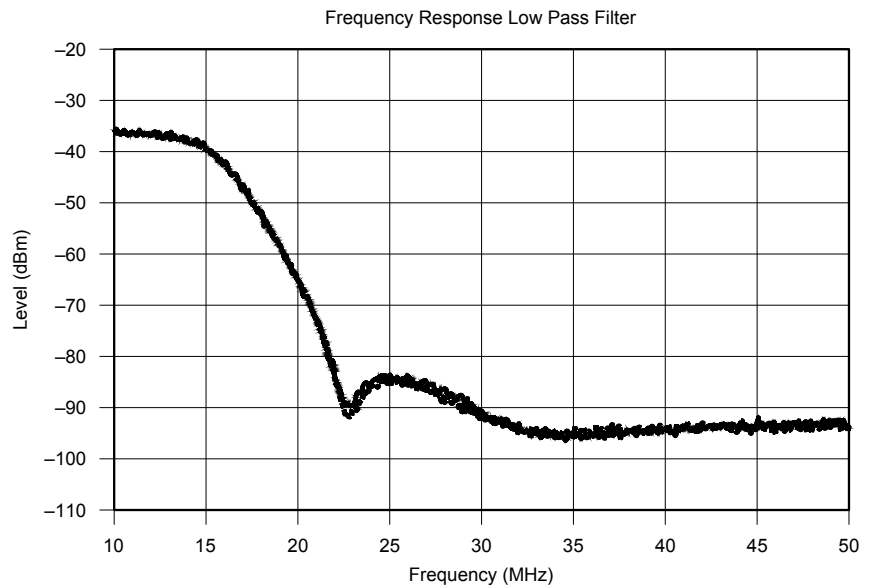
Stubs can easily be measured with the setup shown in Figure 11. Short coax cables are used for the connections. A stub is basically a length of coax that is open on one end. When the stub is excited at certain frequencies it becomes a short and produces a dip in the frequency response.

An example is shown in Figure 12 for a coaxially stub that is approximately 5 feet long. I used a RBW of 100 kHz. The top trace is the output from the tracking generator and is offset a few dB above the noise-source curve. Averaging was not used. After normalization, the two curves are very close to each other. The first dip at 30.8 MHz is quite pronounced. There will be successive dips at odd multiples of the frequency. Stubs are useful for all sorts of things pertaining to antennas.



QX1605-Steber08

Figure 8 — Frequency response of 20 m band-pass filter.



QX1605-Steber09

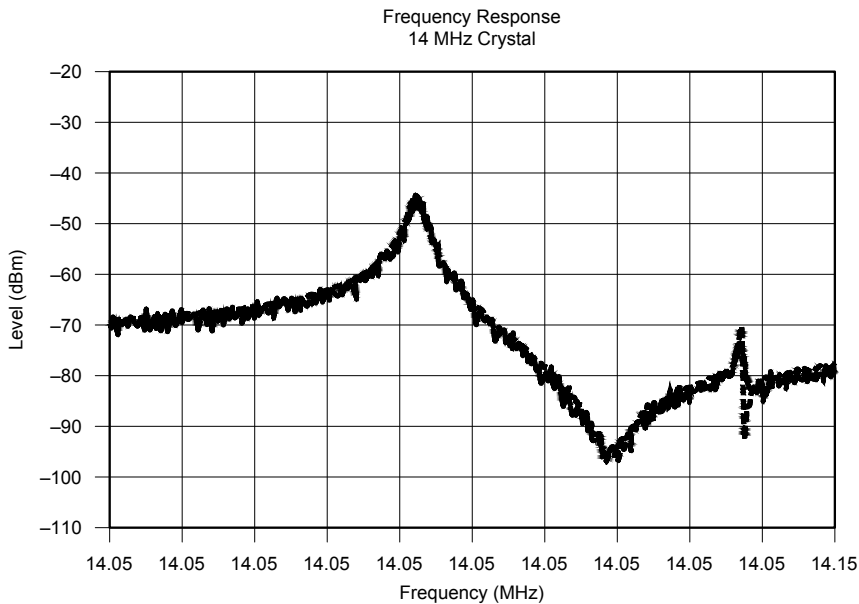
Figure 9 — Frequency response of a low pass filter.

Summary and Conclusions

Presented here were several experiments comparing a low-cost wide-band noise generator to a tracking generator for frequency response measurements of cables and RF filters. In many cases, the results obtained with the noise source were adequate for general use. In some cases the noise source provided results identical to those obtained with the tracking generator, but with

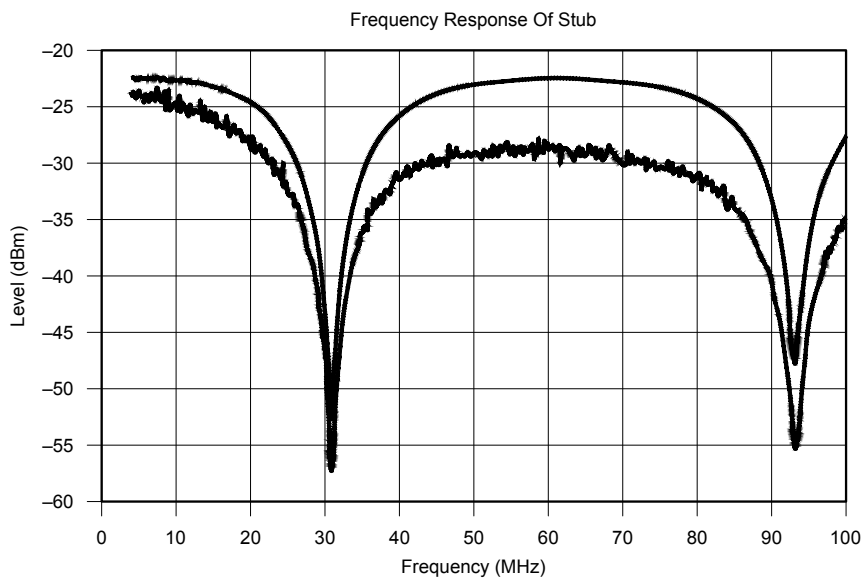
a smaller dynamic range. In general, best results were obtained when measuring band pass filters or low pass filters as opposed to high pass filters. This is probably because a band-pass filters restricts the amount of noise power reaching the first mixer in the spectrum analyzer. This allows the use of smaller values of RBW without fear of overloading the front end.

When measuring filters in the HF bands, a low pass filter placed after the noise source



QX1605-Steber10

Figure 10 — Frequency response of 14 MHz crystal.



QX1605-Steber12

Figure 12 — Frequency response of short stub.

should be used to reduce noise power above those frequencies. A loss of 3 dB or so may be incurred but you will be able to use much smaller values of RBW to obtain more detailed measurements.

Many other tests could be performed with the BG7TBL noise source, particularly at higher frequencies. The dynamic range is lower at the higher frequencies but still adequate for many purposes. My lab is sparsely equipped for work at gigahertz

frequencies. So that work will be left to someone down the line. Hopefully good results will appear here in the future.

If you have a spectrum analyzer without a tracking generator, using a noise source as described in this study may give your instrument new capabilities. Spectrum analyzers vary greatly in capabilities and yours may not produce the same results shown here. Because noise sources have varying flatness, averaging and normalization

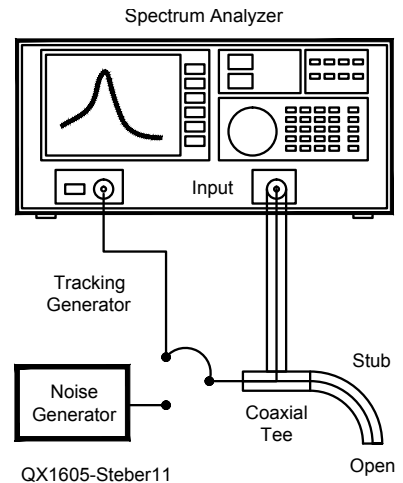


Figure 11 — Test setup for measuring a coaxial stub.

functions can be very useful.

Experimenting with noise sources is enjoyable and educational. Hopefully you have learned something about noise sources and spectrum analyzers from this project. As you explore the subject further you will find there are numerous other applications for noise sources. In any event, let *noise* be part of your *spectrum* and start *analyzing* it now.

George R. Steber, PhD, is Emeritus Professor of Electrical Engineering and Computer Science at the University Of Wisconsin-Milwaukee. He is now semi-retired having served over 35 years. George, WB9LVI, has an Advanced Class license, is a life member of ARRL and IEEE and is a professional engineer. His previous article for QEX, "Experiments With Eddy Current Methods for Thickness Measurement of Thin Metallic Materials" appeared in the Nov 2014 issue. George has worked for NASA and the USAF and still works on various projects at the University. He is currently involved in cosmic ray research and is developing methods to study them on a global basis. In his spare time he enjoys WSPR/JT9 Amateur Radio, racquetball, astronomy, and jazz. You may reach George at steber@execpc.com with "Noise" in subject line and with email mode set to text.

Notes

- ¹Maxim, "Building a Low-Cost White-Noise Generator", Mar 14, 2005, www.maximintegrated.com/an3469.
- ²G. Steber, "An Unusual Vector Network Analyzer", *QEX*, No. 244, Sep/Oct 2007.
- ³Agilent, "Spectrum and Signal Analyzer Measurements and Noise", Application Note, cp.literature.agilent.com/litweb/pdf/5966-4008E.pdf.
- ⁴Agilent, "Performance Spectrum Analyzer Series Swept and FFT Analysis", Application Note, cp.literature.agilent.com/litweb/pdf/5980-3081EN.pdf.

Geodetic and Maidenhead Locator System Conversion

Extending the definition of Maidenhead grid locators from the currently defined 8 characters to 16 characters improves location precision to within inches.

A geodetic system is a coordinate system used to locate places on the Earth using a set of reference points. Specifically, latitude and longitude coordinates used together locate places on Earth's surface, for example the coordinate set (34.065380 N, 84.554930 W). The Maidenhead Locator System, see Figure 1, uses the geodetic latitude and longitude numbers expressed differently as alternating pairs of letters and numbers.¹ This limits

the number of characters needed for radio transmission, for example EM42uf.

It is common in the Amateur Radio world to represent geographical locations using the first two or three Maidenhead pairs. Additional accuracy is gained by including additional pairs. Up to eight characters has been ratified, although several online conversion tools extend the system into smaller squares. It is interesting to note that the extended system results are not always compatible.

Two things are discussed in this paper.
1) The algorithm proposed for additional character pairs beyond the defined eight.
2) The precision gained by adding additional character pairs.

Proposed Algorithm

The proposed algorithm is simple. Continue the original pattern until the necessary precision is reached. Table 1

¹Notes appear on page 35

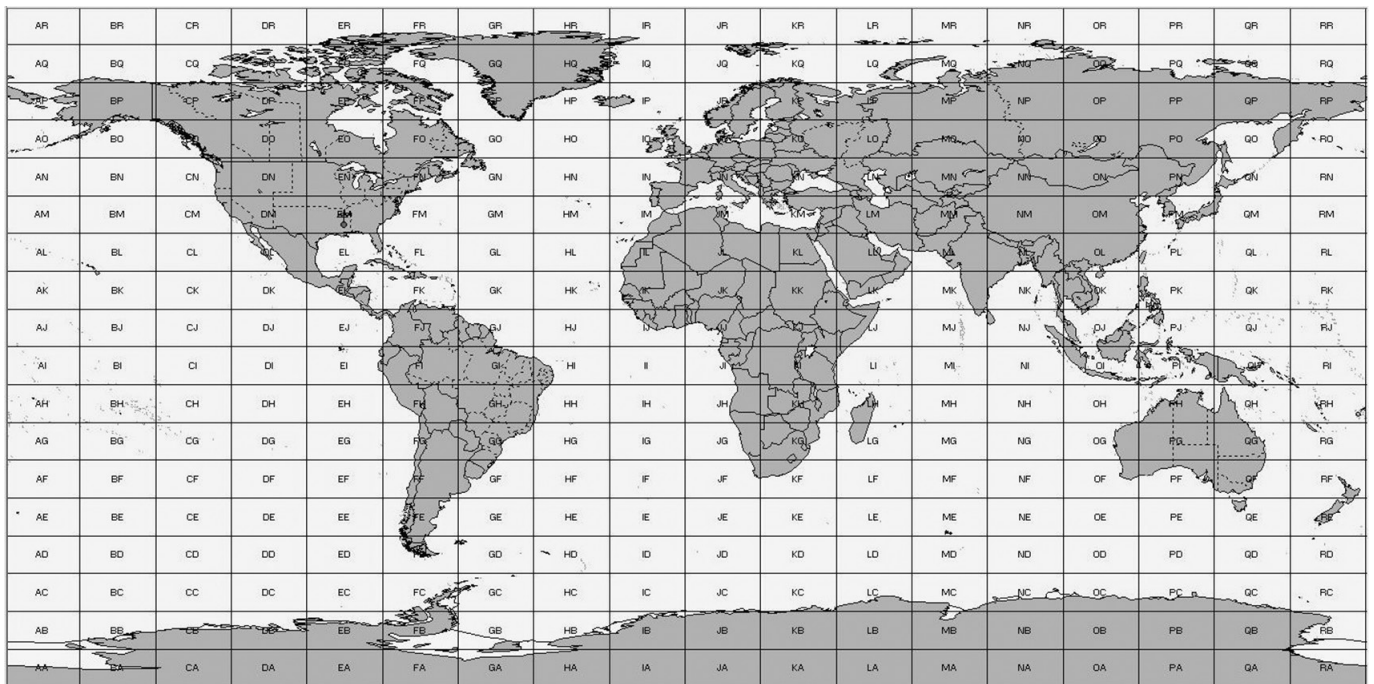


Figure 1 — This map, generated using DX Atlas 2.3 (Alex Shovkoplyas, VE3NEA, www.dxatlas.com), illustrates the two character Maidenhead grid squares.

shows sixteen characters and *number of bins* in degrees. Characters one through eight are defined. I am proposing a definition for characters nine through sixteen. Notice that the first two characters encode eighteen bins of 20 degrees of longitude, and 10 degrees of latitude respectively. Characters 3 and 4 encode ten bins of two degrees of longitude, and one degree of latitude respectively. Characters 5 and 6 encode twenty four bins of five minutes of longitude, and 2.5 minutes of latitude respectively, expressed in degrees. Last, characters seven and eight encode ten bins of 30 seconds of longitude and 15-seconds of latitude respectively, expressed in degrees. Since it is difficult to see the relationship between the elements when expressed in degrees, we transformed the numbers by multiplying them by 3600 to express the values in *seconds*, as shown in Table 2.

Table 3 shows the two important relationships used to codify the algorithm. The values for characters 9 through 16 in Table 2 are calculated from the relationships detailed in Table 3. For example, the number of bins alternates between 24 and 10 based upon the pairs. Numbered pairs have ten bins tagged zero through nine, and the lettered pairs use letters *a* through *x*. Furthermore, the character 9, longitude number of 1.25 (Table 2), was calculated by dividing 300, the character 5 number, by 240.

Tables 13 through 28 represent each of the sixteen characters, and are calculated from the Table 2 values. These Tables are similar to those introduced by Edmund Tyson, N5JTY, in the January 1989 *QST*. There, additional calculations are also given in milliseconds. Note that the number of bins is twice what I show in Table 1 to account for positive and negative coordinates. The positive numbers represent the northern hemisphere and the eastern half of the globe. The negative numbers represent the southern hemisphere and the western half of the globe.

Algorithm Implementation

I chose to implement the algorithm in a *Microsoft Excel* spread sheet, although any other program or language can be used. You can download my spread sheet from the *QEXfiles* web page. Table 4 shows an example for entering decimal latitude and longitude numbers into the spreadsheet to obtain the 16 character Maidenhead grid square. The spread sheet uses color to enhance readability. Anything related to latitude is orange and anything related to longitude is green. Grid square information has a yellow background and lettered in red. This example shows that entering a latitude of 34.065380 and a longitude of -84.554930 results a 16 character Maidenhead grid

locator of EM74rb35jq85av30.

The algorithm and calculations in degrees are shown in the left two columns of Table 5. Columns three and four show the algorithm and calculations in milliseconds. It is interesting to note that the calculations take fewer steps when performed in milliseconds.

It is also comforting to see that the calculations in degrees and in milliseconds produce the same result. The fifth column, labeled *Accuracy*, is used to verify my code. Values 15 and 16 are the same as the original latitude and longitude values.

Just in case you do not have your

Table 1 – Degrees
Characterization of grid characters by degrees.

Character	Longitude	Latitude	Character	Number of bins
1	20	10	2	18
3	2	1	4	10
5	0.0833333	0.0416667	6	24
7	0.0083333	0.0041667	8	10
9	0.0003472	0.0001736	10	24
11	0.0000347	0.0000174	12	10
13	0.0000014	0.0000007	14	24
15	0.0000001	0.0000001	16	10

Table 2 – Seconds
Characterization of grid characters by seconds.

Character	Longitude	Latitude	Character	Number of bins
1	72000	36000	2	18
3	7200	3600	4	10
5	300	150	6	24
7	30	15	8	10
9	1.2500000	0.6250000	10	24
11	0.1250000	0.0625000	12	10
13	0.005208333	0.002604167	14	24
15	0.000520833	0.000260417	16	10

Table 3.
Character relationships.

Relationships 1

Since	Character 1	to	Character 5	in seconds	is equal to	240
and	Character 2	to	Character 6	in seconds	is equal to	240
therefore	Character 5	to	Character 9	in seconds	is equal to	240
and	Character 6	to	Character 10	in seconds	is equal to	240
and	Character 9	to	Character 13	in seconds	is equal to	240
and	Character 10	to	Character 14	in seconds	is equal to	240

Relationships 2

Since	Character 1	to	Character 3	in seconds	is equal to	10
and	Character 2	to	Character 4	in seconds	is equal to	10
therefore	Character 9	to	Character 11	in seconds	is equal to	10
and	Character 10	to	Character 12	in seconds	is equal to	10
and	Character 13	to	Character 15	in seconds	is equal to	10
and	Character 14	to	Character 16	in seconds	is equal to	10

Table 4
Coordinate to Maidenhead sixteen-character conversion.

	Latitude	Longitude	Maidenhead Grid
Enter in decimal degrees:	34.065380		
Enter longitude in decimal degrees:		-84.554930	
			EM74rb35jq85av30

Table 5
Algorithm and calculations example – coordinates to Maidenhead

LONGITUDE

<i>Algorithm and calculations in degrees</i>		<i>Algorithm and calculations in milliseconds</i>		<i>Accuracy</i>
-84.554930	Longitude degrees	Longitude milliseconds	-304397748	
E	Character 1 from Table 13	Character 1 from Table 13	E	
-80	Extract value 1	Extract value 1	-288000000	-80.00000000
-4.55493	Remaining lon degrees	Remaining lon milliseconds	-16397748	
7	Character 3 from Table 15	Character 3 from Table 15	7	
-4	Extract value 3	Extract value 3	-14400000	-84.00000000
-0.55493	Subtract	Remaining lon milliseconds	-1997748	
-33.2958	Remaining lon minutes			
r	Character 5 from Table 17	Character 5 from Table 17	r	
-30	Extract value 5	Extract value 5	-1800000	-84.50000000
-3.2958	Subtract			
-197.748	Remaining lon seconds	Remaining lon milliseconds	-197748	
3	Character 7 from Table 19	Character 7 from Table 19	3	
-180	Extract value 7	Extract value 7	-180000	-84.55000000
-17.748	Remaining lon seconds	Remaining lon milliseconds	-17748	
j	Character 9 from Table 21	Character 9 from Table 21	j	
-17.5	Extract value 9	Extract value 9	-17500	-84.55486111
-0.248	Remaining lon seconds	Remaining lon milliseconds	-248	
8	Character 11 from Table 23	Character 11 from Table 23	8	
-0.125	Extract value 11	Extract value 11	-125	-84.55489583
-0.123	Remaining lon seconds	Remaining lon milliseconds	-123.00	
a	Character 13 from Table 25	Character 13 from Table 25	a	
-0.11979	Extract value 13	Extract value 13	-125	-84.55493056
-0.00321	Remaining lon seconds	Remaining lon milliseconds	2.00	
3	Character 15 from Table 27	Character 15 from Table 27	3	
-0.003125	Extract value 15	Extract value 15	1.562	-84.55493012
-0.00008	Remaining lon seconds	Remaining lon milliseconds	0.438	

LATITUDE

34.065380	Latitude degrees	Latitude milliseconds	122635368	
M	Character 2 from Table 14	Character 2 from Table 14	M	
30	Extract value 2	Extract value 2	108000000	30.00000000
4.06538	Remaining lat degrees	Remaining lat milliseconds	14635368	
4	Character 4 from Table 16	Character 4 from Table 16	4	
4	Extract value 4	Extract value 4	14400000	34.00000000
0.06538	Subtract	Remaining lat milliseconds	235368	
3.9228	Remaining lat minutes			
b	Character 6 from Table 18	Character 6 from Table 18	b	
2.5	Extract value 6	Extract value 6	150000	34.04166667
1.4228	Subtract			
85.368	Remaining lat seconds	Remaining lat milliseconds	85368	
5	Character 8 from Table 20	Character 8 from Table 20	5	
75	Extract value 8	Extract value 8	75000	34.06250000
10.368	Remaining lat seconds	Remaining lat milliseconds	10368	
q	Character 10 from Table 22	Character 10 from Table 22	q	
10	Extract value 10	Extract value 10	10000	34.06527778
0.368	Remaining lat seconds	Remaining lat milliseconds	368	
5	Character 12 from Table 24	Character 12 from Table 24	5	
0.3125	Extract value 12	Extract value 12	312.5	34.06536458
0.0555	Remaining lat seconds	Remaining lat milliseconds	55.50	
v	Character 14 from Table 26	Character 14 from Table 26	v	
0.05469	Extract value 14	Extract value 14	54.69	34.06537978
0.00081	Remaining lat seconds	Remaining lat milliseconds	0.810	
0	Character 16 from Table 28	Character 16 from Table 28	0	
0	Extract value 16	Extract value 16	0	34.06537978
0.0008100	Remaining lat seconds	Remaining lat milliseconds	0.8100	

Table 6
Coordinate conversion: Degrees-Seconds to Decimal Degrees.

	<i>Latitude</i>	<i>Longitude</i>
Enter degrees:	38	-102
Enter minutes:	18.67625998	17.50775174
Coordinates in decimal degrees:	38.311271	-102.2917959

Table 7**Coordinate conversion: Degrees-Minutes-Seconds to Decimal Degrees**

	<i>Latitude</i>	<i>Longitude</i>
Enter degrees:	38	-102
Enter minutes:	18	17
Enter seconds:	40.57559896	30.46510428
Coordinates in decimal degrees:	38.311271	-102.2917959

Table 8**Maidenhead to coordinate conversion.**

Enter grid locator: EM91ad60mw45qt80

	Decimal degrees	Degrees	Minutes	Degrees	Minutes	Seconds
Latitude:	31.128920		7.735200	31	7	44.111979
Longitude:	-81.945670	-81	56.740200	-81	56	44.411979

coordinates in decimal form, or you do not know how to convert degrees-minutes or degrees-minutes-seconds to decimal, Tables 6 and 7 are included as separate spreadsheet tabs to facilitate the conversions. You then must copy the calculated decimal solution to the spreadsheet Table 4.

To convert a Maidenhead grid locator into coordinates, use the *Grid to Degree Converter* spreadsheet tab. Type the grid locator into the yellow box and read the result in decimal degrees, degrees-minutes, and degrees-minutes-seconds to the right. This is illustrated in Table 8. [Table 8 builds the latitude and longitude systematically starting from the corner nearest to 0 deg latitude by 0 deg longitude of the ever decreasing size of grid squares, rather than reporting the center coordinator of those squares. The author welcomes reader inputs.—Ed]. The algorithm and calculations are shown in Table 9.

Maidenhead Grid Precision

How precise are the Maidenhead grid pairs? In other words, how close to the precise geo-location are you in relation to the number of grid pairs? How precise is precise enough? How does this vary with changes in latitude since as you relocate closer to the poles, longitude lines converge, or get closer together?

The spreadsheet tab labeled *Accuracy* shows the results in miles and feet for each pair of grid characters at latitude 34, see Table 10. Notice that with four characters, or two pairs, the location is within 32.1 miles. The location is within about one-third of a mile when eight characters are included in the calculation. With twelve characters, the precision is within about 12 feet, while a 16 character calculation gets you within one inch.

Table 9**Algorithm and calculations example – Maidenhead to coordinates.**

Get # characters	16
Extract character 1	E
Extract character 2	M
Extract character 3	9
Extract character 4	1
Extract character 5	a
Extract character 6	d
Extract character 7	6
Extract character 8	0
Extract character 9	m
Extract character 10	w
Extract character 11	4
Extract character 12	5
Extract character 13	q
Extract character 14	t
Extract character 15	8
Extract character 16	0
Calculate character 1 value	-288000000
Calculate character 2 value	108000000
Calculate character 3 value	0
Calculate character 4 value	3600000
Calculate character 5 value	-6900000
Calculate character 6 value	450000
Calculate character 7 value	-90000
Calculate character 8 value	0
Calculate character 9 value	-13750
Calculate character 10 value	13750
Calculate character 11 value	-625
Calculate character 12 value	312.5
Calculate character 13 value	-36.45838
Calculate character 14 value	49.479173
Calculate character 15 value	-0.520833
Calculate character 16 value	0
Add longitudes together	-295004412
Add latitudes together	112064112
Convert lon to decimal degrees	-81.94566999
Convert lat to decimal degrees	31.12891999
Longitude degrees	-81
Latitude degrees	31
Longitude minutes	-56.74019965
Latitude minutes	7.735199653
Lon Mins	-56
Lat Mins	7
Lon Secs	-44.41197921
Lat Secs	44.11197917

Table 10**Precision based upon number of Maidenhead characters.**

<i>Latitude 1</i>	<i>Longitude 1</i>	<i>Latitude 2</i>	<i>Longitude 2</i>	<i>Distance in miles</i>	<i>Distance in feet</i>	<i>Grid characters</i>
34.065380	-84.554930	30.000000	-80.000000	387.5939897	2046496.2659	2
34.065380	-84.554930	34.000000	-84.000000	32.1297237	169644.9411	4
34.065380	-84.554930	34.041667	-84.500000	3.5496850	18742.3367	6
34.065380	-84.554930	34.062500	-84.550000	0.3456742	1825.1599	8
34.065380	-84.554930	34.065278	-84.554861	0.0080980	42.7576	10
34.065380	-84.554930	34.065365	-84.554896	0.0022294	11.7711	12
34.065380	-84.554930	34.065380	-84.554931	0.0000354	0.1871	14
34.065380	-84.554930	34.065380	-84.554930	0.000017	0.0900	16

Table 11**Distance between two Maidenhead locaters.**

		<i>Latitude decimal</i>	<i>Longitude decimal</i>	<i>Miles</i>
Enter grid square 1:	EM42uf13fd66rq60	32.221470	-90.323030	
Enter grid square 2:	EM31id77sc01go90	31.154541	-93.268740	
Calculated miles				188.3716945

Table 12**Grid 1 – Grid 2 algorithm.***Grid 1 algorithm and calculations*

Get # characters	16
Extract character 1	E
Extract character 2	M
Extract character 3	4
Extract character 4	2
Extract character 5	u
Extract character 6	f
Extract character 7	1
Extract character 8	3
Extract character 9	f
Extract character 10	d
Extract character 11	6
Extract character 12	6
Extract character 13	r
Extract character 14	q
Extract character 15	6
Extract character 16	0
Calculate character 1 value	-288000000
Calculate character 2 value	108000000
Calculate character 3 value	-36000000
Calculate character 4 value	7200000
Calculate character 5 value	-900000
Calculate character 6 value	750000
Calculate character 7 value	-240000
Calculate character 8 value	45000
Calculate character 9 value	-22500
Calculate character 10 value	1875
Calculate character 11 value	-375
Calculate character 12 value	375
Calculate character 13 value	-31.25004
Calculate character 14 value	41.666672
Calculate character 15 value	-1.562499
Calculate character 16 value	0
Add longitudes together	-325162907.8
Add latitudes together	115997291.7
Convert lon to decimal degrees	-90.32302995
Convert lat to decimal degrees	32.22146991
Longitude degrees	-90
Latitude degrees	32
Longitude minutes	-19.38179688
Latitude minutes	13.28819444
Lon Mins	-19
Lat Mins	13
Lon Secs	-22.90781254
Lat Secs	17.29166667

Grid 2 algorithm and calculations

Get # characters	16
Extract character 1	E
Extract character 2	M
Extract character 3	3
Extract character 4	1
Extract character 5	i
Extract character 6	d
Extract character 7	7
Extract character 8	7
Extract character 9	s
Extract character 10	c
Extract character 11	0
Extract character 12	1
Extract character 13	g
Extract character 14	o
Extract character 15	9
Extract character 16	0
Calculate character 1 value	-288000000
Calculate character 2 value	108000000
Calculate character 3 value	-43200000
Calculate character 4 value	3600000
Calculate character 5 value	-4500000
Calculate character 6 value	450000
Calculate character 7 value	-60000
Calculate character 8 value	105000
Calculate character 9 value	-6250
Calculate character 10 value	1250
Calculate character 11 value	-1125
Calculate character 12 value	62.5
Calculate character 13 value	-88.54178
Calculate character 14 value	36.458338
Calculate character 15 value	0
Calculate character 16 value	0
Add longitudes together	-335767463.5
Add latitudes together	112156349
Convert lon to decimal degrees	-93.26873987
Convert lat to decimal degrees	31.15454138
Longitude degrees	-93
Latitude degrees	31
Longitude minutes	-16.12439236
Latitude minutes	9.272482639
Lon Mins	-16
Lat Mins	9
Lon Secs	-7.46354178
Lat Secs	16.34895834

Distance Between Grids

Use the spreadsheet tab named *Grid to Grid Distance* to determine the distance from one Maidenhead grid locator to another. Enter the two grids in the yellow boxes near the top. The coordinates are calculated in decimal degrees and the distance in miles is given. This distance is calculated by the Spherical Law of Cosines with the law rearranged so that latitude can be used directly rather than the co-latitude. An example is shown in Table 11. The Grid 1 and Grid 2 algorithms calculations are shown in Table 12. Units of milliseconds are used in most steps for accuracy and ease of translating into other programming languages.

Bill Echols, N15F, was first licensed as WN2NYR in 1970 while in high school in Poughkeepsie, NY. He became WA2NYR a year later. He held a German call sign, DA2EJ, while living overseas in the early 80s. Bill has spent his career working in broadcasting, two way radio, trunked radio systems, two way paging, analog cellular, and now mesh radio design for a premier ac power generation, transmission, and distribution company. He restores vacuum tube receivers for fun. Bill is building a new station in Florida where he hopes to soon be back contesting and DXing.

Notes

¹www.arrl.org/grid-squares.

² E. H. Tyson, N5JTY, "Conversion between Geodetic and Grid Locator Systems", QST, Jan 1989, pp. 29 – 30, 43.

**Table 13 – Longitude.
18 bins of 20 degrees (7200000 ms).**

Degrees	Letter	Milliseconds
-180		-648000000
-160	A	-576000000
-140	B	-504000000
-120	C	-432000000
-100	D	-360000000
-80	E	-288000000
-60	F	-216000000
-40	G	-144000000
-20	H	-72000000
0	I	0
20	J	72000000
40	K	144000000
60	L	216000000
80	M	288000000
100	N	360000000
120	O	432000000
140	P	504000000
160	Q	576000000
180	R	648000000

**Table 14 – Latitude.
18 bins of 10 degrees (3600000 ms).**

Degrees	Letter	Milliseconds
-90		-324000000
-80	A	-288000000
-70	B	-252000000
-60	C	-216000000
-50	D	-180000000
-40	E	-144000000
-30	F	-108000000
-20	G	-72000000
-10	H	-36000000
0	I	0
10	J	36000000
20	K	72000000
30	L	108000000
40	M	144000000
50	N	180000000
60	O	216000000
70	P	252000000
80	Q	288000000
90	R	324000000

**Table 15 – Longitude.
20 bins of 2 degrees (7200000 ms).**

Degrees	Letter	ms
-20		-72000000
-18	0	-64800000
-16	1	-57600000
-14	2	-50400000
-12	3	-43200000
-10	4	-36000000
-8	5	-28800000
-6	6	-21600000
-4	7	-14400000
-2	8	-7200000
0	9	0
2	0	7200000
4	1	14400000
6	2	21600000
8	3	28800000
10	4	36000000
12	5	43200000
14	6	50400000
16	7	57600000
18	8	64800000
20	9	72000000

**Table 16 – Latitude.
20 bins of 1 degree (3600000 ms).**

Degrees	Number	ms
-10		-36000000
-9	0	-32400000
-8	1	-28800000
-7	2	-25200000
-6	3	-21600000
-5	4	-18000000
-4	5	-14400000
-3	6	-10800000
-2	7	-7200000
-1	8	-3600000
0	9	0
1	0	3600000
2	1	7200000
3	2	10800000
4	3	14400000
5	4	18000000
6	5	21600000
7	6	25200000
8	7	28800000
9	8	32400000
10	9	36000000

Table 17 – Longitude.
48 bins of 5 minutes (300000 ms).

Minutes	Letter	ms
-120		-7200000
-115	a	-6900000
-110	b	-6600000
-105	c	-6300000
-100	d	-6000000
-95	e	-5700000
-90	f	-5400000
-85	g	-5100000
-80	h	-4800000
-75	i	-4500000
-70	j	-4200000
-65	k	-3900000
-60	l	-3600000
-55	m	-3300000
-50	n	-3000000
-45	o	-2700000
-40	p	-2400000
-35	q	-2100000
-30	r	-1800000
-25	s	-1500000
-20	t	-1200000
-15	u	-900000
-10	v	-600000
-5	w	-300000
0	x	0
5	a	300000
10	b	600000
15	c	900000
20	d	1200000
25	e	1500000
30	f	1800000
35	g	2100000
40	h	2400000
45	i	2700000
50	j	3000000
55	k	3300000
60	l	3600000
65	m	3900000
70	n	4200000
75	o	4500000
80	p	4800000
85	q	5100000
90	r	5400000
95	s	5700000
100	t	6000000
105	u	6300000
110	v	6600000
115	w	6900000
120	x	7200000

Table 18 – Latitude.
48 bins of 2.5 minutes (150000 ms).

Minutes	Letter	ms
-60.0		-3600000
-57.5	a	-3450000
-55.0	b	-3300000
-52.5	c	-3150000
-50.0	d	-3000000
-47.5	e	-2850000
-45.0	f	-2700000
-42.5	g	-2550000
-40.0	h	-2400000
-37.5	i	-2250000
-35.0	j	-2100000
-32.5	k	-1950000
-30.0	l	-1800000
-27.5	m	-1650000
-25.0	n	-1500000
-22.5	o	-1350000
-20.0	p	-1200000
-17.5	q	-1050000
-15.0	r	-900000
-12.5	s	-750000
-10.0	t	-600000
-7.5	u	-450000
-5.0	v	-300000
-2.5	w	-150000
0.0	x	0
2.5	a	150000
5.0	b	300000
7.5	c	450000
10.0	d	600000
12.5	e	750000
15.0	f	900000
17.5	g	1050000
20.0	h	1200000
22.5	i	1350000
25.0	j	1500000
27.5	k	1650000
30.0	l	1800000
32.5	m	1950000
35.0	n	2100000
37.5	o	2250000
40.0	p	2400000
42.5	q	2550000
45.0	r	2700000
47.5	s	2850000
50.0	t	3000000
52.5	u	3150000
55.0	v	3300000
57.5	w	3450000
60.0	x	3600000

Table 19 – Longitude.
20 bins of 30 seconds (30000 ms).

Seconds	Number	ms
-300		-300000
-270	0	-270000
-240	1	-240000
-210	2	-210000
-180	3	-180000
-150	4	-150000
-120	5	-120000
-90	6	-90000
-60	7	-60000
-30	8	-30000
0	9	0
30	0	30000
60	1	60000
90	2	90000
120	3	120000
150	4	150000
180	5	180000
210	6	210000
240	7	240000
270	8	270000
300	9	300000

Table 20 – Latitude.
20 bins of 15 seconds (15000 ms).

Seconds	Number	ms
-150		-150000
-135	0	-135000
-120	1	-120000
-105	2	-105000
-90	3	-90000
-75	4	-75000
-60	5	-60000
-45	6	-45000
-30	7	-30000
-15	8	-15000
0	9	0
15	0	15000
30	1	30000
45	2	45000
60	3	60000
75	4	75000
90	5	90000
105	6	105000
120	7	120000
135	8	135000
150	9	150000

Table 21 – Longitude.
48 bins of 1.25 seconds (1250 ms).

Seconds	Letter	ms
-30.00		-30000
-28.75	a	-28750
-27.50	b	-27500
-26.25	c	-26250
-25.00	d	-25000
-23.75	e	-23750
-22.50	f	-22500
-21.25	g	-21250
-20.00	h	-20000
-18.75	i	-18750
-17.50	j	-17500
-16.25	k	-16250
-15.00	l	-15000
-13.75	m	-13750
-12.50	n	-12500
-11.25	o	-11250
-10.00	p	-10000
-8.75	q	-8750
-7.50	r	-7500
-6.25	s	-6250
-5.00	t	-5000
-3.75	u	-3750
-2.50	v	-2500
-1.25	w	-1250
0.00	x	0
1.25	a	1250
2.50	b	2500
3.75	c	3750
5.00	d	5000
6.25	e	6250
7.50	f	7500
8.75	g	8750
10.00	h	10000
11.25	i	11250
12.50	j	12500
13.75	k	13750
15.00	l	15000
16.25	m	16250
17.50	n	17500
18.75	o	18750
20.00	p	20000
21.25	q	21250
22.50	r	22500
23.75	s	23750
25.00	t	25000
26.25	u	26250
27.50	v	27500
28.75	w	28750
30.00	x	30000

Table 22 – Latitude.
48 bins of 0.625 seconds (625 ms).

Seconds	Letter	ms
-15.000		-15000
-14.375	a	-14375
-13.750	b	-13750
-13.125	c	-13125
-12.500	d	-12500
-11.875	e	-11875
-11.250	f	-11250
-10.625	g	-10625
-10.000	h	-10000
-9.375	i	-9375
-8.750	j	-8750
-8.125	k	-8125
-7.500	l	-7500
-6.875	m	-6875
-6.250	n	-6250
-5.625	o	-5625
-5.000	p	-5000
-4.375	q	-4375
-3.750	r	-3750
-3.125	s	-3125
-2.500	t	-2500
-1.875	u	-1875
-1.250	v	-1250
-0.625	w	-625
0.000	x	0
0.625	a	625
1.250	b	1250
1.875	c	1875
2.500	d	2500
3.125	e	3125
3.750	f	3750
4.375	g	4375
5.000	h	5000
5.625	i	5625
6.250	j	6250
6.875	k	6875
7.500	l	7500
8.125	m	8125
8.750	n	8750
9.375	o	9375
10.000	p	10000
10.625	q	10625
11.250	r	11250
11.875	s	11875
12.500	t	12500
13.125	u	13125
13.750	v	13750
14.375	w	14375
15.000	x	15000

Table 23 – Longitude.
20 bins of 0.125 seconds (125 ms).

Seconds	Number	ms
-1.250	0	-1250
-1.125	1	-1125
-1.000	2	-1000
-0.875	3	-875
-0.750	4	-750
-0.625	5	-625
-0.500	6	-500
-0.375	7	-375
-0.250	8	-250
-0.125	9	-125
0.000	0	0
0.125	1	125
0.250	2	250
0.375	3	375
0.500	4	500
0.625	5	625
0.750	6	750
0.875	7	875
1.000	8	1000
1.125	9	1125
1.250		1250

Table 24 – Latitude.
20 bins of 0.0625 seconds (62.5-ms).

Seconds	Number	ms
-0.6250	0	-625.0
-0.5625	1	-562.5
-0.5000	2	-500.0
-0.4375	3	-437.5
-0.3750	4	-375.0
-0.3125	5	-312.5
-0.2500	6	-250.0
-0.1875	7	-187.5
-0.1250	8	-125.0
-0.0625	9	-62.5
0.0000	0	0.0
0.0625	1	62.5
0.1250	2	125.0
0.1875	3	187.5
0.2500	4	250.0
0.3125	5	312.5
0.3750	6	375.0
0.4375	7	437.5
0.5000	8	500.0
0.5625	9	562.5
0.6250		625.0

Table 25 – Longitude.**48 bins of 0.005208 seconds (5.208 ms).**

Seconds	Number	ms
-0.12500016		-125.00016
-0.11979182	a	-119.79182
-0.11458348	b	-114.58348
-0.10937514	c	-109.37514
-0.1041668	d	-104.1668
-0.09895846	e	-98.95846
-0.09375012	f	-93.75012
-0.08854178	g	-88.54178
-0.08333344	h	-83.33344
-0.0781251	i	-78.1251
-0.07291676	j	-72.91676
-0.06770842	k	-67.70842
-0.06250008	l	-62.50008
-0.05729174	m	-57.29174
-0.0520834	n	-52.0834
-0.04687506	o	-46.87506
-0.04166672	p	-41.66672
-0.03645838	q	-36.45838
-0.03125004	r	-31.25004
-0.0260417	s	-26.0417
-0.02083336	t	-20.83336
-0.01562502	u	-15.62502
-0.01041668	v	-10.41668
-0.00520834	w	-5.20834
0	x	0
0.00520834	a	5.20834
0.01041668	b	10.41668
0.01562502	c	15.62502
0.02083336	d	20.83336
0.0260417	e	26.0417
0.03125004	f	31.25004
0.03645838	g	36.45838
0.04166672	h	41.66672
0.04687506	i	46.87506
0.0520834	j	52.0834
0.05729174	k	57.29174
0.06250008	l	62.50008
0.06770842	m	67.70842
0.07291676	n	72.91676
0.0781251	o	78.1251
0.08333344	p	83.33344
0.08854178	q	88.54178
0.09375012	r	93.75012
0.09895846	s	98.95846
0.1041668	t	104.1668
0.10937514	u	109.37514
0.11458348	v	114.58348
0.11979182	w	119.79182
0.12500016	x	125.00016

Table 26 – Latitude.**48 bins of 0.002604 seconds (2.604-ms).**

Seconds	Number	ms
-0.062500008		-62.500008
-0.059895841	a	-59.895841
-0.057291674	b	-57.291674
-0.054687507	c	-54.687507
-0.05208334	d	-52.08334
-0.049479173	e	-49.479173
-0.046875006	f	-46.875006
-0.044270839	g	-44.270839
-0.041666672	h	-41.666672
-0.039062505	i	-39.062505
-0.036458338	j	-36.458338
-0.033854171	k	-33.854171
-0.031250004	l	-31.250004
-0.028645837	m	-28.645837
-0.02604167	n	-26.04167
-0.023437503	o	-23.437503
-0.020833336	p	-20.833336
-0.018229169	q	-18.229169
-0.015625002	r	-15.625002
-0.013020835	s	-13.020835
-0.010416668	t	-10.416668
-0.007812501	u	-7.812501
-0.005208334	v	-5.208334
-0.002604167	w	-2.604167
0	x	0
0.002604167	a	2.604167
0.005208334	b	5.208334
0.007812501	c	7.812501
0.010416668	d	10.416668
0.013020835	e	13.020835
0.015625002	f	15.625002
0.018229169	g	18.229169
0.020833336	h	20.833336
0.023437503	i	23.437503
0.02604167	j	26.04167
0.028645837	k	28.645837
0.031250004	l	31.250004
0.033854171	m	33.854171
0.036458338	n	36.458338
0.039062505	o	39.062505
0.041666672	p	41.666672
0.044270839	q	44.270839
0.046875006	r	46.875006
0.049479173	s	49.479173
0.05208334	t	52.08334
0.054687507	u	54.687507
0.057291674	v	57.291674
0.059895841	w	59.895841
0.062500008	x	62.500008

Table 27 – Longitude.**20 bins of 0.000520833 seconds (0.520833 ms).**

Seconds	Number	ms
-0.005208330		-5.20833
-0.004687497	0	-4.687497
-0.004166664	1	-4.166664
-0.003645831	2	-3.645831
-0.003124998	3	-3.124998
-0.002604165	4	-2.604165
-0.002083332	5	-2.083332
-0.001562499	6	-1.562499
-0.001041666	7	-1.041666
-0.000520833	8	-0.520833
0.000000000	9	0
0.000520833	0	0.520833
0.001041666	1	1.041666
0.001562499	2	1.562499
0.002083332	3	2.083332
0.002604165	4	2.604165
0.003124998	5	3.124998
0.003645831	6	3.645831
0.004166664	7	4.166664
0.004687497	8	4.687497
0.005208330	9	5.20833

Table 28 – Latitude.**20 bins of 0.0002604 seconds (0.2604 ms).**

Seconds	Number	ms
-0.000260417		-0.2604167
-0.000234375	0	-0.23437503
-0.000208333	1	-0.20833336
-0.000182292	2	-0.18229169
-0.000156250	3	-0.15625002
-0.000130208	4	-0.13020835
-0.000104167	5	-0.10416668
-0.000078125	6	-0.07812501
-0.000052083	7	-0.05208334
-0.000026042	8	-0.02604167
0.000000000	9	0
0.000026042	0	0.02604167
0.000052083	1	0.05208334
0.000078125	2	0.07812501
0.000104167	3	0.10416668
0.000130208	4	0.13020835
0.000156250	5	0.15625002
0.000182292	6	0.18229169
0.000208333	7	0.20833336
0.000234375	8	0.23437503
0.000260417	9	0.2604167

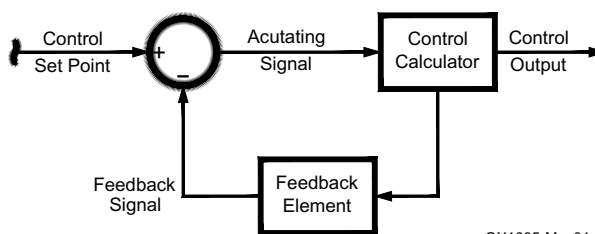
SDR Simplified: Demystifying PID Control Loops

The real story behind how a Proportional-Integral-Differential (PID) control loop works. Ray gives insights into how to build one and tune it for reasonable operation.

An Introduction to Closed Loop Control

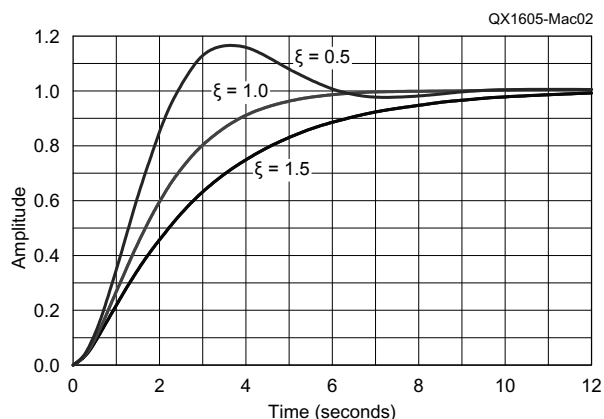
We use closed loop control all the time in Amateur Radio. Regulated power supplies, phase locked loops, and oven control of crystal oscillator temperature are a few examples. All of these systems follow the block diagram shown in Figure 1. The goal is to control a physical property and maintain it at some value. Figure 2 shows the classic plot of the three types of step response of a controlled system can exhibit. The most stable (but not necessarily most desirable) response is over-damped response. This is the same response you get with a step in voltage on a simple RC circuit. It approaches the target voltage slowly until the difference between desired and actual is essentially zero. A faster response is the critically damped response. This is the response you get in an RLC circuit with extremely low Q. The resistance is so large that oscillations cannot get started. The fastest response possible is with an under-damped system. This is the same response you get in an RLC system with some moderate value of Q. The trade off in this system is significant cycles of oscillation above and below the desired value early in the response but with a rapid convergence to the desired value. The other trade-off is that the initial overshoot can be substantial.

Before the advent of computer circuit analysis, it was easiest to design circuits in the frequency domain using Laplace transforms to turn capacitors and inductors into poles and zeros in the frequency analysis. By moving poles and zeros around,



QX1605-Mac01

Figure 1 – Block diagram of a typical control feedback system.



QX1605-Mac02

Figure 2 – The response curves of the classic control loop responses. $\xi=0.5$ shows the under damped response, $\xi=1.0$ shows a critically damped response, and $\xi=1.5$ shows an over damped responses.

you could modify the circuit response from over-damped, to critically-damped, or even to under-damped. The design process of creating a system with poles and zeroes is pretty daunting — but engineers still work this way when the situation fits.

The Full PID Loop

As in all electronics systems, you can evaluate operation in either the frequency domain or the time domain. You can do a lot of mathematical manipulations to convert an analog circuit with several capacitors — and occasionally an inductor or two — into a basic formula that has a single *integral* term, a single *proportional* term, and a single *derivative* term — a proportional-integral-derivative or PID loop. Its form looks like this:

$$\begin{aligned} \text{Control Voltage} = & a \int \text{error}(t) dt \\ & + b \times \text{error}(t) \\ & + c \frac{d[\text{error}(t)]}{dt} \end{aligned} \quad (1)$$

Don't tune out if this equation means absolutely nothing to you, it is really quite simple as we will see.

Figure 3 shows an op-amp circuit that implements a hardware system with the performance of Eq. (1), and implements the control equation block from Figure 1. The top op-amp implements the integral term with the *a* parameter set by the ratio of C1/R1. The middle op-amp is a standard inverting amplifier where *b* is set by the ratio

of R3/R2. The bottom op-amp implements the derivative term where *c* is set by the ratio of R4/C2. Op-amps work by converting the feedback current into a voltage. In these amplifiers, the input current is equal to the feedback current. The top op-amp performs an integrator function because the output will charge or discharge the capacitor C1 as long as the error voltage is not equal to zero. The voltage across a capacitor is the integral of the current through the capacitor. When the error voltage goes to zero the voltage on the capacitor will stay at some value. Likewise, the bottom op-amp implements a derivative function because the current through a capacitor (C2) is equal to the derivative of the voltage across it. If the input voltage does not change, then no current flows and the output of the op-amp is zero. The final amplifier is a summing amplifier with a gain of -1, so the whole system implements Eq. (1). In a real circuit, it may be possible to combine one or more of the circuits around an op-amp to make the circuit simpler, but it helps our illustration to see each term implemented individually.

The Proportional Part

It is possible to implement only a subset of a PID loop. I have used many loops that needed only the proportional and integral terms because the system was so slow that the differential term added nothing to performance. Of course, the simplest PID loop uses only the proportional term (*a* and *c* of Eq. (1) are zero). The problem for purely proportional control is that it requires

that we know the exact transfer function to describe the difference between the set point and the feedback from the driving function. If the system drifts or external factors alter the transfer function, the system will have some small amount of error that is set by the proportional term gain. The error can be made small by increasing the proportional term gain, but the system is likely to overshoot the set point during transients. For this reason, control loops almost never operate in just proportional mode.

The Integral Part of PID

In many systems, we want the error to be as close to zero as possible when the system is in control. The integral portion of the PID equation provides that feature. Oddly, I have never seen this explanation in any control text book! In fact, when the system is in control, *only* the integral portion drives the output; the proportional term is exactly zero. The integral term ramps up to the required drive voltage slowly over time — where “slowly” is relative to your system operation — so that the error becomes zero. This allows the proportional term to operate more quickly to bring the system back into control if something knocks the system out of control. In general, we try to have the proportional term do its work about 10 times faster than the integral portion. The integral term supplies an adaptive feature to the PID loop that will compensate for external and internal drift or error.

The Differential Part of PID

Some systems need to respond very quickly to either a step change of the set point or an external push from stability. The differential term provides that quick but short-duration “kick” to push the system close to equilibrium. In general, we design the integral term to be slowest, the proportional

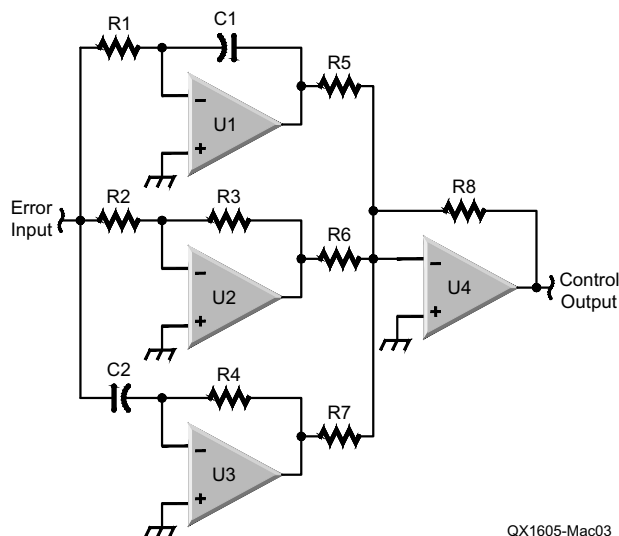


Figure 3 – A representative op-amp circuit that implements the PID control.

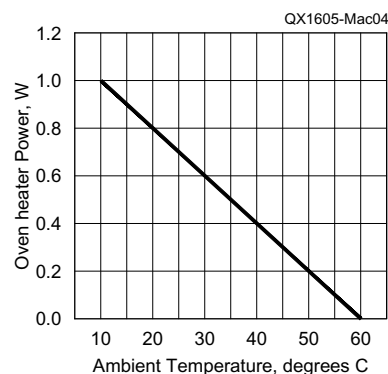
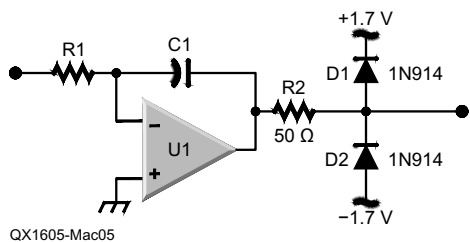
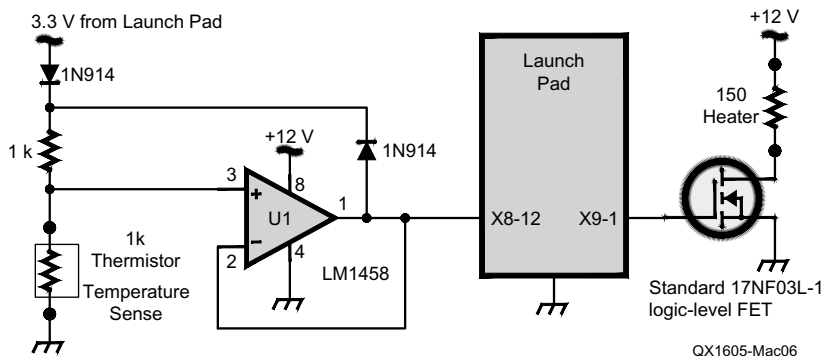


Figure 4 – A plot of power vs. ambient temperature for the OXCO control loop.



QX1605-Mac05

Figure 5 – A schematic showing a clamp of the integral function in an analog implementation.



QX1605-Mac06

Figure 6 – The schematic of an example sampled PID control loop.

term to be ten times faster, and the differential term to be ten times faster than proportional term. The differential term is most useful in a system where a large, quick (but short), drive will move the system almost immediately closer to the control point. An example is a motor driven system like anti-lock brakes where putting a short 10x overdrive pulse of current through the motor will quickly move the actuator. In order for the differential term to be useful, the drive system must have significant overdrive capability compared to the amount of drive normally needed by the proportional and integral terms for slower control changes.

A (More or Less) Real Example

It helps to understand how things work if we can see how to implement a real system. Let's see how we would implement a heater for an oven controlled crystal oscillator (OCXO) that is designed to keep the crystal at $60^{\circ}\text{C} \pm 0.1^{\circ}\text{C}$. The first piece of information is the plot of the amount of heat in watts that is required to maintain the crystal at a given temperature relative to a constant ambient temperature (Figure 4).

Next we need to implement the feedback system to control the temperature. While we could implement the system with op-amps, this type of system is more easily

implemented with a small microcontroller that has an on-board ADC for input and a PWM port for output. Using a computer allows us to create the control loop as a sampled system that directly implements the PID equation. Sampled systems do not actually implement an integrator or differentiator. Instead they approximate those functions as a sum of samples and difference between samples, but the results are essentially identical to integration and differentiation if we sample fast enough.

There is a feature of the integral function for both the op-amp and also the sampled systems that may not be obvious. The integral can grow to be either a very large positive or very large negative number if the error exists for any length of time. The op-amp integrator has a physical limitation: the output cannot exceed the positive rail or the negative rail. Once the output reaches the rail value, it is limited or saturated. We will look at tuning the integral term later, but for now we look at a way to limit the integral saturation to some value less than the rail. In an op-amp, we can use diodes to clamp the output to a value less than the rail as shown in Figure 5. In a sampled computer system, we can implement the "clamp" in software. Clamping the integral term is necessary especially in slow systems such as our heater example.

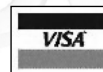
From MILLIWATTS
To KILOWATTSSM
More Watts per DollarSM

In Stock Now!
Semiconductors
for Manufacturing
and Servicing
Communications
Equipment

- **RF Modules**
- **Semiconductors**
- **Transmitter Tubes**

Se Habla Español • We Export

Phone: **760-744-0700**
Toll-Free: **800-737-2787**
(Orders only) **800-RF PARTS**
Website: **www.rfparts.com**
Fax: **760-744-1943**
888-744-1943
Email: **rfp@rfparts.com**



RF PARTS
COMPANY
From Milliwatts to KilowattsSM

Implementing and Tuning

I implemented the example for this explanation using a Texas Instruments Tiva 129 Launchpad because it is an inexpensive and capable system that has the peripherals needed for the control loop: an ADC, a PWM, and a timer. Additionally, you can set the *Code Composer Studio* to a mode that displays debug print in the console, so you do not need a serial connection to the target while debugging. *Code Composer* also comes with a set of functions that mirror the internal ROM functions for controlling the peripherals. These functions really make writing software much easier!

Figure 6 shows a schematic of the example heater control that could be used for an OCXO. My experimental setup uses the 150 Ω resistor to provide up to 1 W of heat with a 12.6 V power supply. The resistor is placed on one side of a cube of aluminum 0.5 inch per side and the thermistor is placed opposite the heating resistor. The two resistors and the aluminum are enclosed in plank foam shipping material to insulate the assembly from ambient. The next step is to determine the set point. I chose an Ametherm 1 k Ω NTC thermistor with response curve B. From the table of relative resistance vs. temperature, we get 318 Ω at 60 °C. This means the feedback voltage will be 1.21 V when the system is in control. Note that we need to limit the input voltage to a value less than 3.3 V using the bipolar transistor. The target ADC value is $(1.21/3.30) \times 4096$ or 1638. The example PWM setup from the Tiva 129 data sheet uses a 10 MHz clock to set the PWM frequency to 25 kHz and gives a range of 0 – 400 for the PWM value. The *Launchpad* uses a 25 MHz crystal, so the actual frequency is 62.5 kHz but still with 0 – 400 PWM range.

Listing 1 shows the sequence of software

commands that implements the PID loop. It is quite simple. Step one, wait for 10 ms timer to elapse. This sets the loop to operate with a constant 10 ms sample period. Step two reads the ADC and compares against the target to determine the error value. The next step calculates each of the three parts of the PID equation and generates the control value. The last step applies the control value to the PWM hardware. The full set of software including the hardware configuration is available on the *QEXfiles* web page, www.arri.org/qexfiles, as well as from dsp-radio-resources.info.

Tuning the loop is a lot easier if you have a laptop to watch the output while you put the assembly in your refrigerator and freezer. Start with the assembly sitting on your desk, which is pretty close to 22 °C. Place the assembly in the foam insulation and close it. Start the system running and watch the error value in the console of *Code Composer Studio*. The error will start out positive and approach zero. You will know how well the system is working by whether the error change slows a lot when close to zero or goes right past zero to become negative. This process can take quite a while depending on the thermal mass of your system. You can adjust the integral parameter larger or smaller to set one of the classic responses. The proportional parameter also affects the response. Setting the proportional parameter too large can cause the system to oscillate because it overcompensates for small errors. In most systems a critically damped response provides the best compromise. That means that the integral term is modest as is the proportional term. You could use an upside down “microduster” or other cold source to give a cold spike to the system to investigate how adding a differential term can rapidly bring the system back into control after a spike of hot or cold.

Errata

Correcting the Formula for Return Loss in the ANSI Standard




Edward Wetherhold, W3NQJ, IEEE Life Member, reports that a correction was approved to the equation for *Return Loss* in the ANSI/EIA-364-108-2000 Standard. The correction places a minus sign before the original and incorrect equation to make the resultant and corrected *Return Loss* (dB) to be positive. The corrected equation is,

$$\text{Return Loss} = -20 \log_{10} |\Gamma| = -20 \log_{10} |s_{11}|$$

where $\Gamma = s_{11}$ is the voltage reflection coefficient.

From **MILLIWATTS**
To **KILOWATTS**
More Watts per Dollar

Transmitting & Audio Tubes

COMMUNICATIONS
BROADCAST
INDUSTRY
AMATEUR

Immediate Shipment from Stock

3CPX800A7	4CX1000A	810
3CPX1500A7	4CX1500B	811A
3CX400A7	4CX3500A	812A
3CX800A7	4CX5000A	833A
3CX1200A7	4CX7500A	833C
3CX1200D7	4CX10000A	845
3CX1200Z7	4CX15000A	6146B
3CX1500A7	4CX20000B	3-500ZG
3CX3000A7	4CX20000C	3-1000Z
3CX6000A7	4CX20000D	4-400A
3CX10000A7	4X150A	4-1000A
3CX15000A7	572B	4PR400A
3CX20000A7	805	4PR1000A
4CX250B	807	...and more!

Se Habla Español • We Export

Phone: **760-744-0700**




Toll-Free: **800-737-2787**

(Orders only) **RF PARTS**

Website: **www.rfparts.com**

Fax: **760-744-1943**
888-744-1943

Email: **rfp@rfparts.com**

RF PARTS
COMPANY

Upcoming Conferences

2016 Society of Amateur Radio Astronomers Annual Conference

July 10-13, 2016, Green Bank,
West Virginia
radio-astronomy.org

The Society of Amateur Radio Astronomers (SARA) solicits papers for presentation at its 2016 Annual Conference to be held July 10 – 13, 2016. Sunday July 10, will start with an introduction to Radio Astronomy at the Jansky Auditorium, followed by learning to operate the forty foot radio telescope — 1,420 MHz (21 cm).

Presentations by SARA members and guests are scheduled on Monday and Tuesday. A high tech tour of the NRAO facility will be conducted on Tuesday July 12.

Papers are welcome on subjects directly related to radio astronomy including hardware, software, education and tutorials, research strategies, observations and data collection and philosophy. SARA members and supporters wishing to present a paper should e-mail a letter of intent, including a proposed title and abstract to the conference coordinator at vicepres@radio-astronomy.org no later than April 20, 2016.

Drafts of papers are due May 4, and final versions of the papers due no later than May 18. Be sure to include your full name, affiliation, postal address, email address, and indicate your willingness to attend the conference to present your paper. Submitters will receive an email response, typically within one week.

Guidelines for presenter papers are located at: radio-astronomy.org/pdf/guidelines-submitting-papers.pdf

50th Anniversary Central States VHF Society Conference

July 28 – 31, 2016, Rochester,
Minnesota
www.csvhfs.org

Call for Papers

The Central States VHF Society is soliciting papers, presentations, and poster displays for the 50th Annual CSVHFS Conference to be held in Rochester, Minnesota, July 28 – 31, 2016. Papers, presentations, and posters on all aspects of weak signal VHF and above Amateur Radio are requested. You do not need to attend the conference, nor present your paper, to have it published in the *Proceedings*.

• Posters will be displayed during the two days of the Conference.

• Topics of interest include (but are not limited to):

- Antennas — including Modeling/Design, Arrays, and Control
- Construction of equipment, such as transmitters, receivers, and transverters
- RF amplifiers (power amps) including single-band and multi-band vacuum tube and solid-state
- Pre-amplifiers (low noise)
- Propagation, including ducting, sporadic E, and meteor scatter, etc.
- Test Equipment — including homebrew, using, and making measurements
- Regulatory topics
- Operating — including contesting, roving, and DXpeditions
- EME
- Digital Signal Processing (DSP)
- Software-defined Radio (SDR)
- Digital Modes — such as WSJT, JT65, etc.

Generally, topics not related to weak signal VHF, such as FM Repeaters and packet-radio, are not accepted for presentation or publication. However, there are always exceptions.

Please contact either the *Technical Program* Chairman, Barry Malowanchuk, ve4ma@shaw.ca, or the *Proceedings* Chairman, Glen Overby, kc0iyt@arrrl.net.

Deadline for submissions:

For the *Proceedings*: **Sunday, May 22, 2016**

For Presentations to be delivered at the conference: **Tuesday, July 5, 2016**

For Posters to be displayed at the conference: **Thursday, July 29, 2016**

Further information is available at the CSVHFS web site (www.csvhfs.org), “The 2016 Conference,” and “Guidance for Proceedings Authors,” “Guidance for Presenters,” and “Guidance for Table-top/Poster Displays.”

The 35th Annual ARRL and TAPR Digital Communications Conference

September 16-18, 2016, St
Petersburg, FL
www.tapr.org

Mark your calendar and start making plans to attend the premier technical conference of the year, the 35th Annual ARRL and TAPR Digital Communications Conference to be held September 16-18, 2016, in St Petersburg, FL. The conference location

is the Hilton St Petersburg Bayfront.

The ARRL and TAPR Digital Communications Conference is an international forum for radio amateurs to meet, publish their work, and present new ideas and techniques. Presenters and attendees will have the opportunity to exchange ideas and learn about recent hardware and software advances, theories, experimental results, and practical applications.

Topics include, but are not limited to: Software Defined Radio (SDR), digital voice (D-Star, P25, Mototrbo, CODEC2, FreeDV), digital satellite communications, Global Position System (GPS), precision timing, Automatic Packet Reporting System™ (APRS), short messaging (a mode of APRS), Digital Signal Processing (DSP), HF digital modes, Internet interoperability with Amateur Radio networks, spread spectrum, IEEE 802.11 and other Part 15 license-exempt systems adaptable for Amateur Radio, using TCP/IP networking over Amateur Radio, mesh and peer to peer wireless networking, emergency and Homeland Defense backup digital communications, using Linux in Amateur Radio, updates on AX.25 and other wireless networking protocols.

Call for Papers

Technical papers are solicited for presentation at the ARRL and TAPR Digital Communications Conference and publication in the Conference Proceedings. Annual conference proceedings are published by the ARRL. Presentation at the conference is not required for publication. Submission of papers are due by July 31st, 2016, and should be submitted to Maty Weinberg, ARRL, 225 Main St, Newington, CT 06111 or maty@arrrl.org.

Hotel

Conference presentations, meetings, and seminars will be held at the Hilton St Petersburg Bayfront. It is highly recommended that you book your room prior to arriving. A special DCC room rate of \$109.00 single/double has been negotiated, and is until August 25, 2016; after that you will pay the regular room rate. Come early, stay late. The conference rate is good for 3 days before and 3 days after DCC.

To book your room, use the reservation link below, or call the hotel and mention the group code DCC when making reservations.

www.hilton.com/en/hi/groups/personalized/S/SPTSHHF-TAPR-20160914/index.jhtml

Hilton St Petersburg Bayfront, 333 1st St S, St Petersburg, FL 33701; 1-800-HILTONS (1-800-445-8667) National reservation line; 1-800-944-5500 Hotel Direct.



NEW!

High Speed Multimedia for Amateur Radio

By Glen Popiel, KW5GP

Build a High Speed Amateur Radio Microwave Network

Using commercial off-the-shelf equipment and developing their own software, groups of hams have created high speed wireless Amateur Radio digital networks with wide area coverage.

The possible uses for these high speed data networks in the Amateur Radio community are endless. Virtually any service that works on the regular Internet can be adapted to an Amateur Radio high speed multimedia (HSMM) network, including video conferencing, instant messaging, voice over Internet protocol (VoIP), network sensors and cameras, remote station control, and many other services. With the capability to send real-time video and data files, the public service and disaster support aspects of Amateur Radio are expanded tremendously.

This book introduces HSMM networking, explains the basics of how it works, and describes the various technologies in use today. Later chapters explain in detail how to deploy your own HSMM network, along with various applications to put it to work. Well illustrated step-by-step instructions will guide you through the process of installing and configuring software needed to get your HSMM network up and running.

Includes:

- Introduction to High Speed Multimedia
- High Speed Multimedia Technologies
- HSMM Equipment for Amateur Radio
- TCP/IP for HSMM
- HSMM Applications
- Security and Filtering
- Backup and Redundancy
- Deploying HSMM Networks
- The Future of HSMM

High Speed Multimedia for Amateur Radio

ARRL Item No. 0529

Member Price! Only \$24.95 (retail \$27.95)



ARRL The national association for
AMATEUR RADIO®



www.arrl.org/shop

Toll-Free US 888-277-5289 or
elsewhere +1-860-594-0355

Quicksilver Radio

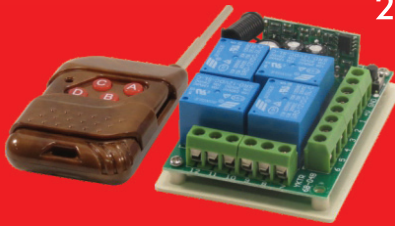
Test Equipment

USB Microscope



Up to 500X magnification. Captures still images and records live video. Built in LED Lighting. A must for working on surface mount components.

Wireless Relay Switch



200'+ Range. We have single, four, and eight channel models.

GO-PWR Plus™



Portable power to go or backup in the shack. Includes Powerpoles, bright easy to read meter, and lighted switch. For U1 size (35 ah) and group 24 (80 ah) batteries.



Digital Voltmeter/ Ammeter

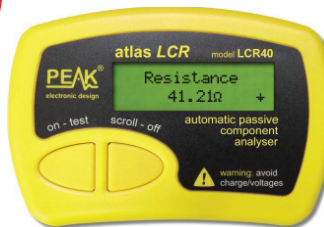
Two line display shows both current and voltage. Included shunt allows measurement up to 50A and 99V. Snaps into a panel to give your project a professional finish.

LCR and Impedance Meter



Newest Model. Analyzes coils, capacitors, and resistors. Indicates complex impedance and more.

Automatic Passive Component Analyzer



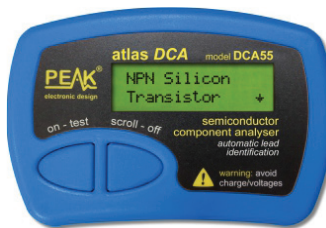
Analyzes coils, capacitors, and resistors.

Advanced Semiconductor Component Analyzer



Analyzes transistors, MOSFETs, JFETs, IGBTs, and more. Graphic display. Enhanced functionality with included PC software.

Semiconductor Component Analyzer



Analyzes transistors, MOSFETs, JFETs and more. Automatically determines component pinout.

Capacitance and ESR Meter



Analyzes capacitors, measures ESR.

Get All Your Ham Shack Essentials at Quicksilver Radio Products. Safe and Secure Ordering at:

www.qsradio.com



